

Design av flytende vindturbin

Responseundersøkelse av TLP-forankret
konstruksjon

Sindre Jin S Moldenhagen

Marin teknikk

Innlevert: juni 2015

Hovedveileder: Carl Martin Larsen, IMT

Norges teknisk-naturvitenskapelige universitet
Institutt for marin teknikk

Preface

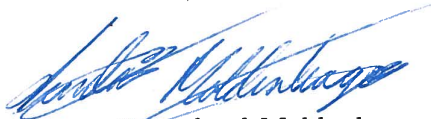
This thesis constitutes the final work with my master thesis in marine hydrodynamics at the Norwegian University of Science and Technology (NTNU) in Trondheim. The work has been carried out during the spring semester of 2015 at MTS.

The thesis investigates the effect of placing the spokes/arms of a TLP at the center of the substructure rather than at the bottom. The focus has been the rigid body motion and forces in the mooring system. A lot of effort has been made to describe the theoretical background of the analysis and the establishment of a model. TLP-based wind turbines are still a relatively new field and this project is intended to contribute to increase the information about innovative solutions for the TLP-concept.

Learning the different computer program has also been challenging and time consuming, but hopefully beneficial as they are widely used in the commercial industry.

I would like to thank my supervisor, Professor Carl Martin Larsen for support, guidance and interesting conversation during the project period. I will also like to thank my fellow student Jan-Tore Haugan Horn for help with the computer programs in the SESAM package. Gratitude is also given to Dr. Erin Bachynskei for openly shearing her work and computer model.

Trondheim, June 10, 2015



Sindre J. Sønneland Moldenhagen

List of Symbols

kW	-	Kilowatt
MV	-	Mega Watt
GWh	-	Gigawatt hour
kN	-	Kilo Newton
kNm	-	Kilo newton Meter
TLP	-	Tension Leg Platform
TLB	-	Tension Leg Buoy
$NREL$	-	"National Renewable Energy Laboratory"
APA	-	"American Psychological Association"
u_x	-	Wind Speed dependent of height x
u_r	-	Reference wind speed
z_x	-	Height for of wind speed u_x
z_r	-	Reference height
α	-	Atmospheric Stability Coefficient
f	-	Frequency in Hz
$S(f)$	-	Hz Dependent Spectrum
$S(\omega)$	-	ω Dependent Spectrum
U_{10}	-	Mean wind speed 10m over the sea level
κ	-	Surface Drag Coefficient
T	-	Wave Period [s]
λ	-	Wave length [m]
ζ	-	Wave Height [m]
ζ_a	-	Wave Amplitude [m]

ω	-	Angular frequency [rad/s]
c	-	Wave celerity [m/s]
V	-	Velocity Vector
ρ	-	Fluid Density
E_n	-	Energy
θ	-	Wave direction
ϵ	-	phase
γ	-	Peakedness parameter
ω_p	-	Peak Frequency
H_s	-	Significant wave height [m]
T_p	-	Peak Period
M_y	-	Moment y-axis
M_z	-	Moment z-axis
N_x	-	Normal Force
I_y	-	Inertia y-axis
I_z	-	Inertia z-axis
A	-	Cross Section Area
σ	-	Stress
MPa	-	Mega Pascal
t	-	Plate thickness
C_p	-	Capacity factor
τ	-	Time step
m_n	-	n-th Degree Spectral Moment
RAO	-	Response Amplitude Operator
r_s	-	Radius of spoke [m]
l_s	-	Length of spoke [m]
l_h	-	Length of main hull/substructure [m]
z_s	-	Vertical position of spoke [m]

Abstract

The global focus on renewable energy has made it interesting to investigate floating offshore wind turbines further out offshore as the sites often has more stable wind conditions. There has already been installed multiple commercial offshore wind farms globally but they are mainly bottom fixed structures in shallow waters. In the recent years, research project such as the OC3-Hywind project and the WindFloat1 has been tested in full scale by commercial interested parties.

The purpose of this project has been to investigate the effect of position the spokes/arms for the tethers at the center of the substructure. This has been carried out by comparing two identical substructures with different mooring system.

The natural periods and damping were investigated by a simple decay test. The design criterion of having natural periods out side the most energetic wave period range was achieved for critical motions such as surge, heave and pitch. The damping in heave and pitch was dominated by linear damping as the motions and thus the relative velocities became small. The surge/sway and yaw motion was dominated be quadratic damping due to drag over the spokes/arms.

A limited response analysis was carried out for 5 conditions. The data sampled was not entirely comparable due to the difference in the length of the time domain simulation, but gave an indication of the response. Coupled effects occurred for both models although the natural period and the wave period was the dominant amplitudes in the spectra. The heave spectra indicates that the concept model may be subjected to greater coupling effects with roll and pitch than the reference model.

The forces in the tendon during the most severe sea state did not become negative which indicates that there were no slack conditions during the time period. However, the margin was relatively low and since the sea state was only representative for one wave seed. A more thorough study should be made to increase the statistical certainty of the no-slack condition.

Two cases of contact between substructure and tendon have been investigated. The first case was contact due to translation in the horizontal plane. This case of contact requires a very large horizontal force as the substructure will be considerably submerged thus creating a large vertical force. The induced vertical displacement for this case will be of such magnitude that this contact case can be regarded as inferior to other problems related to large vertical displacement.

Sammendrag

Den globale satsing på fornybar energi har gjort det interessant å undersøke flytende offshore vindturbiner lenger ut til havs der vindforholdene ofte er mer gunstige og stabile. Det har allerede blitt installert flere kommersielle offshore vindparker globalt sett, men de er i hovedsak bunnfaste strukturer i grunt farvann. I de senere år har forskningsprosjektet som OC3-Hywind-prosjektet og WindFloat1 blitt testet i fullskala av kommersielle organisasjoner.

Formålet med dette prosjektet har vært å undersøke effekten av å posisjonere eikene/armene for strekkstagene på midtre del av skroget. Dette har blitt utført ved å sammenligne to identiske skrog med forskjellig fortøyningsystem.

Egen-perioder og demping ble undersøkt ved en enkel "Decay-test". Designkriteriet er at egen periodene ligge utenfor de mest energirike bølgeperiodene. Dette ble oppnådd for de mest kritiske bevegelsene som jag, hiv og stamp. Dempingen i hiv og stamp er dominert av lineær demping på grunn av små bevegelser og dermed relativt små hastigheter. Dette på grunn av at kvadratisk demping er proporsjonal med hastigheten i andre. Jag, svai og giring er dominert av kvadratisk demping på grunn av drag over eikene/armene.

En begrenset responsanalyse ble utført for fem forskjellige forhold. Utvalget av dataene var ikke helt sammenlignbare på grunn av forskjellen i lengden av tidsdomenesimulering, men ga en indikasjon på responsen. Koblede effekter var synlige for begge modellene, selv om egenperioden og bølgeperioden var de dominerende amplitudene i spektrene. Hivspekteret indikerer at konseptmodellen kan bli utsatt for større koblingseffekter med rull og stamp enn referansemodellen.

Kreftene i strekkstagene under den største sjøtilstand ble ikke observert til å bli negativ, noe

som indikerer at det ikke var slakk tilstand i strekkstag i løpet av tidsperioden. Det skal sies at marginen var relativt lav for enkelte amplituder, og siden det kun er tatt data fra en sjøtilstaden, er ikke dette statistisk grundig nok. En grundigere undersøkelse bør gjøres for å øke den statistiske sikkerheten

To tilfeller av kontakt mellom understell og strekkstag har blitt undersøkt. Det første tilfellet var kontakt på grunn av translasjon i horisontalplanet. Dette tilfellet av kontakt krever en veldig stor horisontal kraft som medfører at skroget vil bli betydelig nedsenket og dermed skape en stor vertikal kraft. Den induserte vertikale forskyvning for dette tilfellet vil være av en slik størrelsesorden at dette kontakt tilfellet kan anses som underordnet andre problemer i forbindelse med stor vertikal forskyvning.

M.Sc. thesis 2015

for

SINDRE MOLDENHAGEN

DESIGN OF FLOATING WIND TURBINES

Renewable energy is considered to be the only sustainable way for future energy supply. Norway is blessed with topography and sufficient rainfall that makes it possible to produce electricity from hydropower at a very large scale. However, future growth in domestic and industrial energy demand and export will require unwanted encroachments on rivers and lakes. Alternative energy production is therefore encouraged. Wind energy is an obvious alternative, but wind turbines are not always wanted on land. Offshore wind turbines have therefore been proposed. For several reasons one would prefer to have such installations at some distance from the coast, but the water depth on the Norwegian continental shelf is too large for the use of bottom fixed turbines. It is therefore proposed to have floating units, and the design of cheap but reliable mooring systems for such structures will hence be crucial for the economy of this concept.

The purpose of the present project is to investigate the performance of tension leg anchor systems for floating wind turbines, and in particular study the dynamics of a floating wind turbine with tension leg anchors. The vertical position of tether attachment on the wind turbine column should in particular be investigated.

This project is a continuation of the pre-project during fall 2014. Part of the literature study may hence be taken from the pre-project.

The work may be carried out in steps as follows

1. Literature study that should concentrate on floating wind turbine technology, and methods for calculation of hydrodynamic loads and motions of floating wind turbines as needed for the design of the anchor system
2. Establish a model for dynamic analysis of a floating wind turbine with anchor system consisting of vertical tethers
3. Apply the model to study the influence from vertical position of tether attachments on system dynamics, and also how the response becomes influenced by the length of the horizontal beams with tether attachments.

The work may show to be more extensive than anticipated. Some topics may therefore be left out after discussion with the supervisor without any negative influence on the grading.

The candidate should in her/his report give a personal contribution to the solution of the problem formulated in this text. All assumptions and conclusions must be supported by mathematical models and/or references to physical effects in a logical manner.

The candidate should apply all available sources to find relevant literature and information on the actual problem.

The report should be well organised and give a clear presentation of the work and all conclusions. It is important that the text is well written and that tables and figures are used to support the verbal presentation. The report should be complete, but still as short as possible.

The final report must contain this text, an acknowledgement, summary, main body, conclusions and suggestions for further work, symbol list, references and appendices. All figures, tables and equations must be identified by numbers. References should be given by author name and year in the text, and presented alphabetically by name in the reference list. The report must be submitted in two copies unless otherwise has been agreed with the supervisor.

The supervisor may require that the candidate should give a written plan that describes the progress of the work after having received this text. The plan may contain a table of content for the report and also assumed use of computer resources.

From the report it should be possible to identify the work carried out by the candidate and what has been found in the available literature. It is important to give references to the original source for theories and experimental results.

The report must be signed by the candidate, include this text, appear as a paperback, and - if needed - have a separate enclosure (memory stick or DVD/ CD) with additional material.

Trondheim, February 2015

Carl M. Larsen

Deadline: 10. June 2015

Contents

1	Introduction	3
2	Literature Study	7
2.1	Existing concept for Floating Wind Turbines	7
2.1.1	WindFloat	8
2.1.2	Hywind	9
2.2	Annotated Bibliography	10
2.2.1	Shifting Towards Offshore Wind Energy	10
2.2.2	Experimental and Computational Comparison of the OC3-HyWind and Tension-Leg-Buoy Floating Wind Turbine conceptual design	11
2.2.3	Dynamic response in frequency and time domain of a floating founda- tion for offshore wind turbines	11
2.2.4	Effects of hydrodynamic modelling in fully coupled simulation of a semi-submersible wind turbine	12
2.2.5	Higher Order Loads from Steep Waves on Floating Wind Turbines	12
3	Theoretical Background	13
3.1	Environmental forces	13
3.2	Wind Forces	14
3.2.1	Steady Wind	14
3.2.2	Fluctuating and turbulent wind	14
3.3	Wave Forces	16
3.3.1	General Characteristics of Waves	16

3.3.2	Linear Wave Theory	17
3.3.3	Non-Linear Wave Theory	20
3.3.4	Modelling of Sea States	20
3.4	JONSWAP Spectrum	23
3.5	Rigid Body Motion	25
3.6	Hydrodynamic Coefficients	26
3.6.1	Added Mass estimation	26
3.6.2	Estimation of Stiffness - Mooring System	28
3.7	Natural Periods	29
3.8	Damping	30
3.9	Fast Fourier Transform	33
4	Description of TLP-Concept	35
4.1	Substructure	37
4.2	Mooring System	37
5	Computer Modelling	39
5.1	GeniE - Panel Model	39
5.2	HydroD - Hydrodynamic Calculations	41
5.3	SIMA - Time Domain Simulation	42
5.3.1	SIMO	42
5.3.2	RIFLEX	43
5.3.3	Modelling in SIMA	43
6	Hydrodynamic Results	45
6.1	Added Mass	45
6.2	Potential Damping	49
6.3	Excitation Forces	52
7	Decay Test and Damping	53
7.1	Surge and Sway	54
7.2	Heave, Pitch/Roll and Yaw	55

7.3	Summary and Concluding Remarks	57
8	Response Analysis	59
8.1	Surge Spectrum	61
8.2	Heave Spectrum	61
8.3	Pitch Spectrum	62
9	Slack Tethers and Contact with Substructure	63
9.1	Axial Force in Tendon	64
9.2	Tendon Contact with Substructure	65
10	Conclusion and Discussion	69
11	Recommendation for Future work	71
	References	73
	References	73
A	Reference Model	i
B	Decay Test	ix
C	Damping Calculations	xiii
D	Response Spectra	xxi
D.0.1	Case 1	xxi
D.0.2	Case 2	xxv
D.0.3	Case 3	xxx
D.0.4	Case 4	xxxv

List of Figures

1.1	Concept illustration	5
2.1	The WindFloat 1 in Northern Portugal	8
2.2	The HyWind Turbine at "Karmøy", Norway	9
3.1	Wind Profiles	15
3.2	Regular travelling wave properties, (Veritas, 2010)	16
4.1	Tethers and Substructure with spokes	36
4.2	Definition of axis and motions	36
5.1	Panel model with mesh in GeniE	40
5.2	Morison model in GeniE	40
5.3	Composite model in HydroD	42
5.4	SIMA model; 1) Pre-tension Force, 2) Spoke/Arm, 3) Substructure, 4) Tendon, 5) Anchor	44
6.1	Added mass; Force translation and moment rotation mode	47
6.2	Added mass; Force rotation and moment translation mode	48
6.3	Potential damping; Force translation and moment rotation mode	50
6.4	Potential damping; Force rotation and moment translation mode	51
6.5	Excitation forces and moments from HydroD (Postresp)	52
7.1	Time domain response: Surge	54
7.2	Time domain response: Sway	55

7.3	Time domain response: Heave	55
7.4	Time domain response: Pitch	56
7.5	Time domain response: Sway	56
7.6	Time domain response: Multiple peaks	57
8.1	Surge spectra for case 5	61
8.2	Heave spectra for case 5	62
8.3	Pitch spectra for case 5	62
9.1	Time domain: Axial force in tendon 1	64
9.2	Time domain: Moment about y-axis for the arm	65
9.3	Two extreme cases of contact	66
9.4	Deflection of beam (Ruina, 2012)	66
9.5	Time Domain: Heave and pitch response	67
A.1	Reference model in HydroD	ii
A.2	Added mass; Force translation and moment rotation mode	iii
A.3	Added mass; Force rotation and moment translation mode	iv
A.4	Potential damping; Force translation and moment rotation mode	v
A.5	Potential damping; Force rotation and moment translation mode	vi
A.6	Excitation forces and moments from HydroD (Postresp)	vii
B.1	Decay test: Surge	ix
B.2	Decay test: Heave	x
B.3	Decay test: Roll	x
B.4	Decay test: Pitch	xi
B.5	Decay test: Yaw	xi
D.1	Surge spectra for C1-1	xxi
D.2	heave spectra for C1-1	xxii
D.3	Pitch spectra for C1-1	xxii
D.4	Surge spectra for C1-2	xxii
D.5	heave spectra for C1-2	xxiii

D.6 Pitch spectra for C1-2	xxiii
D.7 Surge spectra for C1-3	xxiii
D.8 heave spectra for C1-3	xxiv
D.9 Pitch spectra for C1-3	xxiv
D.10 Surge spectra for C2-1	xxv
D.11 heave spectra for C2-1	xxv
D.12 Pitch spectra for C2-1	xxvi
D.13 Surge spectra for C2-2	xxvi
D.14 heave spectra for C2-2	xxvi
D.15 Pitch spectra for C2-2	xxvii
D.16 Surge spectra for C2-3	xxvii
D.17 heave spectra for C2-3	xxvii
D.18 Pitch spectra for C2-3	xxviii
D.19 Surge spectra for C2-4	xxviii
D.20 heave spectra for C2-4	xxviii
D.21 Pitch spectra for C2-4	xxix
D.22 Surge spectra for C3-1	xxx
D.23 heave spectra for C3-1	xxx
D.24 Pitch spectra for C3-1	xxxi
D.25 Surge spectra for C3-2	xxxi
D.26 heave spectra for C3-2	xxxi
D.27 Pitch spectra for C3-2	xxxii
D.28 Surge spectra for C3-3	xxxii
D.29 heave spectra for C3-3	xxxii
D.30 Pitch spectra for C3-3	xxxiii
D.31 Surge spectra for C3-4	xxxiii
D.32 heave spectra for C3-4	xxxiii
D.33 Pitch spectra for C3-4	xxxiv
D.34 Surge spectra for C4-1	xxxv
D.35 heave spectra for C4-1	xxxv

D.36 Pitch spectra for C4-1	xxxvi
D.37 Surge spectra for C4-2	xxxvi
D.38 heave spectra for C4-2	xxxvi
D.39 Pitch spectra for C4-2	xxxvii
D.40 Surge spectra for C4-3	xxxvii
D.41 heave spectra for C4-3	xxxvii
D.42 Pitch spectra for C4-3	xxxviii

List of Tables

- 4.1 Substructure 37
- 4.2 Mooring system 37

- 7.1 Decay test parameters 54
- 7.2 Natural periods for the concept model and reference model 57

- 8.1 Conditions for response analysis 60

Chapter 1

Introduction

Seabed anchored structures dominates the commercial offshore wind energy business today. There are numerous sites in Europe where offshore wind is a recognizable contributor to the overall power consumption. Examples are Denmark with the “Horns Rev” offshore wind farm with a total installed power of 165.2MW. This farm was commissioned in 2002 based on the pilot project at “Middlegrunden“ in Denmark. Another example is the ”Walney“ wind farm in United Kingdom, which with its 367MW installed power is the largest offshore wind farm to day (Kaldellis & Kapsali, 2013). A common denominator for these farms and projects is that the water depths are relatively shallow. Piled structures are, because of water depth, the preferred solution regarding cost.

When the water depth increases, a piled structure or a bottom based platform becomes expensive. It is in this segment that a floating base platform could be able to compete in price. The requirements is that construction, installation and maintenance cost must be competitive with other source of power.

Today there exist two full-scale offshore wind turbines in operation. The HyWind concept is based on a spar-type platform (Myhr, Maus, & Nygaard, 2011). This is a project from Statoil ASA, commissioned in 2009, and is still in operation outside ”Karmøy” in Norway. The other concept is the WindFloat 1 outside the coast of northern Portugal (Roddier, Cermelli, Aubault, & Weinstein, 2010). The base for the turbine is a 3-column semi-submersible.

Problem Formulation

The main work has been to design a concept TLP-model with the fastening arms for the tethers placed closer to the center part of the hull as illustrated in figure 1.1.

The work has is divided into three main parts. A literature survey where the goal is to map and identify similar projects and papers published in this field. The literature survey has been done as part of the preparation project, prior to the thesis. In addition, the literature study contains relevant theory used in the work. The second part consist of the design of a concept model and a reference model. This work is done using GeniE for the design part and HydroD for the calculation of the hydrodynamic properties.

The last part of the work is a time domain analysis of the two models. For calculations of motions response and forces, the SIMO/RIFLEX software SIMA developed by MARINTEK and Statoil has been used. The result and conclusion of this thesis should lead to increased knowledge of the behaviour of the concept model in comparison with the concept model.

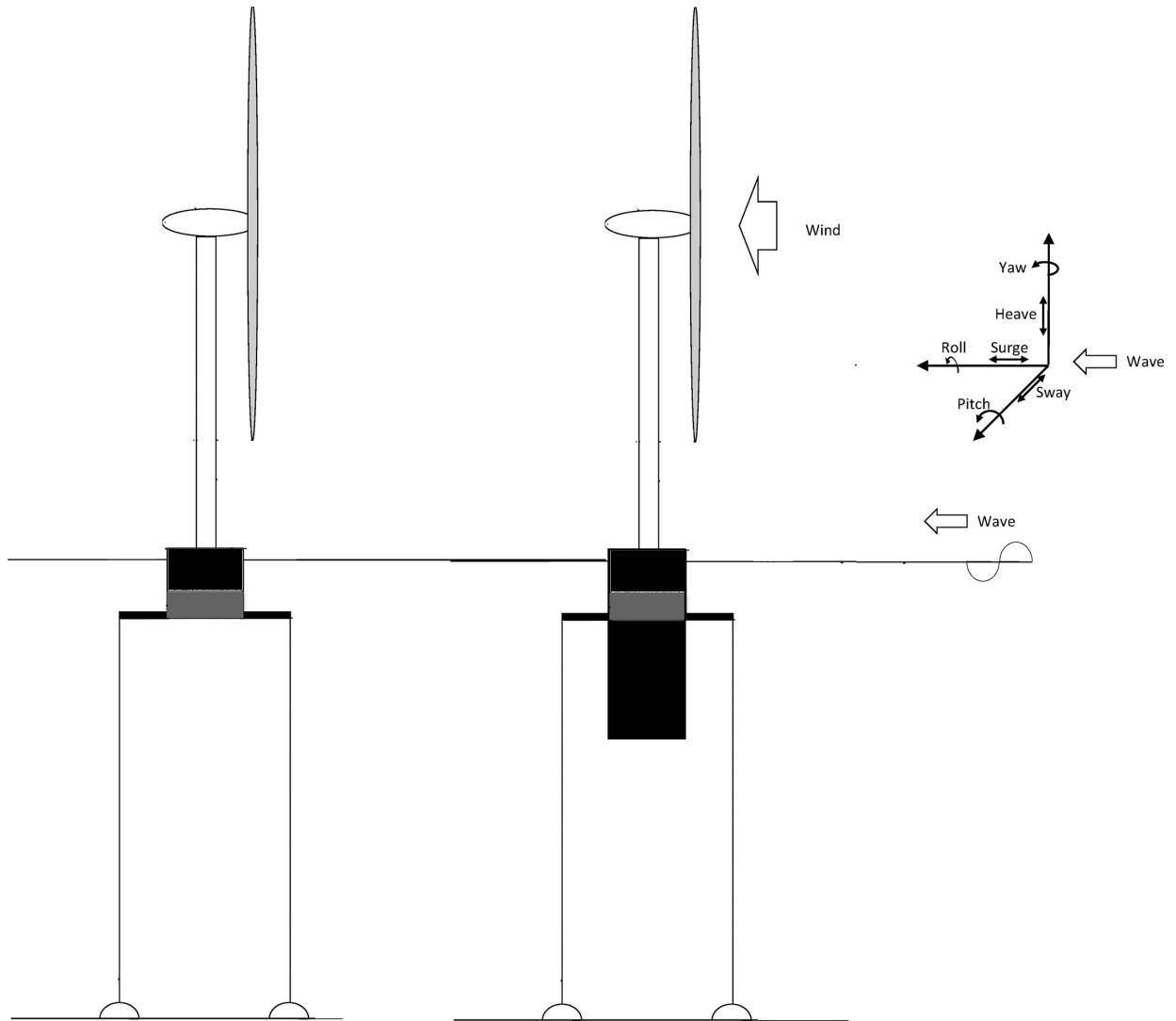


Figure 1.1: Concept illustration

Chapter 2

Literature Study

A literature search into the topic of Offshore FWTs is a major part of the project. This chapter will cover important aspects of work done in this field and later form the basis for citations and sources in the master thesis. Some of the related work presented will cover floating concepts than other TLPs.

2.1 Existing concept for Floating Wind Turbines

Various concepts for a floating wind turbine exists in the literature and computer models are the most common. However, a limited number of floating platforms exists in model scale and are tested. Data from these experiments are hard to retrieve as they are research material and often protected. There are only 2 floating offshore wind turbines built in full scale and in operational condition.

2.1.1 WindFloat

The WindFloat technology is based on a three column semi-submersible platform (Roddiier et al., 2010), shown in figure 2.1. Each column are fitted with entrapment plates that acts as heave skirts. This increases the added mass and shifts the natural period of the semi-submersible away from the wave energy. The heave skirts also increases the viscous damping in roll, pitch and heave.

The mooring system is a asymmetrical catenary mooring system with 6 mooring lines. The asymmetry means that by statistical data, the mooring system has been designed with directional purpose with regard to waves and wind.

The wind turbine tower is placed on one of the columns and ballast tanks are used for the stability. The outer hull of the columns are divided into horizontal parts where the lower sections have thicker hull plating. This ensures that the parts with the highest static water pressure has sufficient strength and that the structure requires less steel.

The main advantage of this design is the assembly and installation of the wind turbine offshore. Everything can be done in a dry dock because of the low draught and the design gives very good stability in towing condition. The downside is the cost of steel.

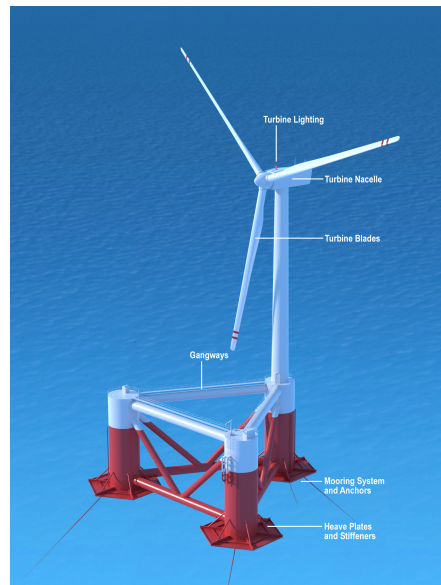


Figure 2.1: The WindFloat 1 in Northern Portugal

2.1.2 Hywind

The Hywind concept was developed by "Norsk Hydro" and later absorbed into Statoil when the two companies merged (Vera Ingunn, 2010). Several platform designs were considered but the ultra stable spar concept was favoured. The concept is designed for deep waters between 120 - 700m. The floating section has a depth of 100m and is moored with 3 mooring lines, see figure 2.2. Above the surface, only the turbine itself is visual. For the pilot project, a 2.3MW turbine from Simens was used but the concept is aimed at accommodating larger turbines of 5MW or more. Statoil reckons that the concept is ready for commercial use within a time frame of 12-15 years.

The Construction of this type of offshore wind turbine is somewhat more complicated than for the WindFloat 1. Assembly of tower and platform as well as the turbine it self can be done in calm waters inshore. However, because of the large draught, the choice of assembly site is less flexible. The ideal location for this would be in a deep fjord, which there is an abundance of in Norway.



Figure 2.2: The HyWind Turbine at "Karmøy", Norway

2.2 Annotated Bibliography

There exists a number of different solution for a floating platform for this purpose, all with different advantages and drawbacks. I have done a research into "TLP/Spar"-platform as this can reduce the stresses in the tendons/mooring lines and thus reduce the production cost related to this system.

The literature reviewed in this project are obtained by various means. Some articles and papers are picked from websites such as sciencedirect.com and scholar.google. Other has been recommended by my supervisor and some are picked from courses I have attended on the same topic. The basis for selection has been from the hydrodynamic perspective and with regard to motions and forces acting on the structure as well as articles that reasons for the use of offshore wind turbines.

2.2.1 Shifting Towards Offshore Wind Energy

The review article by (Kaldellis & Kapsali, 2013) gives a good overview of offshore wind activity today and future expectations. Wind power has mainly been built on land, but lately many countries has invested in offshore wind farms. Recent technological progress has made it possible to narrow the gap between land based wind turbines and offshore wind turbines in the near future.

The article makes good use of well explained graphs and plots. However, some of the pictures that are included in the graphs may seem a bit unnecessary and makes the composition a bit messy. Especially since some of the pictures are very small photos.

The focus is on shallow water wind turbines and seen from an economical perspective. Some comments are given on the floating concepts in existence but only from an economical and historical perspective. The article contain very little technical description, is therefore for technical purpose more orientation material, and could be used for motivational reference.

2.2.2 Experimental and Computational Comparison of the OC3-HyWind and Tension-Leg-Buoy Floating Wind Turbine conceptual design

The Hywind from Statoil (inherited from the merge with Norsk Hydro) is based on a Spar-structure, which gives good stability and small motions. The conference proceeding by (Myhr et al., 2011) gives a comparison between the Hywind-Spar and two different TLB's. The comparison is done both by computation and by experiment in marine cybernetics lab at MTS, Trondheim. The results are oriented around the eigen frequency of the different models.

The article is a bit short and thus thorough explanation of acronyms and expression is a bit thin. The tables are clean and well explained thus the data is easy to understand. The figures presented gives a good view of the model and the physical boundary conditions associated.

The proceeding contains many important aspects that are similar to my work and is a good reference in future work. The Tension-Leg-Buoy is similar in design of a TLP. The difference is just a matter of design.

2.2.3 Dynamic response in frequency and time domain of a floating foundation for offshore wind turbines

For the calculations of response, one often use frequency domain or time domain analysis. The article written by (Zhang, Tang, Hu, Ruan, & Chen, 2013) presents a fully coupled model with wave and wind loads and the article presents motion equations both for time and frequency domain.

The geometry of the platform is well explained and the physical properties presented in a clear way. There are many equations presented that may be a bit incomprehensible depending on the readers background. However, the parameters and variables are fairly well explained.

The article describes much of the same software and codes that I use in my thesis as well as the general equation used. The articles gives good references that I may use in my work.

2.2.4 Effects of hydrodynamic modelling in fully coupled simulation of a semi-submersible wind turbine

The article by (Kvittem, Bachynski, & Moan, 2012) goes into details on the hydrodynamics behind SIMO/RIFLEX. The program is also coupled with Aerodyn from NREL to simulate turbulent wind fields. Together, these programs can make very competent simulations on wind and wave induced response. Morrison equation and potential flow theory are methods for calculations of forces acting on a structure in waves. For short waves, diffraction forces becomes important and the article discuss solutions to this problem. The article also discuss the result of power production when using either Potential flow theory or Morrison's equation.

The article has many equations that may seem a bit under explained depending on your standpoint, but good references are given. However, the references are given in the numbered format. APA style may be better if the reader knows the field of the topic.

The article describes much of the same software and codes that I use in my thesis as well as the general equation used.

2.2.5 Higher Order Loads from Steep Waves on Floating Wind Turbines

Higher order wave loads has been of interest when investigating the "slamming and ringing" response of slender structure. A master student (Bekkeheien, 2013) recent graduated from the department of marine technology presented a master thesis about this topic. The thesis is written with the Hywind in mind. The thesis contains both a literature study and a response analysis compared with measured data. The thesis shows that the fear for higher order loads has been somewhat exaggerated and that there is no sign of slamming effects in the measured data. Although higher order forces are not a big issue in the design of the Hywind, a TLP is a much stiffer system with lower natural periods in some of the degrees of freedom. This means that this phenomena should be considered and much of the theory need is presented in this thesis.

Chapter 3

Theoretical Background

The motions of a TLP is well defined in the horizontal plane as for other floating structures. Surge, sway and yaw motions tend to occur at the wave frequency and lower. The vertical motions of a TLP is more complex because of the large stiffness from the tendons. Floating structures with natural frequencies in the order of 1-5 seconds may also be subjected to other types of resonant forces such as steady-state "springing" and transient "ringing". These are motions due to resonance oscillations in heave, pitch and and roll of the platform.

3.1 Environmental forces

The environmental forces that affects the TLP is much the same as for other floating structures. In addition, the wind forces acting on the rotor blades will be an significant contributor to the wind forces. The forces consists of:

Wind forces

- Steady wind
- Fluctuating and turbulent wind

Wave forces

- Linear waves

- Non-linear waves

Current forces

- Current Drag forces
- Coexisting Wave and Current Drag Forces

3.2 Wind Forces

The wind forces acting on a Wind turbine is the source power but is also a great contributor to the forces acting on the structure. It is mainly the thrust on the rotor blades that will set up a moment around the base of the tower. Turbulent fields that hits the rotor blades at different instance of time is also an effect that may cause instabilities an induced motions.

3.2.1 Steady Wind

Steady wind condition is a simple theoretical approach to a wind condition. I reality, turbulence of varied degree will occur in the wind field. For simulation purposes, steady wind is used to analyse the performance of the wind turbine. The control system of a pitch controlled wind turbine can be optimized with regard to more stable torque and power production.

3.2.2 Fluctuating and turbulent wind

One of the strongest arguments for moving the wind turbines offshore is the access to more stable wind conditions. That is, wind with less turbulence and more stable velocity. Terrain and obstacles such as trees, buildings and other indentations in the landscape contributes to slow the wind down at lower altitudes. This results in a wind profile that may cause reduced wind velocities in the wind field that the wind turbine sees. This is best illustrated by figure 3.1. The disturbance in the wind field is greatly affected by the terrain. The reduction in wind speed is not only affecting the lower parts.

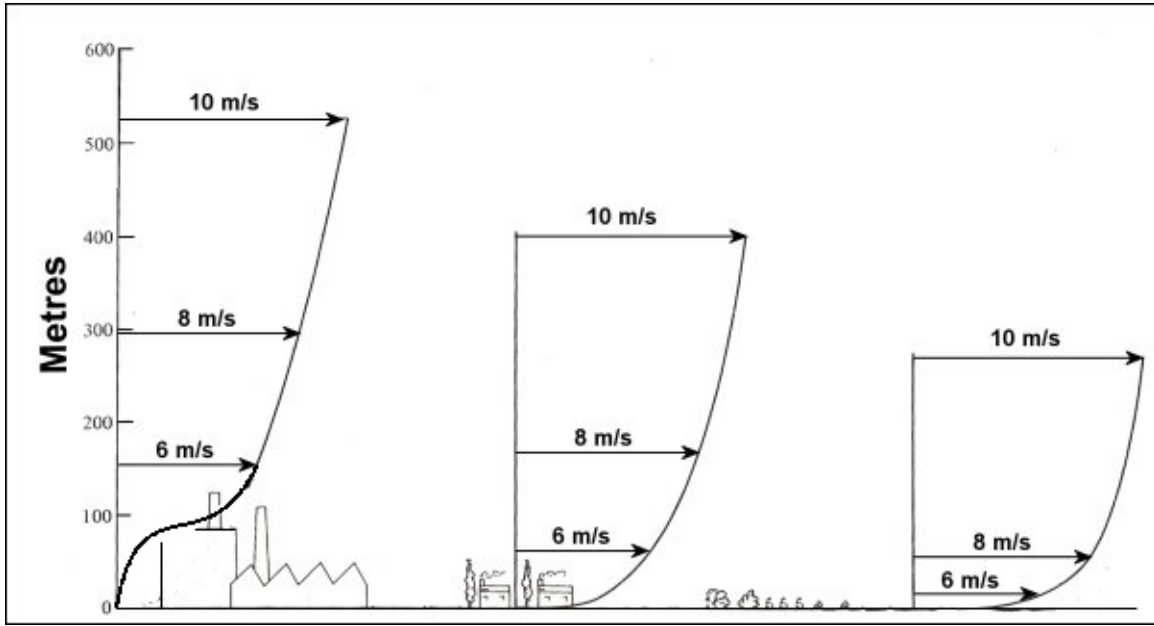


Figure 3.1: Wind Profiles

The wind profile is often described as the vertical distribution of horizontal mean wind speeds within the lowest portion of the boundary layer, which can be the terrain or the ocean surface. A common way to describe the profile is the wind profile power law presented in equation (3.1) (Elliot, Holladay, Barchet, Foote, & Sandusky, 1986).

$$u_x = u_r \left(\frac{z_x}{z_r} \right)^\alpha \quad (3.1)$$

Here u_x is the wind speed at the height z_x . u_r is the wind speed at the reference height z_r . α is an empirical derived coefficient dependent on the atmospheric stability. Like for wave states, there exists different spectrum that may be used to describe a wind state. Harris wind spectrum may be used and is explained in (Faltinsen, 1993). The spectrum is formulated in equation (3.2).

$$\frac{f \cdot S(f)}{U_{10}^2} = \frac{4\kappa \tilde{f}}{(2 + \tilde{f}^2)^{\frac{5}{6}}} \quad (3.2)$$

Here U_{10} is the one hour mean speed at 10m above sea level. f is the frequency in Hz and $\tilde{f} = \frac{Lf}{U_{10}}$. L is the scale length and κ is the the surface drag coefficient.

3.3 Wave Forces

Waves can be as periodic elevation of the water surface. In reality the surface elevation is random and chaotic in nature thus a real sea state is best described by a random wave model. The two most common way to describe a sea state is a linear and a non-linear model. A linear random wave model is a sum of many small linear wave components with different amplitude, frequency and direction. The phases are random with respect to each other. The non-linear random wave model allows for sum- and difference frequency wave component caused by non-linear interaction between the individual wave components (Veritas, 2010).

3.3.1 General Characteristics of Waves

The simplest component in a sea state is a regular wave propagating with constant wave period (T), wave length (λ) and wave height (ζ). Other important parameters are the wave angular frequency $\omega = \frac{2\pi}{T}$, the phase velocity or wave celerity $c = \frac{\lambda}{T}$ and the wave number $k = \frac{2\pi}{\lambda}$. The wave parameters are illustrated in figure 3.2. The period is defined as the time it takes for a crest to crest passing at on fixed point in space. The wave length is the the distance from crest to crest and the the wave height is the distance from the trough to the crest (marked as H in the figure 3.2). The z -coordinate is defined as zero at the mean of the free surface.

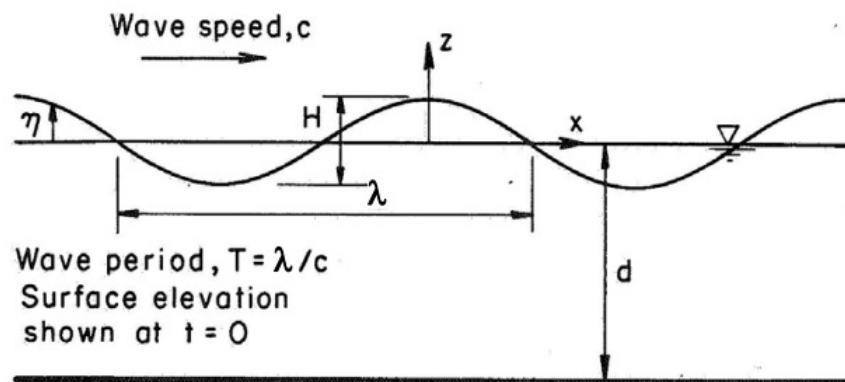


Figure 3.2: Regular travelling wave properties, (Veritas, 2010)

3.3.2 Linear Wave Theory

Linear wave theory can be applied when the wave height is much smaller than the wave length and the water depth. the criteria for deep water is usually defined as $d \geq \frac{\lambda}{2}$, where d is the depth. Waves at finite depth can be modelled in a similar manner, but the expressions will contain hyperbolic functions. According to (Faltinsen, 1993) The wave profile for a two-dimensional regular sinusoidal surface wave travelling in deep waters can be given equation (3.3)

$$\zeta(x, t) = \zeta_a \sin(\omega t - kx) \quad (3.3)$$

The fluid particle velocity and acceleration in the horizontal plane can be found by derivation of the velocity potential with respect to direction x or y and time t respectively. The velocity potential is given by equation (3.4)

$$\phi = \frac{g\zeta_a}{\omega} e^{kz} \cos(\omega t - kx) \quad (3.4)$$

The Dynamic free-surface condition states that the water pressure on the surface equals the atmospheric pressure P_0 . This can be derived from Bernoulli's equation and by ensuring that the constant relation between static, dynamic and atmospheric pressure equals $\frac{P_0}{\rho}$ the dynamic free surface condition can be expressed as equation (3.5):

$$\rho g + \frac{\partial \phi}{\partial x} + \frac{1}{2} \left(\left(\frac{\partial \phi}{\partial x} \right)^2 + \left(\frac{\partial \phi}{\partial y} \right)^2 + \left(\frac{\partial \phi}{\partial z} \right)^2 \right) = 0 \quad (3.5)$$

On $z = \zeta(x, y, z)$. This equation is not linear. We do not know where the free surface is before the problem is solved. However, the free-surface condition can be linearised by assuming that the structure has no forward speed and that there is no current. Furthermore it is assumed that the wave amplitude is small relative to a characteristic wave length and body dimension.

The kinematic boundary condition states that no fluid is to pass through the solid body. This means that $\frac{\partial \phi}{\partial n} = 0$ on the body surface. Here $\frac{\partial}{\partial n}$ denotes differentiation along the the normal of the body surface. The positive normal direction is defined into the fluid from the body. For a body that moves in the fluid with velocity U , which can be both translatory or

rotary, the generalized equation can be written as equation (3.6)

$$\frac{\partial \phi}{\partial n} = U \cdot n \quad (3.6)$$

The free-surface can be defined as $z = \zeta(x, y, t)$. The substabtial derivative $\frac{DF}{Dt}$ of a function $F(x, y, z, t)$ can be described as the rate of change with time of the function F if we follow a fluid particle in space. This can be expressed by equation (3.7)

$$\frac{DF}{Dt} = \frac{\partial F}{\partial t} + \mathbf{V} \cdot \nabla F \quad (3.7)$$

We then define the function presented as equation (3.8)

$$F(x, y, z, t) = z - \zeta(x, y, t) \quad (3.8)$$

We assume that a fluid particle on the free-surface will stay on the free-surface. This means that equation (3.8) will always be satisfied and that $\frac{DF}{Dt} = 0$. The kinematic boundary condition can then be expressed as

$$\frac{\partial}{\partial t}(z - \zeta(x, y, t)) + \nabla \phi \cdot \nabla(z - \zeta(x, y, t)) = 0 \quad (3.9)$$

or

$$\frac{\partial \zeta}{\partial t} + \frac{\partial \phi}{\partial x} \frac{\partial \zeta}{\partial x} + \frac{\partial \phi}{\partial y} \frac{\partial \zeta}{\partial y} - \frac{\partial \phi}{\partial z} = 0 \quad \text{on} \quad z = \zeta(x, y, t) \quad (3.10)$$

Here the fluid velocity can be describe from the velocity potential presented in equation (3.4) in the follwing way:

$$V = \nabla V = \mathbf{i} \frac{\partial \phi}{\partial x} + \mathbf{j} \frac{\partial \phi}{\partial y} + \mathbf{k} \frac{\partial \phi}{\partial z} \quad (3.11)$$

By a Taylor expansion we can transfer the free-surface condition from the free-surface position $z = \zeta(x, y, t)$ to the mean free-surface at $z = 0$. By keeping the linear terms in the wave amplitude from equation (3.5) and equation (3.10), we can express the dynamic and kinematic boundary conditions as:

$$\frac{\partial \zeta}{\partial t} = \frac{\partial \phi}{\partial z} \quad \text{on} \quad z = 0 \quad (\text{Dynamic condition}) \quad (3.12)$$

$$\rho g + \frac{\partial \phi}{\partial t} = 0 \quad \text{on} \quad z = 0 \quad (\text{Kinematic condition}) \quad (3.13)$$

These are basic assumption and simplification when calculation loads with linear waves. In many cases such as a body floating in swells, these assumption is good and may produce reliable results. However, in some cases as in ringing and slamming loads these assumptions are not good enough as the waves will behave much different than what is described here.

3.3.3 Non-Linear Wave Theory

Non-linear wave theory is applied when the need for modelling steep waves is present. A steep wave has a steeper crest and wider trough than a linear wave. This can be modelled with an expansion of the surface elevation in powers of the linear wave height H . Stokes Fifth order wave theory, described by (Fenton, 1985) can be applied.

First order Stokes waves are identical to linear waves. In Stokes fifth order wave theory, the wave steepness is used as an expansion parameters. The result is obtained by solution of the steady wave equation as a number of power series expansion, truncated after the fifth order (Bekkeheien, 2013).

This is particularly useful when investigating slamming loads on a structure. This will not be big topic in my work and thus not be further described in this report.

3.3.4 Modelling of Sea States

For those of us who have seen the ocean on a stormy day knows that the waves does not behave as simply as described by equation (3.3). The sea surface is far more chaotic and random. A common theory applied is based on the stochastic process described by (Myrhaug, 2007).

A real sea state can be modelled as the sum of sinusoidal wave components. A simple random wave model in the linear long-crested wave model given by equation (3.14)

$$\zeta(x, t) = \sum_{n=1}^N \zeta_{A_n} \cos(\omega_n t - k_n x + \epsilon_n) \quad (3.14)$$

The parameters are described in 3.3.2. If the wave is observed in a fixed point in space, the $k_n x$ term can be neglected and the expressions becomes a function of only time t . The ϵ_n term is the stochastic variable which is statistically independent, identical and rectangularly distributed between 0 and 2π . It is assumed that the process is stationary, ergodic and that wave elevation is normal distributed with zero mean.

The total energy for a sea state is the sum of N linear wave components and can be written as:

$$\frac{E_n}{\rho g} = \sum_{n=1}^N \frac{1}{2} \zeta_{An}^2(\omega_n) \quad (3.15)$$

A wave spectrum, denoted $S(\omega)$, is a common way to describe a sea state. The spectrum contain all necessary statistical characteristic of $\zeta(t)$. The spectrum also contain all the energy of the sea state at given frequencies. For a small time interval $\Delta\omega$ this can be expressed equation (3.16)

$$\frac{1}{2} \zeta_a^2 = S(\omega_n) \Delta\omega \quad (3.16)$$

With the assumption that the wave elevation $\zeta(t)$ is normal distributed and has zero mean, the variance σ^2 can be expressed as equation (3.17) when $N \rightarrow \infty$ and $\Delta\omega \rightarrow 0$

$$\sigma^2 = \int_0^\infty S(\omega) d\omega \quad (3.17)$$

The free surface elevation can now be expressed by the spectrum as:

$$\zeta(t) = \sum_{n=1}^N \sqrt{2S(\omega_n) \Delta\omega} \cos(\omega_n t + \epsilon_n) \quad (3.18)$$

Up to now, the waves has been considered to be long crested. In reality they are likely to appear as short crested. This can be taken into account by introducing an additional dimension y . The angle between x-axis and the propagation direction is θ and the wave number k has to be decomposed with respect to the direction of propagation. By a similar approach discussed above, the wave elevation can be described be the directional spectrum $S(\omega, \theta)$. This is shown in equation (3.19). For further details, see section 1 in (Myrhaug, 2007)

$$\zeta(x, y, t) = \sum_{i=1}^I \sum_{j=1}^J = \sqrt{2S(\omega_i \theta_j) \Delta\omega \Delta\theta} \cos(\omega_i t - k_i x \cos(\theta_j) - k_i y \sin(\theta_j) + \epsilon_{ij}) \quad (3.19)$$

3.4 JONSWAP Spectrum

There exists many different spectrum in the literature. The JONSWAP spectrum is commonly used in the North Sea and will be the focus. This spectrum is the result of a multinational measurement project in the south part of the North sea. It was observed that the spectrum for this are had a very sharp peak. It is based on the spectrum of Pierson-Moskowitz type which has the form presented in equation (3.20).

$$S(\omega) = \frac{A}{\omega^5} \exp\left(-\frac{B}{\omega^4}\right) \quad (3.20)$$

The JONSWAP spectrum uses top frequency ω_p instead of the wind velocity. Here, $A = \alpha g^2$ and $B = \frac{5}{4}\omega_p^4$. Inserted in equation (3.20), the result becomes equation (3.21)

$$S(\omega) = \alpha \frac{g^2}{\omega^5} \exp\left[-\frac{5}{4}\left(\frac{\omega_p}{\omega}\right)^4\right] \quad (3.21)$$

The peak is further amplified by multiplication with the peakedness parameter given by equation (3.22)

$$\gamma \exp\left[-\frac{1}{2}\left(\frac{\omega - \omega_p}{\sigma \omega}\right)^2\right] \quad (3.22)$$

$$\sigma = \begin{cases} \sigma_a & \text{for } \omega \leq \omega_p; \\ \sigma_b & \text{for } \omega > \omega_p. \end{cases}$$

γ usually has a value between 1 and 7. If $\gamma = 1$, the spectrum becomes the PM spectrum. It should also be noted that the JONSWAP spectrum can be transformed into Hz frequency. Since the energy in the spectrum should be the same regardless of what frequency is used, the following relation is valid.

$$\int_0^\infty S(f)df = \int_0^\infty S(\omega)d\omega = \int_0^\infty S(\omega)2\pi d\omega \quad (3.23)$$

If the spectrum is known with its 3 parameters α , γ and σ , several important parameters can be derived from the spectral moments given by the general equation presented as equation (3.24). For more details, see (Myrhaug, 2007) or (Faltinsen, 1993)

$$m_n = \int_0^{\infty} \omega^n S(\omega) d\omega \quad (3.24)$$

3.5 Rigid Body Motion

The rigid body motion for a steady-state sinusoidal motion can be described by equation (3.25) according to (Faltinsen, 1993).

$$\sum_{k=1}^6 [(M_{ik} + A_{kj})\ddot{\eta}_k + B_{kj}\dot{\eta}_k + C_{kj}\eta_k] = F_j e^{-i\omega_0 t}, \quad (j = 1, 2, 3, 4, 5, 6) \quad (3.25)$$

Here, M_{jk} is the respective component of the mass matrix for the structure. It contains the structural mass and mass-moment of inertia, A_{jk} is the respective component of the added mass matrix, B_{jk} is the respective component of the damping matrix and C_{jk} is the respective component of the restoring matrix.

The restoring matrix can be divided into a hydrostatic part and a mooring part. The total restoring matrix is given as the sum of these two parts. The restoring effects due to the hydrostatic effects are small compared with the restoring from the TLP mooring system. F_j is the complex amplitude of the exciting force or moment. The force and moment components are given by the real part of $F_j e^{-i\omega_0 t}$

3.6 Hydrodynamic Coefficients

The hydrodynamic coefficients used in the calculation of the rigid body motions are computed in HydroD. An estimation of these coefficient is important for a verification point of view. This section will give a brief over view of such estimations.

3.6.1 Added Mass estimation

According to (Newman, 1977) chapter 4, 2-D added mass coefficients can be applied for each component if interaction effects are neglected. A cylinder with diameter D has a transverse added mass per unit length (A_t) given by equation (3.26).

$$A_t[D] = \rho\pi D^2/4 \quad (3.26)$$

Similarly, for a square section with side lengths has h , the transverse added mass per unit length can be expressed by equation (3.27)

$$A_t[h] = 4.754\rho\left(\frac{h}{2}\right)^2 \quad (3.27)$$

In surge, the added mass will be a summation of contribution from the cylindrical hull and the spokes/arms. This can be expressed for all direction in the XY plane by introducing an angle θ about the z-axis. The summation is presented in equation (3.28) where the first term is the contribution form the cylindrical hull and second term is the contribution from the spoke/arms depending on whether the cross section is square or cylindrical.

$$A_{11} \approx A_t[D](l_h) + \sum_{i=1}^3 l_s A_t[d_s \text{ or } h_s] \cos^2 \theta_i \quad (3.28)$$

The heave added mass includes contribution from the cylindrical hull and the spokes/arms. The cylindrical hull has approximately the same added mass as an sphere with diameter D and this is equal to the displaced mass of half the sphere. The contribution from the

spokes/arms can be found by applying equation (3.26) and equation (3.27) depending on the cross section properties. This can be expressed as equation (3.29)

$$A_{33} \approx \rho\pi \frac{1}{12} D_h^3 + \sum_{i=1}^3 l_s A_t [d_s \text{ or } h_s] \quad (3.29)$$

The added mass in pitch and coupled surge and pitch can be calculated by integration the sectional added mass. For more information see (Bachynski, 2014) chapter 4.

3.6.2 Estimation of Stiffness - Mooring System

The stiffness of the mooring line system can be estimated assuming that the tethers remains straight for small motions. From (Faltinsen, 1993) and (Bachynski, 2014) The stiffness of the mooring system can be expressed as follows:

$$k_{11} = \frac{F_t}{l_0}, \quad k_{33} = \frac{E_t A_t}{l_0} \quad (3.30)$$

$$K_{11} \approx \sum_{i=1}^3 k_{11} \quad (3.31)$$

$$K_{33} \approx \sum_{i=1}^3 k_{33} \quad (3.32)$$

$$K_{51} = K_{15} \approx \sum_{i=1}^3 k_{11} z_s \quad (3.33)$$

$$K_{55} \approx \sum_{i=1}^3 [k_{11} z_s^2 + k_{33} r_s^2] \cos^2 \theta \quad (3.34)$$

$$K_{66} \approx \sum_{i=1}^3 k_{11} r_s^2 \quad (3.35)$$

3.7 Natural Periods

To avoid first-order wave excitation, the natural period in Surge and sway should be longer than 25 s. The decoupled undamped natural period in surge T_{n1} can be expressed as in equation (3.36).

$$T_{n1} = 2\pi \sqrt{\frac{M_{11} + A_{11}}{K_{11}}} \quad (3.36)$$

The roll, pitch and heave natural period should be shorter than 3.5 s to avoid first-order excitation. The natural period in heave can be estimated using both hydrostatic and mooring stiffness in the term K_{33} (equation (3.37)).

$$T_{n3} = 2\pi \sqrt{\frac{M_{33} + A_{33}}{C_{33} + K_{33}}} \quad (3.37)$$

3.8 Damping

The damping of a floating body such as a TLP, can be divided into linear and quadratic damping. The linear damping is mainly related to the body's ability to create waves, i.e. radiation damping and structural damping. The quadratic (non-linear) damping is mainly related to Morison drag forces, i.e. viscous damping and is proportional with the velocity squared. For higher velocities, this is the dominant contribution to the damping. The following deduction of damping is from lecture notes in Marin Operation and cited by (Lygren, 2011)

The damping force can be expressed as in equation (3.38) where B_1 is the linear damping coefficient and B_2 is the quadratic damping coefficient. \dot{x} is the velocity, either translatory or angular. The damped motion of a system, in the degree of freedom considered, can be described by equation (3.39), where M is the sum of the structural and added mass.

$$F_{damp} = B_1\dot{x} + B_2\dot{x}|\dot{x}| \quad (3.38)$$

$$M\ddot{x} + F_{damp} + kx = 0 \quad (3.39)$$

By dividing the equation (3.39) and inserting for F_{damp} , equation (3.40) is obtained. Here b_1 and b_2 are the damping coefficients divided by the mass.

$$\ddot{x} + b_1\dot{x} + b_2\dot{x}|\dot{x}| + \frac{k}{M}x \quad (3.40)$$

This expression can be linearised by demanding that the energy dissipated per cycle in the linear model must equal the energy dissipated per cycle by the damping force in equation (3.38).

$$\int_0^{T_n} (b_1 \dot{x} + b_2 \dot{x} |\dot{x}|) dx = \int_0^{T_n} b_e \dot{x} dx \quad (3.41)$$

Performing the integration and solving for b_e gives equation (3.42)

$$b_e = b_1 + \frac{16x_n}{3T_n} b_2 \quad (3.42)$$

Here, x_n and T_n is the motion amplitude and period of the cycle respectively.

Logarithmic decrement is a common method to calculate the damping from a decaying signal. This method can also be used for a time series obtained from a decay test. The solution of a free oscillating system can be written as equation (3.43)

$$u(t) = e^{-\lambda \omega_o t} (A \sin(\omega_d t) + B \cos(\omega_d t)) \quad (3.43)$$

Here, λ is the damping ratio which is the ratio between actual, and critical damping. ω_o is the undamped natural frequency and ω_d is the damped natural frequency (equation (3.45)). The damping ratio λ has the following relations given in equation (3.44).

$$\lambda = \frac{B}{B_c} = \frac{B}{2M\omega_o} \quad (3.44)$$

$$\omega_d = \omega_o \sqrt{1 - \lambda^2} \quad (3.45)$$

The logarithmic decrement δ , is defined as the natural logarithm of the ratio between two successive peaks. The relation to the damping ratio can be expressed as equation (3.46)

$$\delta = \ln \frac{x_t}{x_{t+T_d}} = \ln \frac{e^{-\lambda\omega_0 t}}{e^{-\lambda\omega_0(t+T_d)}} = \lambda\omega_0 T_d = \lambda 2\pi \frac{\omega_0}{\omega_d} \quad (3.46)$$

T_d is the damped natural period. By inserting equation (3.45) into equation (3.46), the logarithmic decrement can be expressed as equation (3.47). Thus, the damping ratio can then be expressed as equation (3.48). For light damped systems, a reasonable assumption is that $\omega_o \approx \omega_n$. This will be used in the damping calculations.

$$\delta = 2\pi \frac{\lambda}{\sqrt{1 - \lambda^2}} \quad (3.47)$$

$$\lambda = \frac{\delta}{\sqrt{4\pi^2 + \delta^2}} \quad (3.48)$$

The linear damping coefficient defined in equation (3.42) can now be defined as equation (3.49) by inserting equation (3.48), solving for B_e and dividing on the mass M .

$$b_e = \frac{B_e}{M} = \frac{4\pi}{T_0} \frac{\delta}{\sqrt{4\pi^2 + \delta^2}} \quad (3.49)$$

The measurements of the equivalent linearised damping in equation (3.49) can be fitted to equation (3.42) by linear regression. By plotting b_e with $\frac{16x_n}{3T_n}$ on the x-axis, b_2 can be found as the slope, and b_1 as the intersection point on the y-axis. This means that the linear damping is the value of the linearised damping for zero motion amplitude and a constant slope of b_e means a constant quadratic damping coefficient. This method will be used later in Chapter 7.

3.9 Fast Fourier Transform

The Fast Fourier Transform is an algorithm to perform the discrete Fourier transform. It is commonly used to transform a sample from the time domain into the frequency domain. The method was first described in 1965 by (Cooley & Tukey, 1965). This is also the method that is implemented in the post-processing part of SIMA.

Given a time series $x(t)$, the continuous Fourier transform of x can be defined as in equation (3.50).

$$\hat{x}(f) = \int x(t) \exp(-2 + \pi i f t) dt \quad (3.50)$$

Here, f is the frequency and $i = \sqrt{-1}$ which is the imaginary part.

Chapter 4

Description of TLP-Concept

The TLP consists of 4 main parts, a mooring system, substructure, tower and a wind turbine. The water depth is 150 m. The mooring system consists of 3 lines (tethers) mounted at the end of 3 spokes which is located at the lower mid section of the substructure. This is the concept which will be compared to a model with the spokes/arms located at the bottom of the structure. The angle between the spokes is 120 degrees and the tethers goes straight down to attachment points on the sea floor. The stiff mooring system causes the natural frequencies in heave, roll and pitch to be outside of the energetic wave frequency range. The substructure provides the buoyancy force needed carry the weight and required pretension. Concrete ballast is used at the bottom of the substructure to ensure stability in moderate sea states when the mooring system is not attached. This is important during tow-out and installation.

The coordinate system has its origin in the still water level at the center of the substructure. The rigid-body translatory motions are referred to as surge, sway and heave and the angular motions are referred to as roll, pitch and yaw. The fore perpendicular is defined as the tip of spoke in positive x-direction.

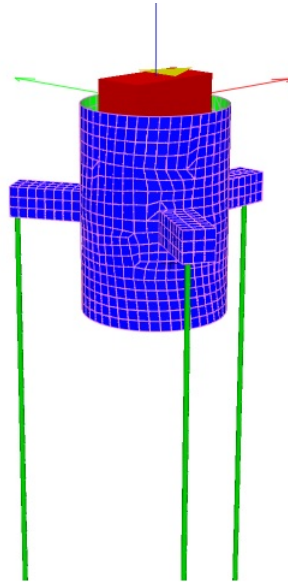


Figure 4.1: Tethers and Substructure with spokes

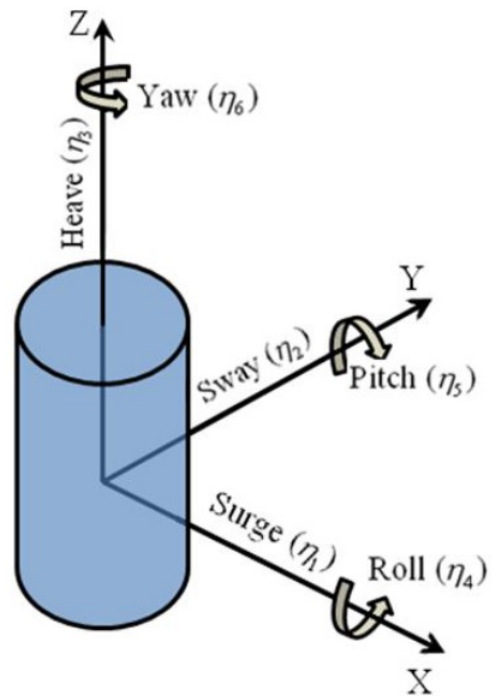


Figure 4.2: Definition of axis and motions

4.1 Substructure

The substructure is made from steel and filled with concrete for ballast. The main dimensions of the substructure are listed in table 4.1. In addition, the spokes has an radius of 27 m and a square cross section of 4 by 4 meters. This is included in the calculations of the added mass and displacement. The comparison model will have the same properties, but different location of the spokes/arms.

Table 4.1: Substructure

Description	Value	Unit
Radius of main hull	9	[m]
Draft	40	[m]
Total mass	8155 467.677	[kg]
Displacement	10218.831	[m ³]
Center of Mass	-29.94	[m]
Center of Buoyancy	-20	[m]
Mass moment of inertia pitch/roll	8 685 700 000	[kgm ²]
Mass moment of inertia yaw	326 120 000	[kgm ²]

4.2 Mooring System

The three tethers are mounted at the end of the spokes with a radius of 26 m from the center of the substructure. The restoring forces are mostly due to the mooring system thus eigen periods can be tuned by the mooring system. The properties of the mooring system is given in table 4.2

Table 4.2: Mooring system

Description	Value	Unit
Unstretched length of tendon	129.5	[m]
Tendon diameter	0.127	[m]
Mass pr. unit length	116	[kg]
Axial stiffness	1 411 831.74	[kN/m]
Depth to failead from sea surface	-20.6	[m]
Pre-tension pr. tendon	7 580 000	[N]
Number of tendons	8 685 700 000	[-]

Chapter 5

Computer Modelling

The computer modelling has been carried out using GeniE and HydroD developed by Det Norske Veritas and SIMA developed by MARINTEK. This section gives a brief description of the different computer programs and how they were used. The procedure followed is taken from the pre-studies prior to the master thesis and is based upon the design from (Bachynski, 2014).

5.1 GeniE - Panel Model

GeniE is part of the Sesam package developed by DNV, and is a software for design and analysis of offshore structures. A panel model is sufficient for calculating hydrodynamic properties when structural properties are disregarded. An element size of 1 meter is considered sufficient by (Lygren, 2011). This gave 4648 wetted elements for the structure. The tethers and spokes were modelled as Morison elements and made separately from the panel model. The two models were exported to HydroD for hydrodynamic calculations. The Panel model is shown in figure 5.1 and the Morison model in figure 5.2. Note that the tethers are enlarged in the picture for enhanced visibility.

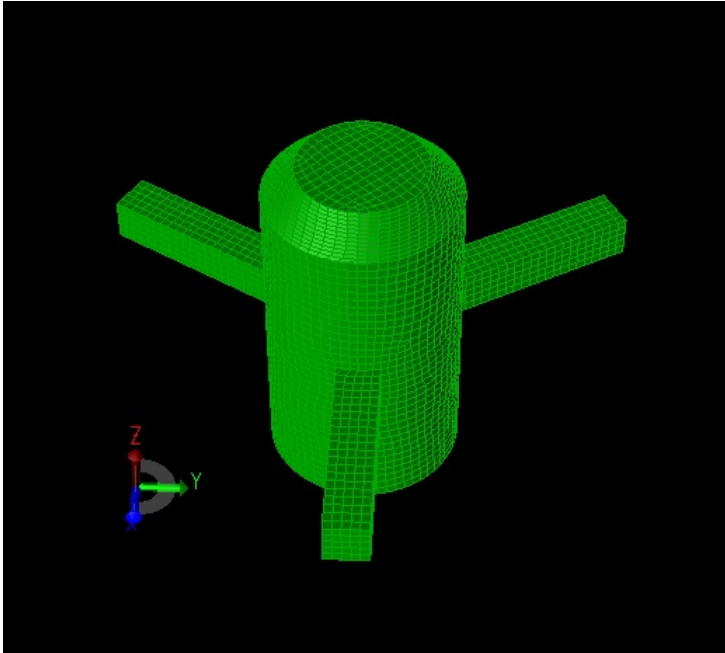


Figure 5.1: Panel model with mesh in GeniE

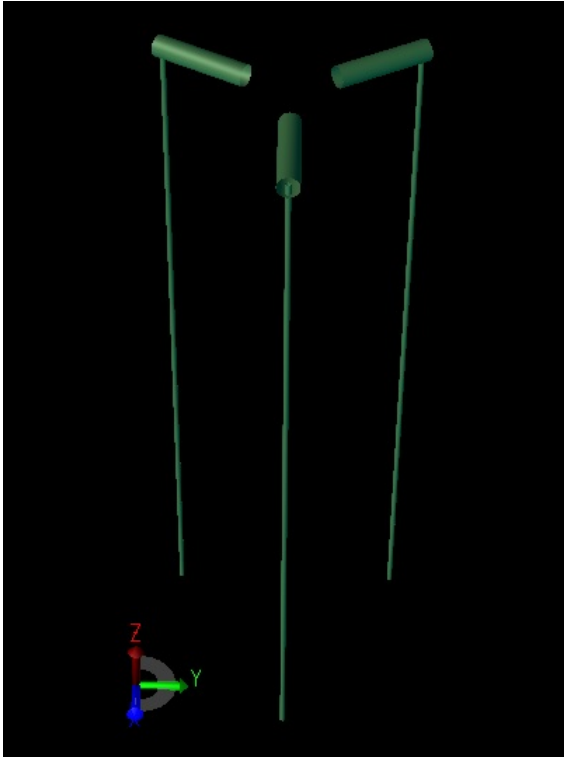


Figure 5.2: Morison model in GeniE

5.2 HydroD - Hydrodynamic Calculations

HydroD is also part of the Sesam package developed by DNV. This software is the graphical user interface for WADAM and WASIM. For the calculations of hydrodynamic properties, WADAM ("Wave Analysis By Diffraction and Morison Theory") is used. Although WADAM can include Morison forces on the spokes and tethers, this is disregarded in HydroD as they will be included later in SIMA. It is not recommended to include this as the result from HydroD is going to be used in an coupled analysis between SIMO and RIFLEX. Thus, The drag- and added mass coefficients are set equal to zero. More information on the program can be found in (. DNV, 2014) and (. DNV, 2010).

The HydroD model is a combination of the panel model and the Morison model designed in GeniE. The two models do not cover the same parts of the structure (substructure and spokes). This means that the model is imported to HydroD as a "composite model". The Morison elements are needed in HydroD only as attachment points for the tension legs.

Frequency dependent added mass, potential damping, the restoring forces (excluding mooring line restoring) and the wave force transfer functions will be used later by SIMA through a wamit result file. The calculations of the first-order wave forces do not require an accurate mass distribution. The only requirement is that the submergence is correct. Calculations of second-order forces on the other hand, require that the mass distribution is correct. To achieve this, the tension legs are modelled with the correct stiffness and tension. The restoring forces from the tension-legs will not be transferred to SIMA but are re-modelled in RIFLEX.

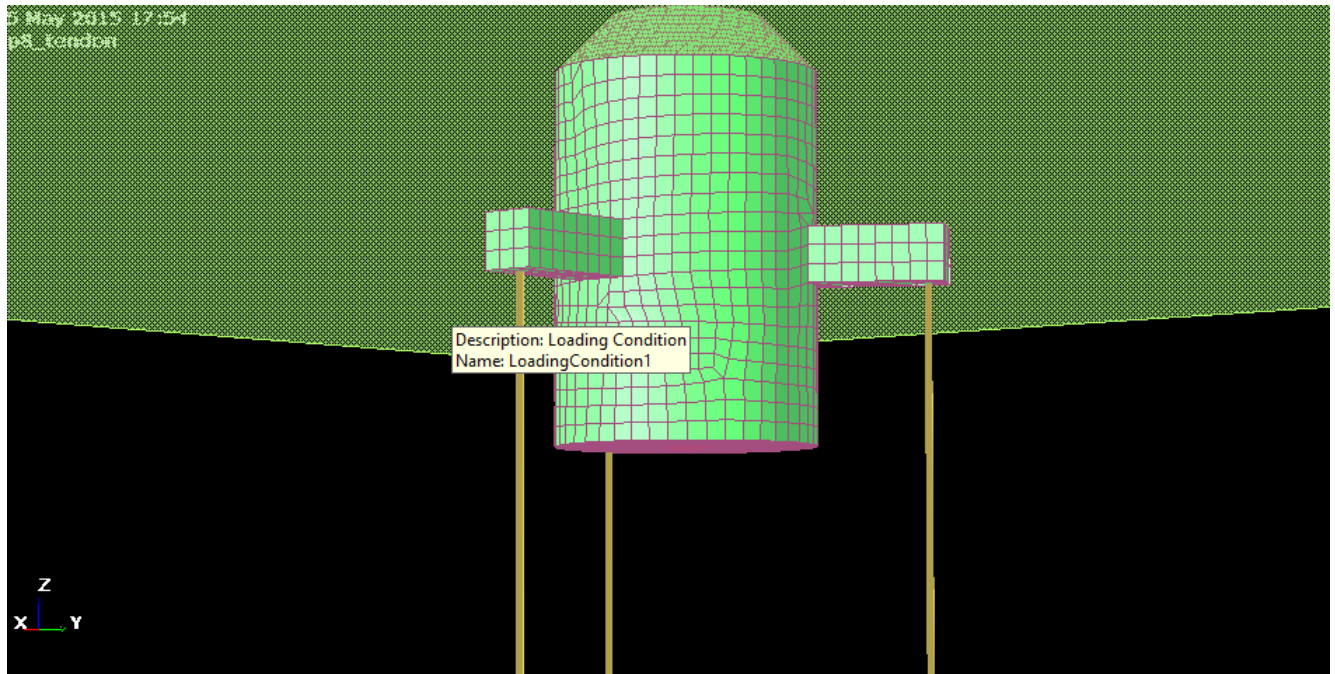


Figure 5.3: Composite model in HydroD

5.3 SIMA - Time Domain Simulation

SIMA is a simulation and analysis tool developed as a Joint Industry Project by MARINTEK and Statoil. It is meant for marine operations and floating systems and includes codes such as SIMO and RIFLEX. Input to SIMA is the frequency depended added mass and potential damping, restoring forces and excitation forces calculated in HydroD.

5.3.1 SIMO

SIMO is short for "Simulation of Marine Operations" and is a time domain simulation program systems of multiple bodies. In SIMO, all structures are modelled as "rigid" thus no elastic modes are included. The model will have motions in six degrees of freedom; surge, sway, heave, roll, pitch and yaw. Since there is no elastic modes, the

5.3.2 RIFLEX

RIFLEX is a nonlinear finite element method program for static and dynamic analysis of slender marine structures. RIFLEX is used to model the mooring system.

5.3.3 Modelling in SIMA

The wamit-file from HydroD contains the hydrodynamic coefficients but the tendons and spokes/arms must be remodelled in SIMA. This is done in a similar way as for the Morison model in Genie. The tethers are suspended between two super-nodes, one which is the anchor and the second the tip of the spoke/arm. The spoke/arm it self is suspended between the hull and the tip where the tethers are connected.

The tip and inner node of the spokes/arms are slaved nodes to a master node in the center of the hull. A dummy line is suspended between this node and the dummy node. The anchor nodes are fixed in all degrees of freedom except for rotation in the x- and y-plane.

The drag forces on the mooring system are to be included in SIMA. The quadratic drag coefficient is set to 0.07 in the tangential direction and 0.7 in the normal direction. Both for the tethers and the spokes/arms. The drag is expected contribute to the damping, especially in heave and yaw where the linear drag is very low due to the circular cross section of the body.

To connect the slender system to the body, a dummy line is used. The cross section is modelled be a simple CSR0 cross section type for the spokes/arms and CSR1 for the tethers. The geometry and material properties are defined for the different cross sections.

In figure 5.4, the spokes/arms with tethers are modelled. 1) represents the pre-tension. For detailed information on the model, see the input to SIMO/RIFLEX in the digital attachment. The pre-tension forces a displacement in the positive z-direction of 0.6 meters. This means that the stretched length of the tethers is 130 meters.

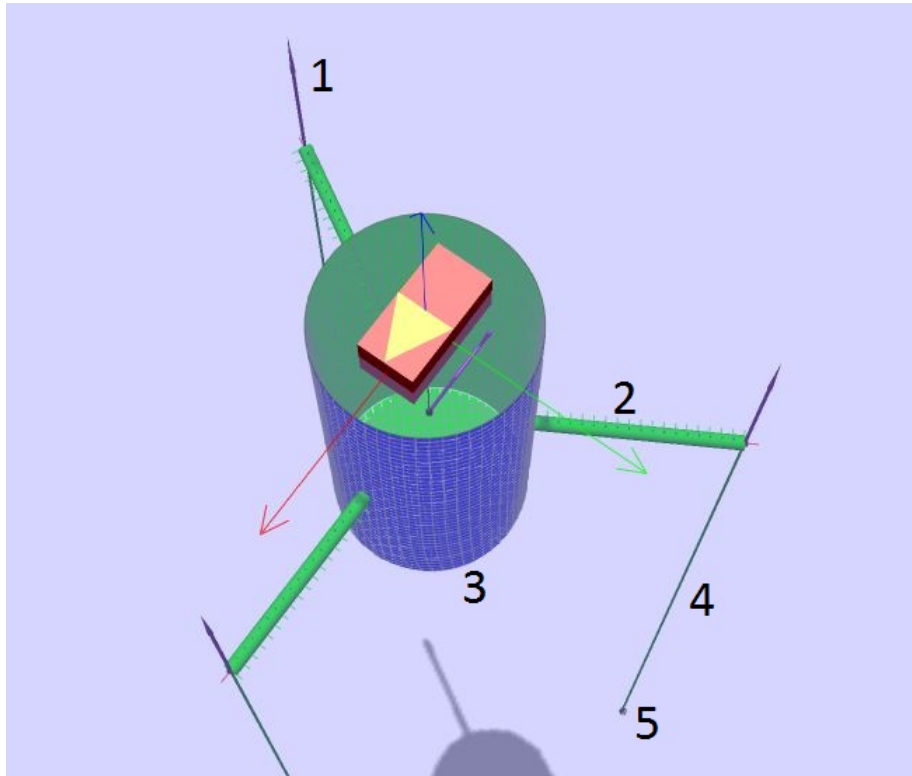


Figure 5.4: SIMA model; 1) Pre-tension Force, 2) Spoke/Arm, 3) Substructure, 4) Tendon, 5) Anchor

Chapter 6

Hydrodynamic Results

In this chapter, added mass, potential damping and excitation forces obtained from the hydrodynamic analysis in HydroD will be presented. These values are exported to SIMA for the calculation of the rigid body motion described in section 3.5. The post processing program Postresp from DNV is used to display graphs and results from the WADAM calculations. See (DNV, 2007) for more information on the program.

6.1 Added Mass

The full added mass matrix consists of 36 coefficients. The frequency depended added mass is shown in figure 6.1 and figure 6.2 on the two following pages. Since there is no forward speed and symmetry about the XZ plane, some of the terms will be zero or close to zero. For the force translation case, in the upper part of figure 6.1, it is shown that A_{11} , A_{22} and A_{33} are nonzero. A_{11} in surge and A_{22} in sway are near equal because of symmetry and A_{33} the smallest because the "wetted area" from motion in heave direction is the smallest.

The moment rotation is presented in the lower part of figure 6.1. A_{55} and A_{44} are non-zero and close to equal. A_{66} is zero as the substructure is a cylinder and no added mass force in yaw direction is generated because of motions in yaw direction (Drag coefficients on the spokes/arms are set equal to zero).

The moment translation is presented in the upper part of figure 6.2. A_{24} and A_{15} are non-zero, equal in magnitude but with opposite signs. In the lower part of figure 6.2, only A_{42} and A_{51} have significant values, again this is due to symmetry.

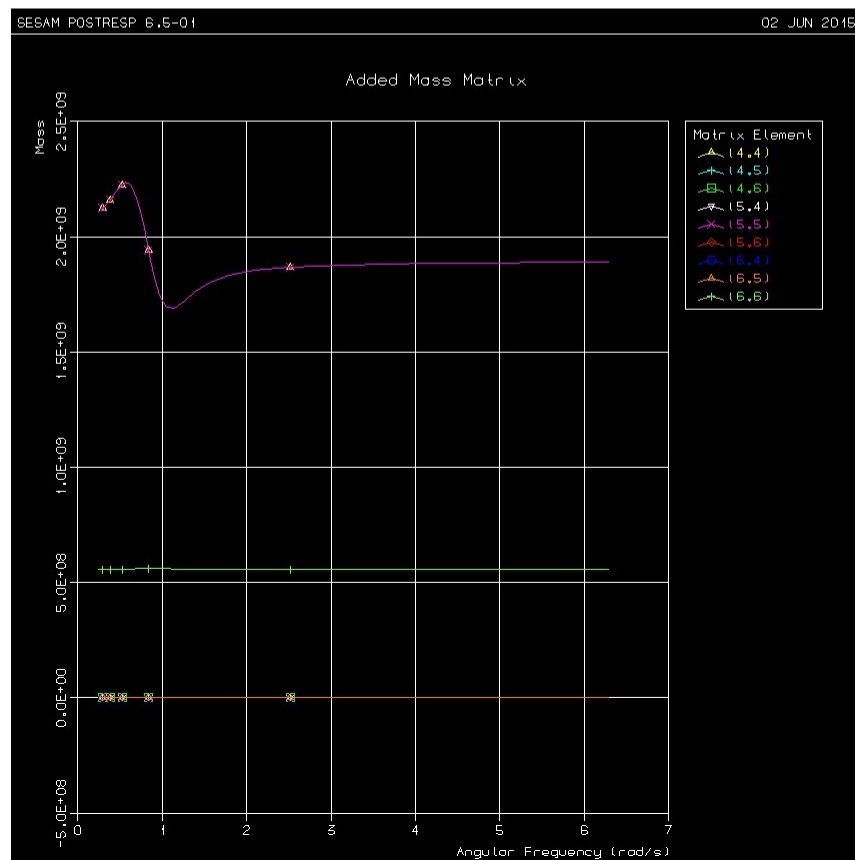
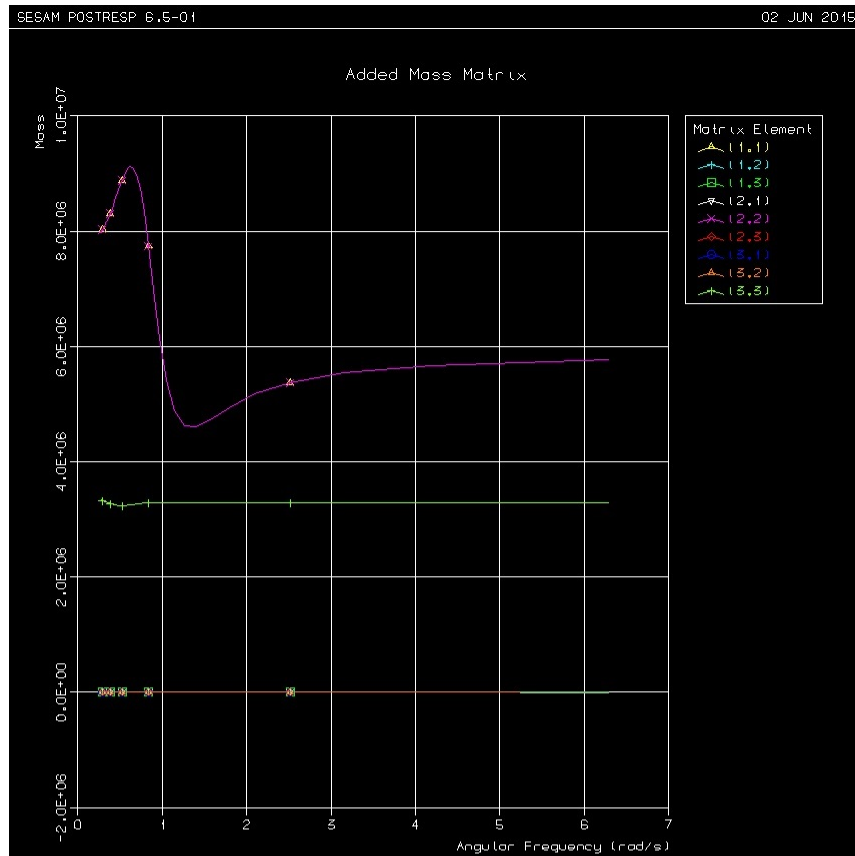


Figure 6.1: Added mass; Force translation and moment rotation mode

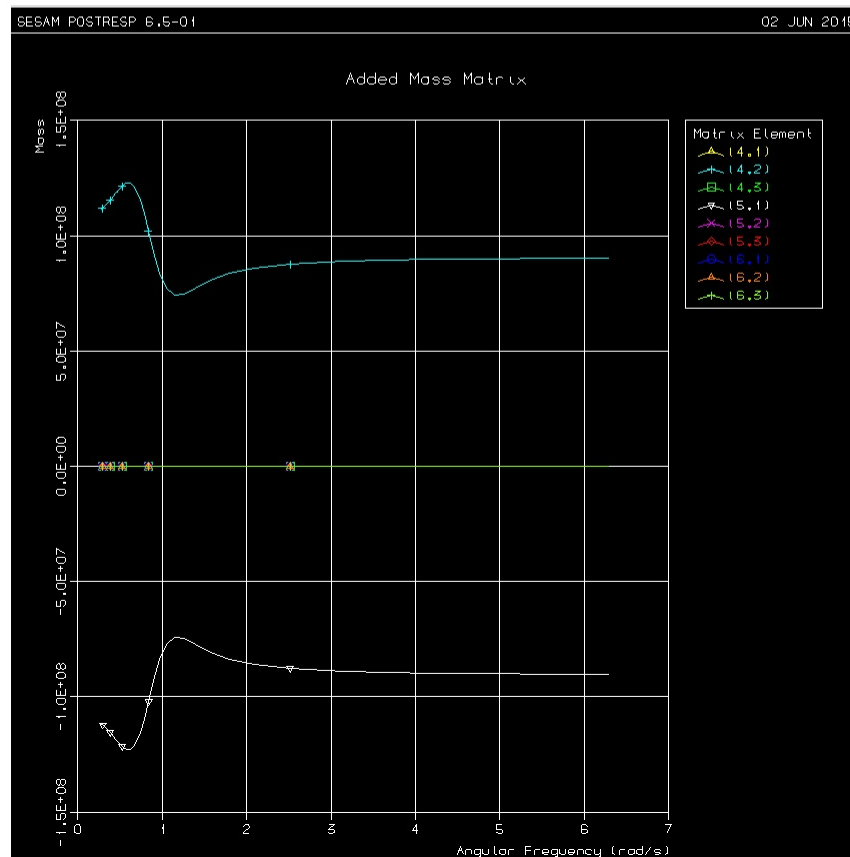
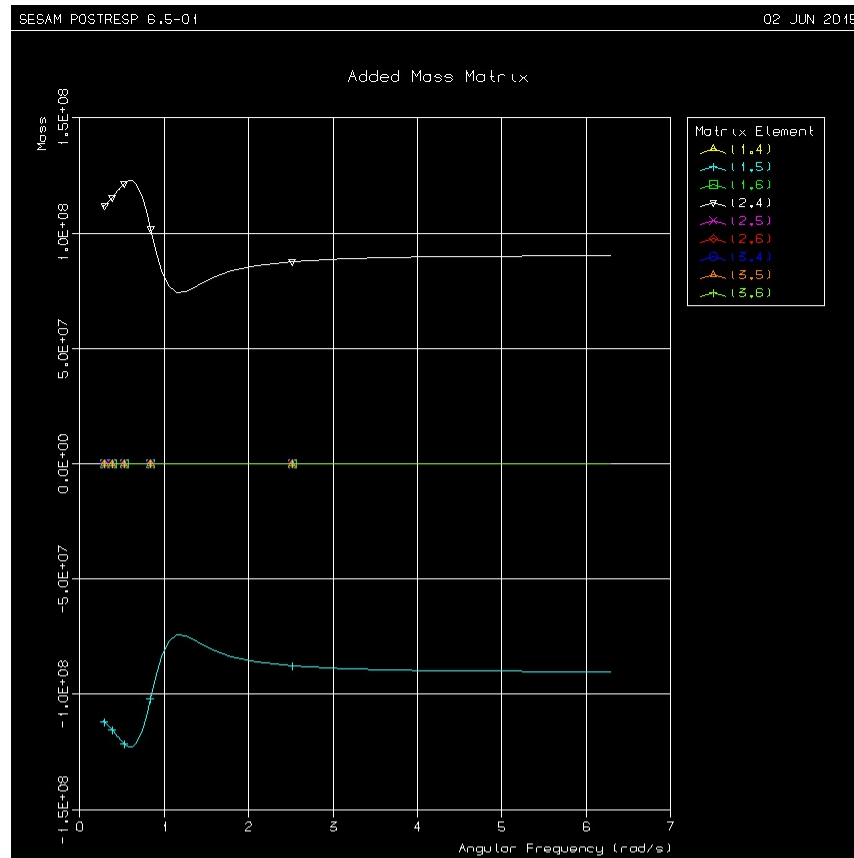


Figure 6.2: Added mass; Force rotation and moment translation mode

6.2 Potential Damping

The frequency dependent potential damping contribution is presented in figure 6.3 and figure 6.4 on the two following pages. The set-up of the graphs is the same as for the presentation of added mass in the previous section. It is the same non-zero terms that appears in the potential damping as in the added mass.

The potential damping approaches zero in both the low and high frequencies. Only the potential damping is presented in these figures. Viscous forces are added to the analysis by using Morison elements as described in section 5.2. Damping is further discussed in section 3.8.

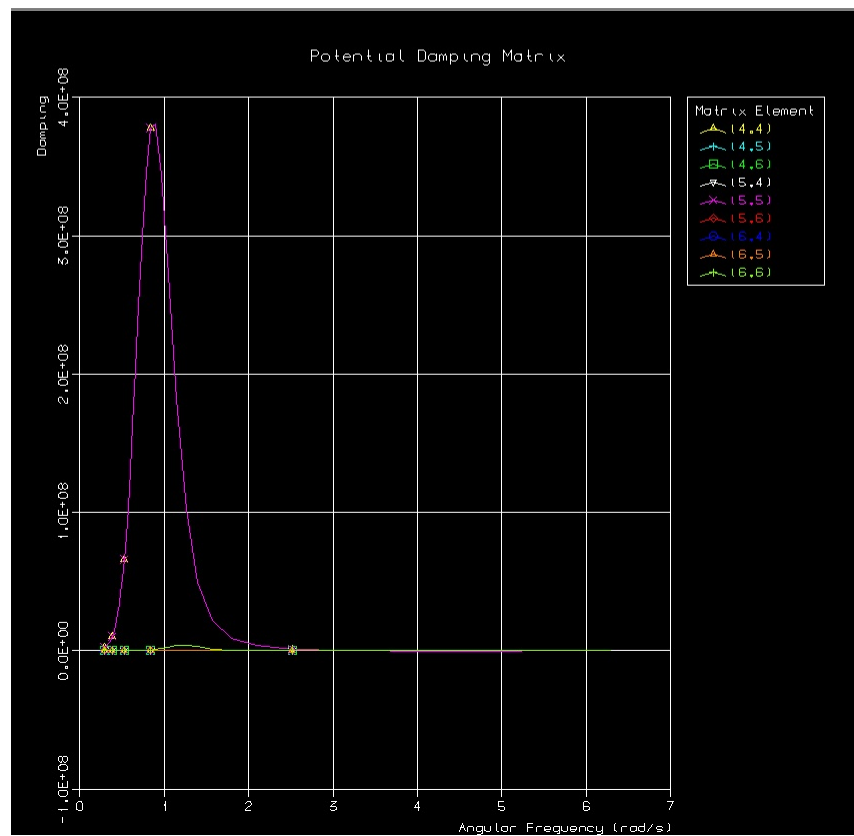
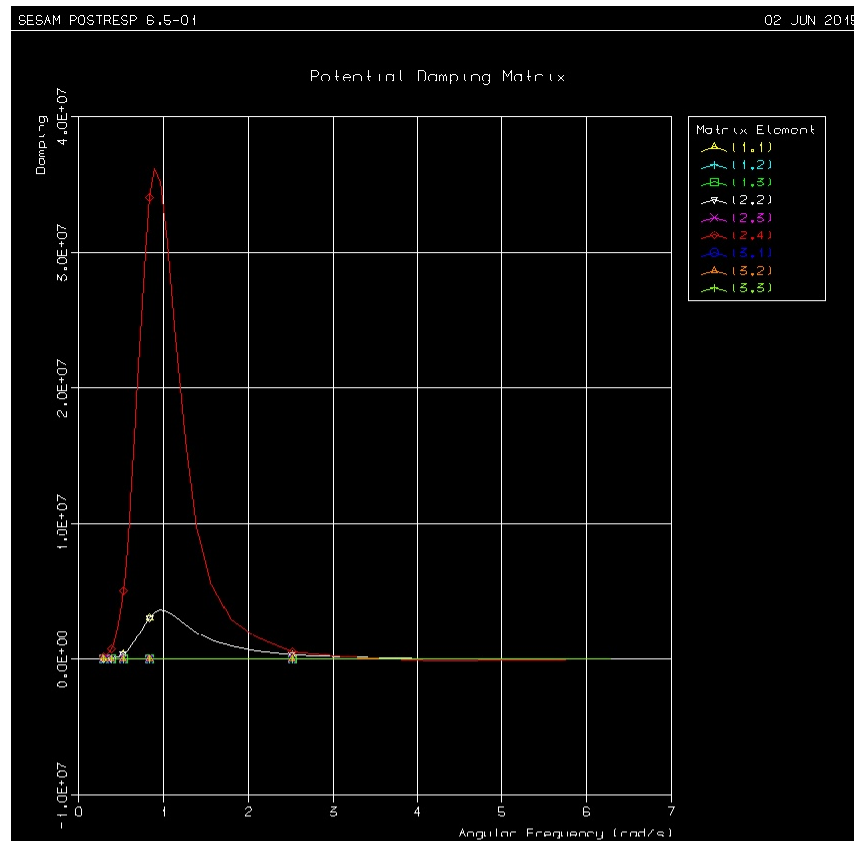


Figure 6.3: Potential damping; Force translation and moment rotation mode

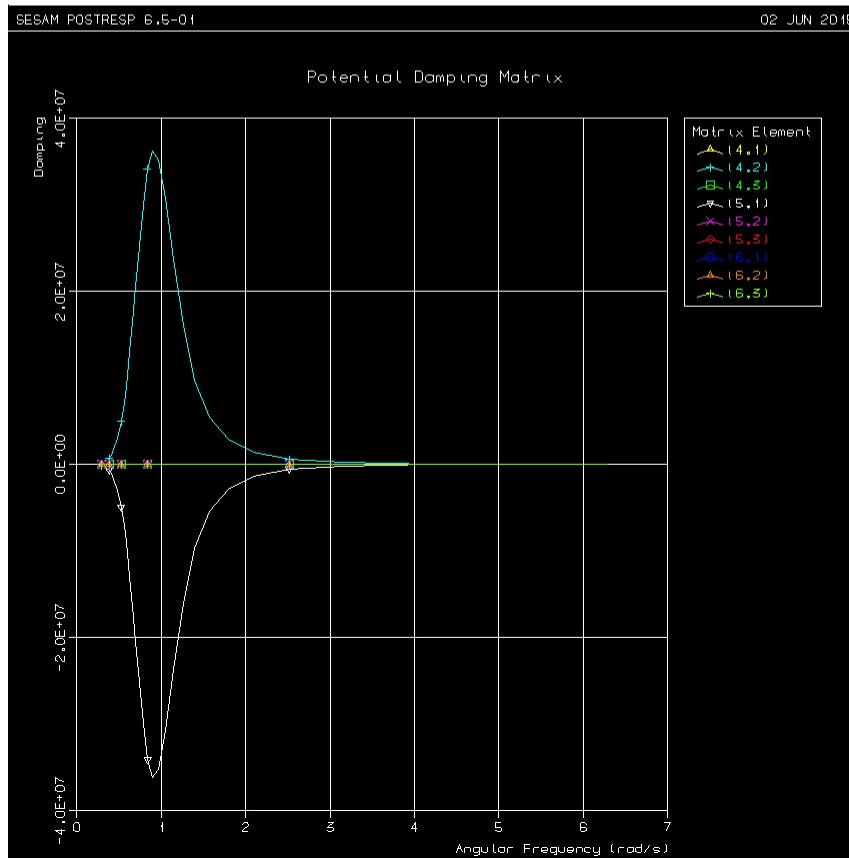
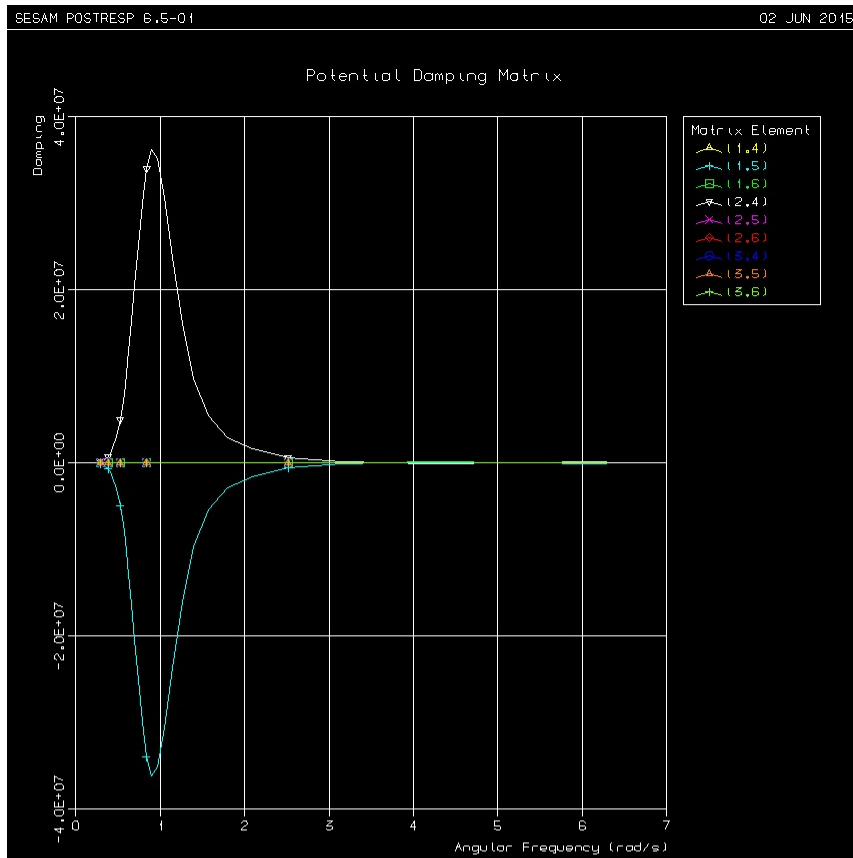


Figure 6.4: Potential damping; Force rotation and moment translation mode

6.3 Excitation Forces

The first-order excitation force and moment transfer functions are presented in figure 6.5. The wave direction in the plots are for 0 degree heading, that is, along the positive x-axis. In the left part of the figure, the translation forces are presented. The force in sway direction (Force2) is zero because of the 0 degree heading. If the heading was 90 degrees, this term would be non-zero and surge (Force3) would be zero.

In the figure to the right, it can be observed that the pitch moment is non-zero. If the heading was 90 degrees, the pitch moment would have been zero and the roll moment would be non-zero. There will be a little difference between roll/pitch and surge/sway as the substructure and mooring system are not entirely symmetric. In either case the yaw moment is zero. We also observe that the forces approaches zero for high frequencies.

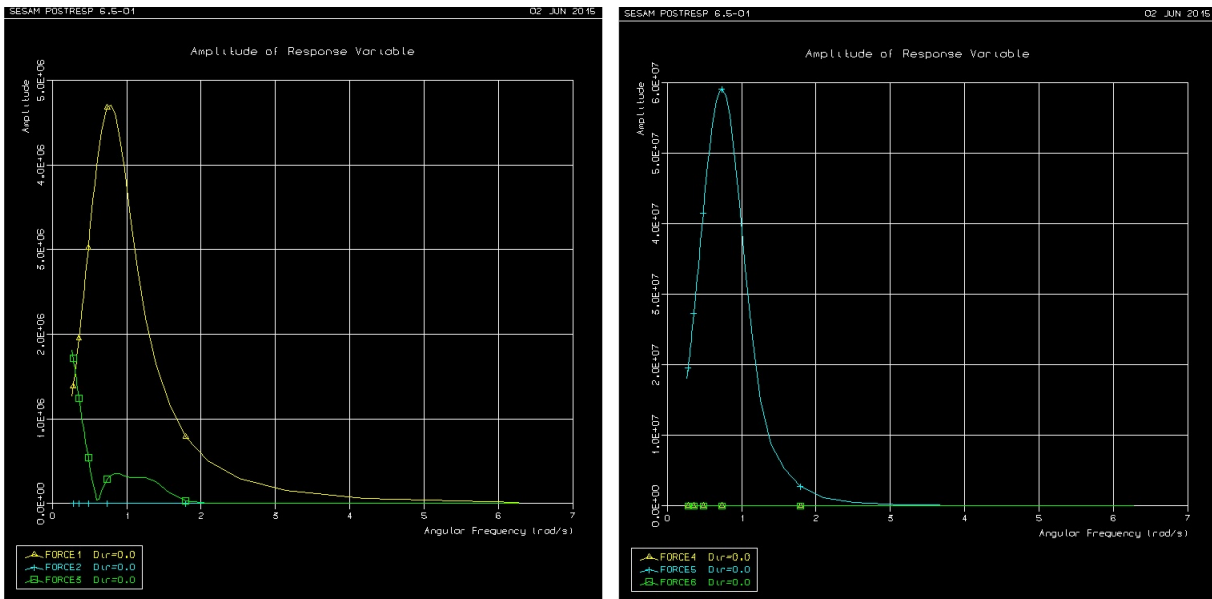


Figure 6.5: Excitation forces and moments from HydroD (Postresp)

The hydrodynamic model has been compared to the results of (Lygren, 2011) for verification. Although the model is not entirely symmetric, the agreement is still very good both in terms of magnitude and frequency dependency. This is a good indication that the results from the hydrodynamic analysis in HydroD are correct.

Chapter 7

Decay Test and Damping

A decay test, simulated in SIMA, has been performed to estimate the damping and the natural periods of the system. The test will also give an indication of whether the computer model is working good or not. The decay test is performed by applying a specified force or moment to force a displacement or rotation. The system is then released and left to oscillate freely. From the time series obtained from the tests, damping and eigen period can be determined. In table 7.1, the parameters for the test are listed. Since the pre-tension also is modelled with a specified force, the displacement force starts with a ramp force, 20 second into the simulation, followed by a constant force. This is done to avoid incremental load problems. The reference model is tested by the same parameters although the z-coordinate is changed to the new position of the spokes/arms. The damping calculations are described in section 3.8. However, some interference in the time domain response made it difficult to calculate this by scripting. Hand calculations have been performed to eliminate peaks from interference. More about this in section 7.3.

Table 7.1: Decay test parameters

Motion	Force/ Moment	Simulation length [s]	Point of application	Ramp duration [s]	Constant force duration [s]
Surge	500 kN	4500	(0,0,-20.6)	50	30
Sway	500 kN	4500	(0,0,-20.6)	50	30
Heave	1 MN	350	(0,0,0)	50	30
Roll	500 kNm	300	(0,0,-20.6)	50	30
Pitch	500 kNm	300	(0,0,-20.6)	50	30
Yaw	500 kNm	300	(0,0,-20.6)	50	30

7.1 Surge and Sway

The response from the time domain calculation for the surge and sway decay test is plotted in figure 7.1 and figure 7.2. The natural periods are determined from the response spectrum in the decay test. This is done by the post processing part of SIMA. Even though the mooring system is not symmetric, the natural period and amplitude is the same as the offset of the tethers remains the same for both the cases. The drag forces over the spokes will also be close to equal if shading effects from the main body is disregarded.

The damping ratio for surge and sway ranges from 0.076 to 0.0213 with the greatest damping ratio for larger amplitudes. This is due to the quadratic drag contribution which is proportional to the velocity squared.

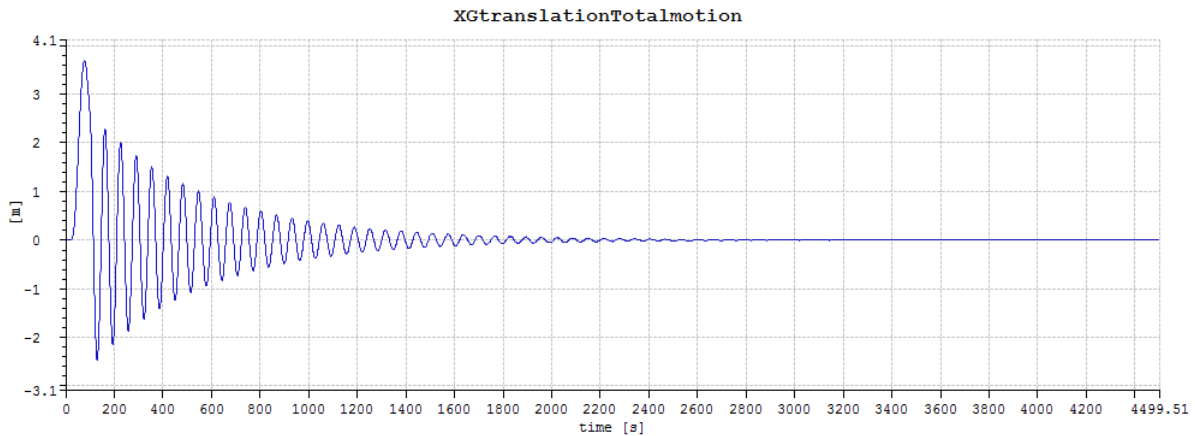


Figure 7.1: Time domain response: Surge

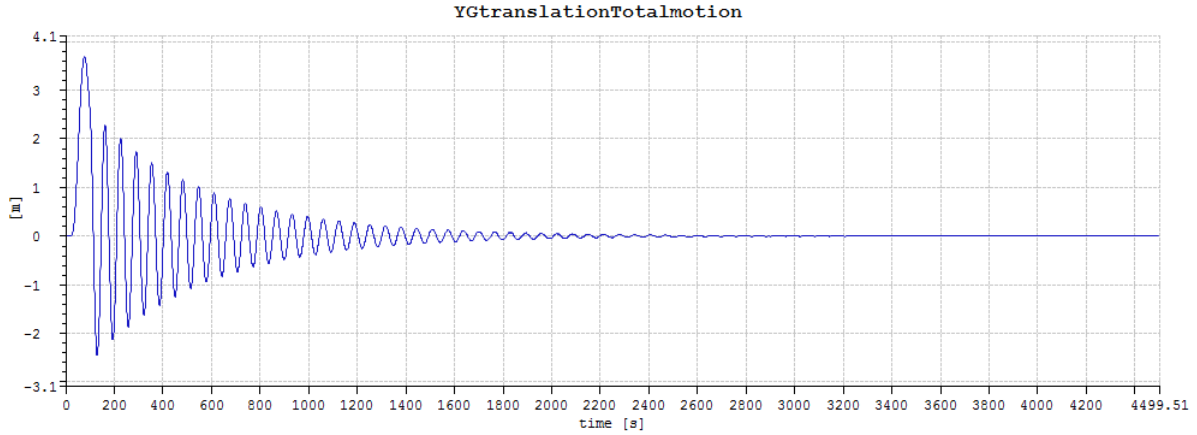


Figure 7.2: Time domain response: Sway

7.2 Heave, Pitch/Roll and Yaw

The response from the decay test for heave, pitch/roll and yaw is presented in figure 7.3, figure 7.4 and figure 7.5 respectively. The damping in heave and pitch/roll turned out to be almost independent of motion amplitude. This means that the damping is dominated by the linear drag force. Viscous effects are small due to small amplitudes of translation and rotation. The yaw response has similar tendency as for surge and sway where the drag force over the spokes/arms is the dominant term for the larger amplitudes.

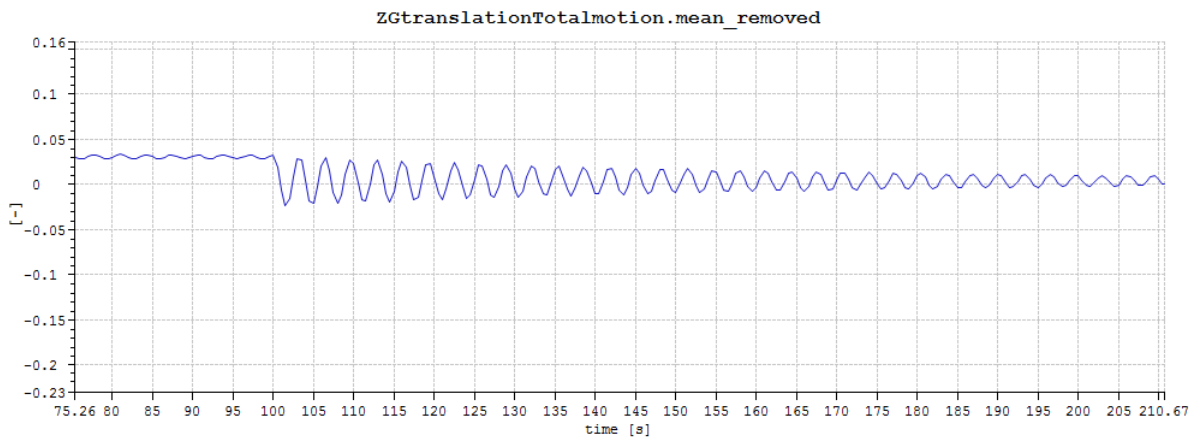


Figure 7.3: Time domain response: Heave

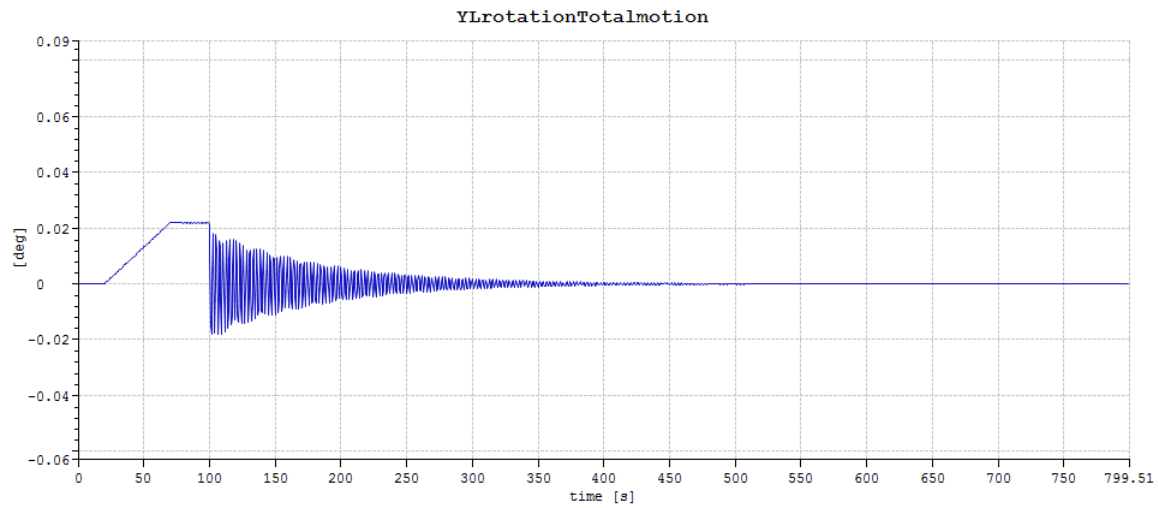


Figure 7.4: Time domain response: Pitch

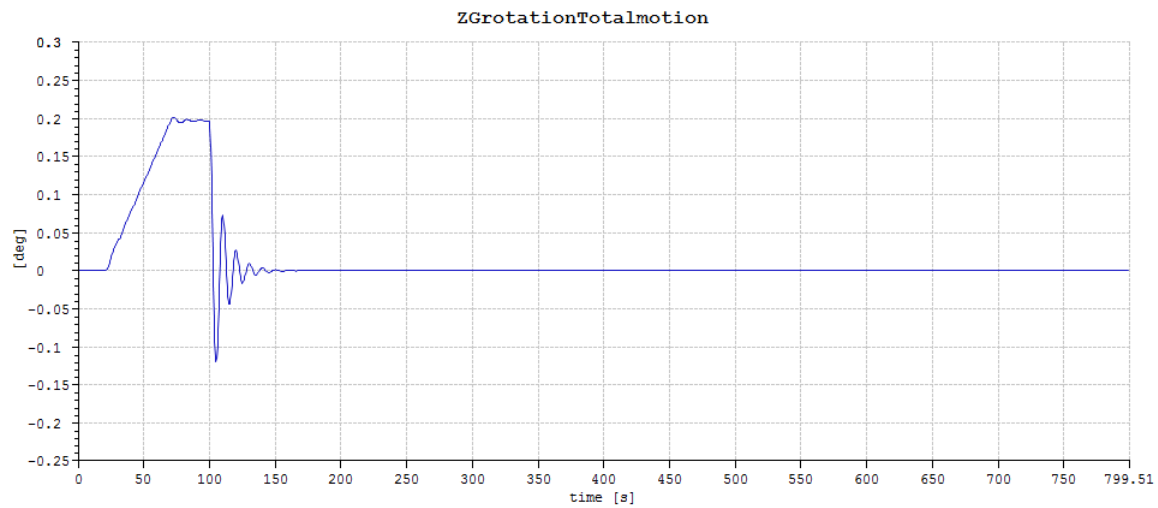


Figure 7.5: Time domain response: Sway

7.3 Summary and Concluding Remarks

The natural periods for the reference model is presented together with concept model in table 7.2 The difference in the natural periods can be explained by the difference in the length of the tethers. The stiffness is depended on the length of the tether as described in section 3.6.2. All the natural periods, except from yaw, are out of range of first order wave excitation. For a simulation with a wind turbine, the yaw period may become important when considering turbulent wind and directional change of the turbine.

Table 7.2: Natural periods for the concept model and reference model

Model/ DOF	Concept model [s]	Reference model [s]
Surge	64	63
Sway	64	63
Heave	3	2.5
Roll	2.56	1.82
Pitch	2.56	1.82
Yaw	9.58	9.14

The damping calculations are partly done by hand as multiple peaks occurred in the response. This made it difficult to sort out the right peaks for logarithmic decay. The reason for the multiple peaks may be numerical or from coupled effects although measures has been done to eliminate transient effects. These multiple peaks are illustrated in figure 7.6. The Matlab script intended for the damping calculation can be found in Appendix C

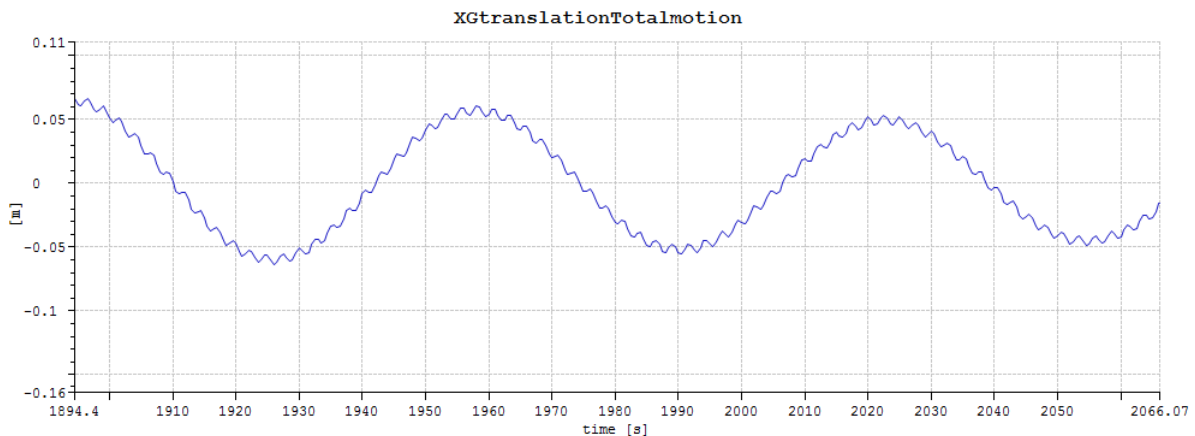


Figure 7.6: Time domain response: Multiple peaks

Chapter 8

Response Analysis

The response calculations has been done for an ideal, fictional location for an offshore wind turbine. The simulations has been carried out over a period of 3 hours with a start up period of 200 seconds to avoid any transient effects. The time step used is 0.01 seconds and data is stored every 0.5 seconds. The parameters for the test is presented in table 8.1 and is used for both the concept model and the reference model.

The five conditions in question are considered normal operation condition. The significant wave height i each condition remains the same while the the peak period is different. The sea state is defined in SIMA as a 3 parameters JONSWAP spectrum described in section 3.4 and the heading of the waves is 0 degrees. The time domain series for the concept model had to be shortened due to some divergence problem for longer simulations. Although the data is not directly comparable, they should give a good indication of where the response occur in the frequency domain

The spectra presented in this section is for the most sever case, with a significant wave height of 6.75 meters and a peak period of 12 seconds. The spectra for the remaining cases can be found in appendix C.

Table 8.1: Conditions for response analysis

Condition	Hs [m]	Tp [s]	Wave seed
C1-1	1.25	4	101
C1-2	1.25	6	102
C1-3	1.25	8	103
C2-1	2.75	6	104
C2-2	2.75	8	105
C2-3	2.75	10	106
C2-4	2.75	12	107
C3-1	3.75	6	108
C3-2	3.75	8	109
C3-3	3.75	10	110
C3-4	3.75	12	111
C4-1	5.25	8	112
C4-2	5.25	10	113
C4-3	5.25	12	114
C5-1	6.75	12	115

8.1 Surge Spectrum

The surge spectra for both the design model and the reference model are presented in figure 8.1. There are two significant peaks in both spectrum occurring at approximately $T = 10$ and $T = 64$. The first peak is likely due to coupled effects with pitch which has a natural period in this domain. The second peak is the natural period of surge.

For a platform designed to carry a wind turbine, the surge motion should not affect the turbines efficiency in the surge motion. The period is relatively long thus will not affect the relative wind speed in any major degree.

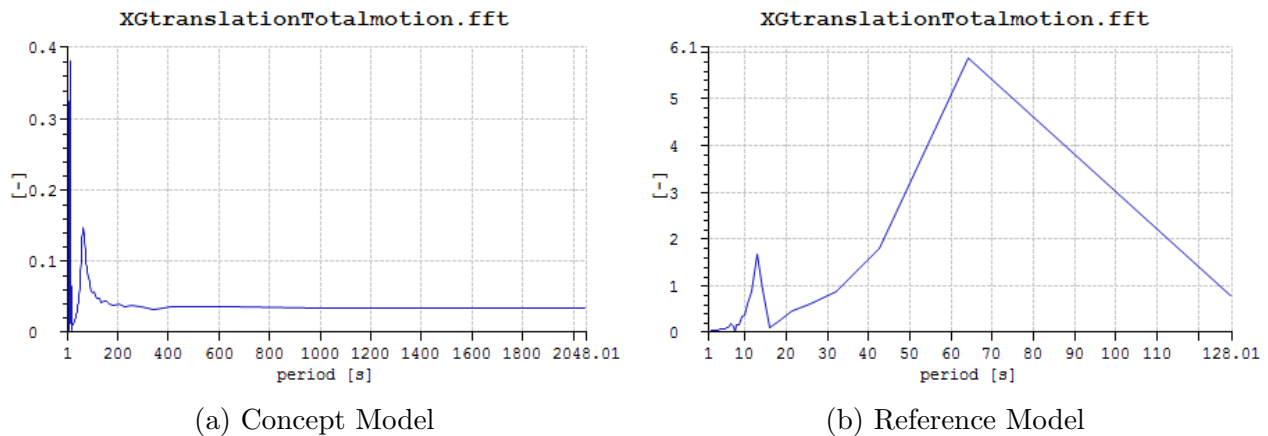


Figure 8.1: Surge spectra for case 5

8.2 Heave Spectrum

The heave spectra for both models are presented in figure 8.2. The greatest peaks occurs around the natural period of the heave motion. A contribution from the heave-surge coupling is expected. This is due to the "set-down effect" which is pendulum motion that the TLP has. The peaks at the lower periods may be caused by the heave-pitch coupling where the period will be half of the pitch period (one pitch motion gives two up and down motions in heave). The heave motion is in general small due to the stiff mooring system.

In the lower periods, there is a higher concentration of peaks that are relatively higher for the concept model than for the reference model. This may suggest that the concept model

may be subjected to more coupled effects from pitch and roll than the reference model.

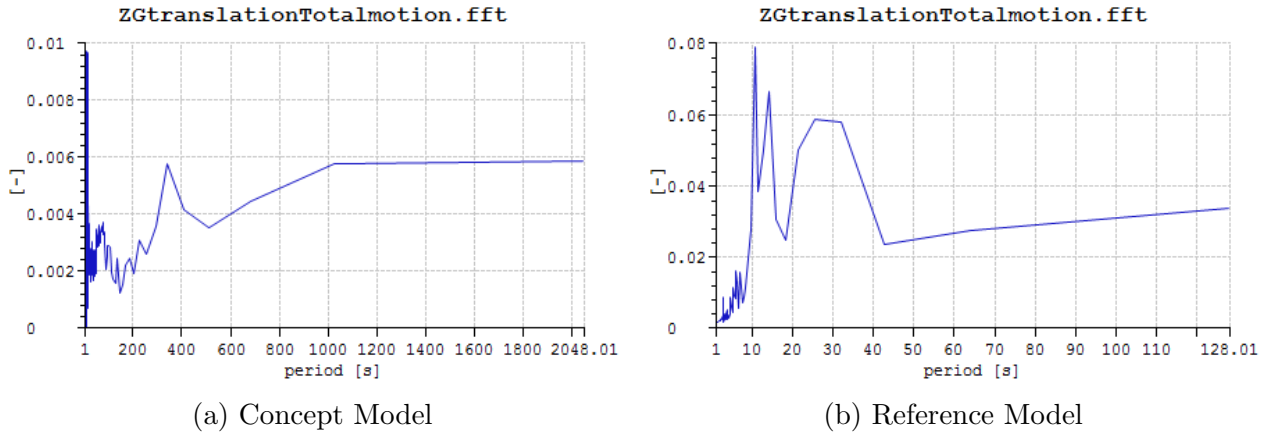


Figure 8.2: Heave spectra for case 5

8.3 Pitch Spectrum

In the pitch spectra for both models presented in figure 8.3, there is a lot of peaks between 5 and 15 seconds. This is also the interval for the most energetic waves. As seen for the other motions, the peak period of the wave is also a dominant contributor to the response in the spectra.

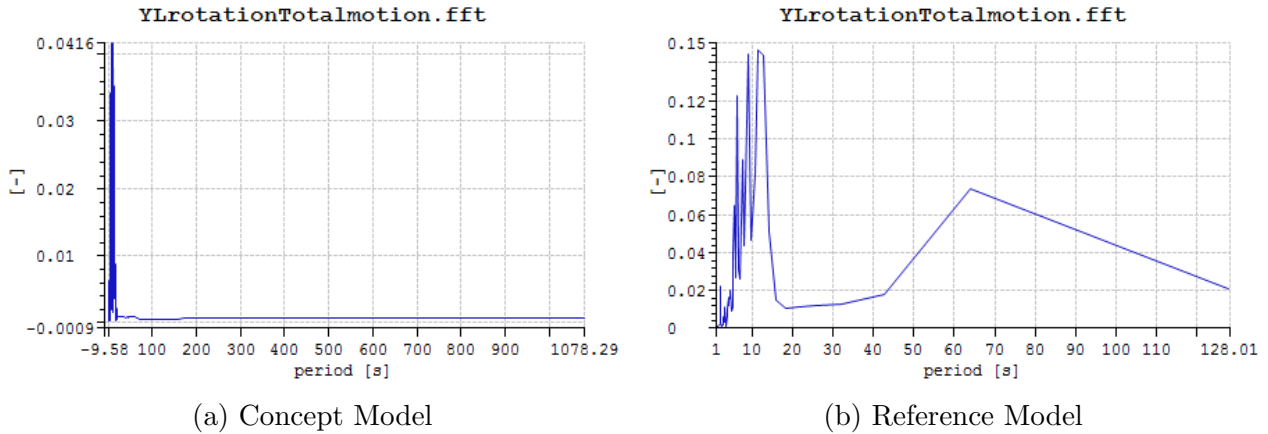


Figure 8.3: Pitch spectra for case 5

Chapter 9

Slack Tethers and Contact with Substructure

Slack in one or several tethers may lead to snapping as the system is very stiff. The pretension described in section 5.2 is there to prevent slack condition from occurring. However, during large displacements and/or acceleration from severe sea states, this may not be enough. In the analysis, such cases can be observed as negative axial forces in tethers, for larger values of negative tension, the simulation may become unstable and diverge.

Contact between hull and tendon may lead to abrasive wear and ultimately failure. Contact on such kind may occur for large horizontal movements or in combination with slack tethers. This extreme case is crucial for the integrity of this concept as the design is based upon spokes/arms that are positioned at the center of the substructure. A good method of describing this phenomena is not yet established but the rotation and translation of the model may give an indication of whether there is a probability of contact.

9.1 Axial Force in Tendon

In the most sever sea state, with significant wave height of 6.75 meters and a peak period of 12 seconds, tendon 1 does not go slack as there are no negative values observed in the time domain response analysis (figure 9.1). The data is collected from element 1 in tendon 1, which is located just below the fairlead node. However, the lowest recorded tension in the tendon is 926 kN which is only 11 percent of the equilibrium tension in calm sea. This analysis is also only for one wave seed which means that there is a great deal of statistical uncertainty connected to whether the tendon will go slack at this sea state.

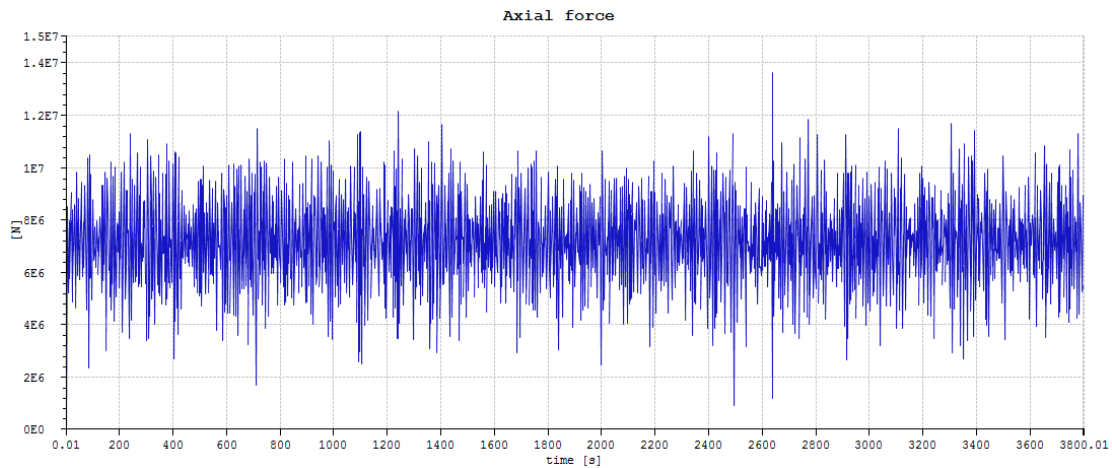


Figure 9.1: Time domain: Axial force in tendon 1

Another aspect of this analysis is the yield of the tendon. The largest observed axial force in the tendon is 13627 kN which is 72.7 percent greater than the pretension. Larger variation of forces may lead to fatigue damage and ultimately failure. The moment recorded in the inner part of the spoke/arm, closest to the substructure is presented in figure 9.2. This part of the structure may also be subjected to fatigue damage and should be investigated further. This will be discussed further in chapter 11.

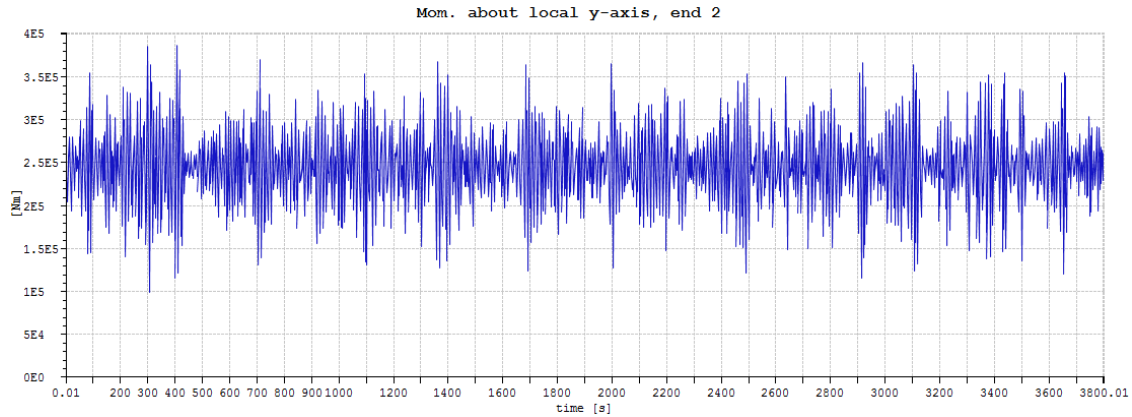


Figure 9.2: Time domain: Moment about y-axis for the arm

9.2 Tendon Contact with Substructure

As mentioned earlier, a good method of predicting contact between spokes/arms and substructure is yet to be established. In this section, two simplified models are presented (figure 9.3) to illustrate extreme cases of contact.

Contact between substructure and tendon due to translation is presented in case a). Tendon 1 is located 27 meters in the positive x-direction and the bottom is located at 20.6 meters in the negative z-direction. If the assumption of small elongation on the tendon is valid, the translation required for contact between substructure and tendon is 103 meters by simple trigonometric calculation. The angle between the spoke/arm and the tendon is in this case 53 degrees. The vertical displacement needed for this to occur is over 50 meters which means that the buoyancy will be considerably increased thus increasing the vertical restoring force because of added buoyancy. A vertical displacement of this magnitude will also lead to other problems such as wind turbine rotor contact with water and shift in center of buoyancy. Hence, contact of this nature is regarded as an inferior problem.

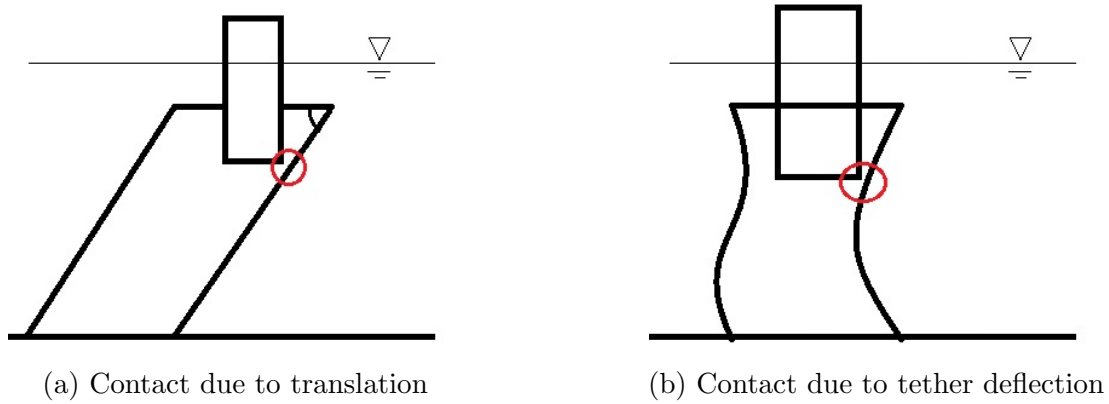


Figure 9.3: Two extreme cases of contact

Case b) represents deflection of the tether in such degree that the tendon makes contact with the substructure. The first mode shape causes the largest horizontal deflection. The beam deflection is illustrated in figure 9.4, where θ_2 is the necessary angle to achieve contact with the substructure. Quick estimation of the horizontal force P , using $\theta_2 = 53^\circ$, it is clear that the corresponding vertical force will be larger than the pretension. This case will therefore likely end up in slack tendon condition before contact is made.

$$\theta_2 = \frac{Pab(2l - b)}{6lEI} \quad (9.1)$$

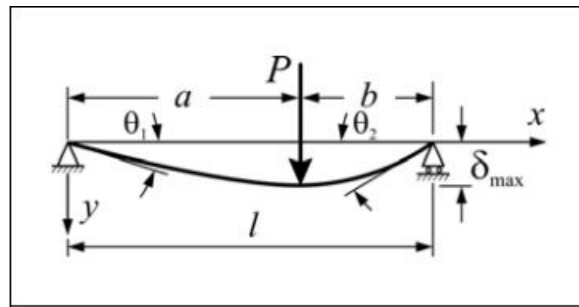


Figure 9.4: Deflection of beam (Ruina, 2012)

The time domain response in heave and pitch is presented figure 9.5 and non of the response values are close to the response needed for the extreme cases of contact. However, the same limitation applies here as this only represent one wave seed, but the margin is higher than for the slack tendon case.

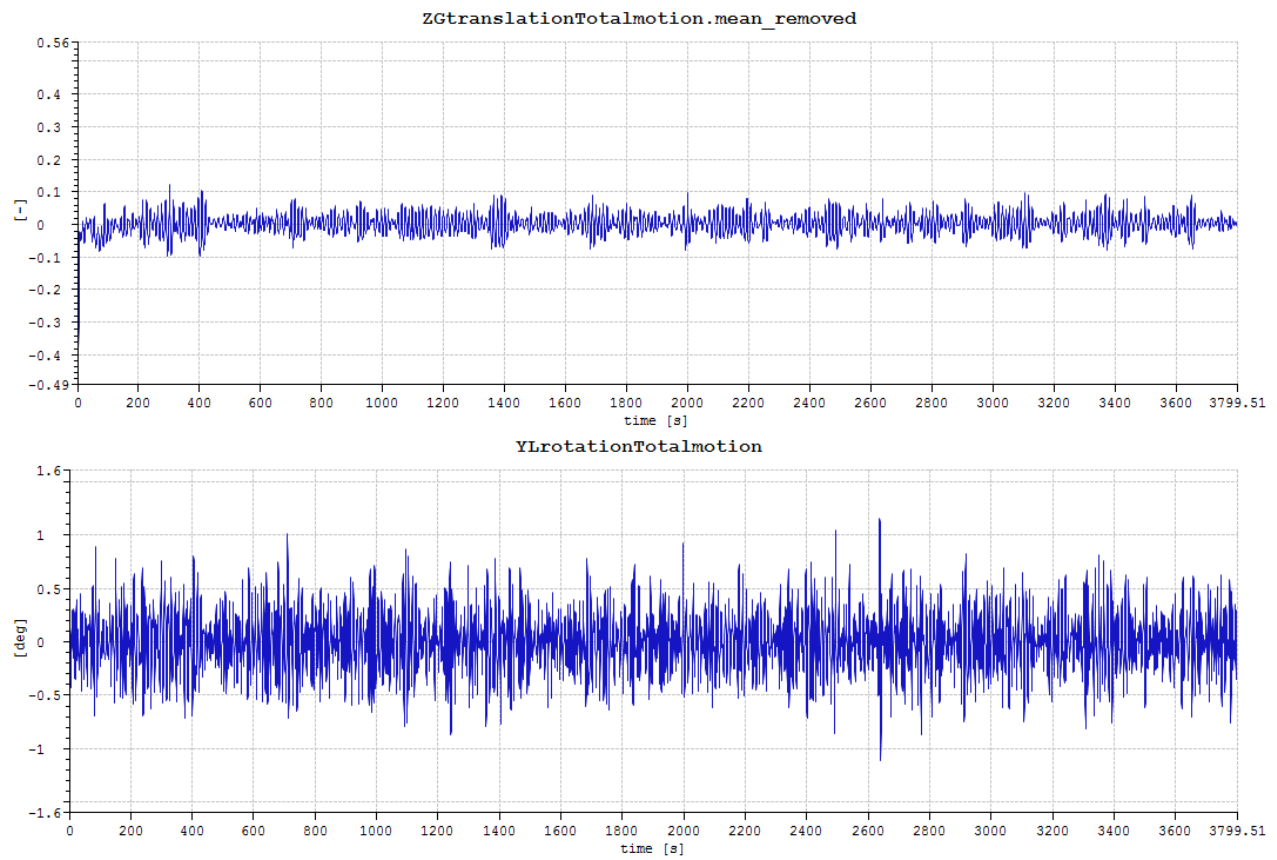


Figure 9.5: Time Domain: Heave and pitch response

Chapter 10

Conclusion and Discussion

The purpose of this project was to establish a model with the spokes/arms for the tethers positioned at the center part of the structure. A comparison of the response and behaviour of this concept were made with a similar model with conventional spokes/arms at the bottom of the substructure. The computer program used to design the models was GeniE from DNV. The Hydrodynamic calculations were performed using HydroD (WADAM) which uses potential theory. The Time domain simulations were done in SIMA by use of SIMO and RIFLEX. The mooring system was modelled as a finite element model, but the substructure was rigid.

Based on the work done in this report, it is difficult to conclude whether the concept design has an advantage or not over the conventional design. Some indication has been discovered that may suggest that there are some disadvantages connected to this concept. The length of the tethers will be increased by moving the tethers up. This can be compensated for by increasing the stiffness, either by cross section geometry or material. This consequence is conflicting with the low cost target which is crucial for offshore wind industry.

From the spectra, the concept model has shown indication of having larger coupling effects which may lead to a higher number of stress cycles. This is disadvantageous from a fatigue point of view. Although contact between substructure and tendon is unlikely from the two cases presented, the study done on this field is very limited. A good conclusion can not be drawn from this. However, the possibility of such contact occurring puts the concept at an disadvantage.

Chapter 11

Recommendation for Future work

The utilization of TLP as a base for a offshore wind turbine is still a very young field with many possibilities for improvement and innovative designs.

A coupled analysis with NREL5 5MW wind turbine in turbulent wind was intended for the project but limitation in time and expertise in SIMA made this complicated. A study into coupled effects such as blade passing frequency and torque differences in on turbine due to turbulent wind should be investigated.

This report only represent one iteration, at best, in a design process. A deeper study into the optimum dimensions and geometry could improve the behaviour and response of the design. In this report, no structural analysis of the hull is included.

Second order forces should be investigated as the system is relatively stiff with low natural periods. Steep waves and slamming effects could have a crucial effect on the structural integrity and the life span of the structure.

The response analysis in this report is simplified and a more thorough analysis should be done to further verify the response. This means that a greater number of wave seed should be used and the several headings. Extreme sea states should also be investigated as well as survival and damaged modes of the structure.

The cost of construction and life cycle is a major constraint for the offshore wind industry. Although this report aims at decreasing the forces in the tethers and thus the scale of the mooring system, a more detailed cost analysis is needed for a good conclusion on this subject.

References

- Bachynski, E. E. (2014). *Design and Dynamic analysis of Tension Leg Platform Wind Turbines, Ph.D Thesis* (Unpublished doctoral dissertation). NTNU.
- Bachynski, E. E., & Moan, T. (2012). Design considerations for tension leg platform wind turbines. *Marine Structures*, *29*(1), 89–114.
- Bekkeheien, M. A. (2013). *Higher Order Loads from Steep Waves on Floating Wind turbines* (Master Thesis). NTNU.
- Cooley, J. W., & Tukey, J. W. (1965). An algorithm for the machine calculation of complex Fourier series. *Math. Comp.* *19* (1965), 297-301.
- DNV, . (2010). Sesam User Manual, WADAM.
- DNV, . (2014). Sesam User Manual, HydroD.
- DNV. (2007). Sesam User Manual, Postresp.
- Elliot, D., Holladay, C., Barchet, W., Foote, H., & Sandusky, W. (1986). *Wind Energy Resource Atlas of the United States*. Solar Technical Information Program.
- Faltinsen, O. (1993). *Sea Loads on Ships and Offshore Structures*.
- Fenton, J. D. (1985). *A Fifth Order Stokes Theory for Steady Waves* (Vol. 111).
- Kaldellis, J. K., & Kapsali, M. (2013). Shifting towards offshore wind energy, Recent activity and future development. *Energy Policy*, *53*(0), 136–148.
- Kvittem, M. I., Bachynski, E. E., & Moan, T. (2012). Effects of Hydrodynamic Modelling in Fully Coupled Simulations of a Semi-submersible Wind Turbine. *Energy Procedia*, *24*(0), 351–362.
- Lygren, J. E. L. n. y. (2011). *M . Sc . THESIS TENSION-LEG FLOATING WIND TURBINE Student* : (Unpublished doctoral dissertation). NTNU.

- Myhr, A., Maus, K. J., & Nygaard, T. A. (2011). Experimental and computational comparisons of the OC3-hywind and tension-leg-buoy (TLB) floating wind turbine conceptual designs. In *Twenty-first international offshore and polar engineering conference, maui, hawaii, usa*.
- Myrhaug, D. (2007). *TMR4180 Marine Dynamic - Irregular Sea*.
- Newman, J. N. (1977). *Marine Hydrodynamics*. MIT Press.
- Roddier, D., Cermelli, C., Aubault, A., & Weinstein, A. (2010). WindFloat: A floating foundation for offshore wind turbines. *Journal of Renewable and Sustainable Energy*, 2(3), 33104.
- Ruina, A. (2012). *Intermediate Dynamics and Vibrations, MAE 4735/5735*. Retrieved from <http://ruina.mae.cornell.edu/Courses/ME4735-2012/>
- Vera Ingunn, M. O. E. (2010). Floating turbine captures wind energy in deep water environment. *Welding Journal (Miami, Fla)*, 89, 54–58.
- Veritas, D. N. (2010). *ENVIRONMENTAL CONDITIONS AND ENVIRONMENTAL LOADS DNV-RP-C205* (Tech. Rep. No. October).
- Zhang, R., Tang, Y., Hu, J., Ruan, S., & Chen, C. (2013). Dynamic response in frequency and time domains of a floating foundation for offshore wind turbines. *Ocean Engineering*, 60(0), 115–123.

Appendix A

Reference Model

Added Mass, Potential Damping and Excitation Forces

The same panel model has been used for the reference model, but the Morison model is different in both HydroD and SIMA. The vertical position of the spokes/arms are moved down to a position of -39.4 m relative to the free water surface. This also means that the unstretched length of the tethers are reduced to 110.6 m. The same center of buoyancy and gravity still applies as well as the total mass, displacement and pre-tension. The hydrodynamic coefficients are presented in the following section of the appendix

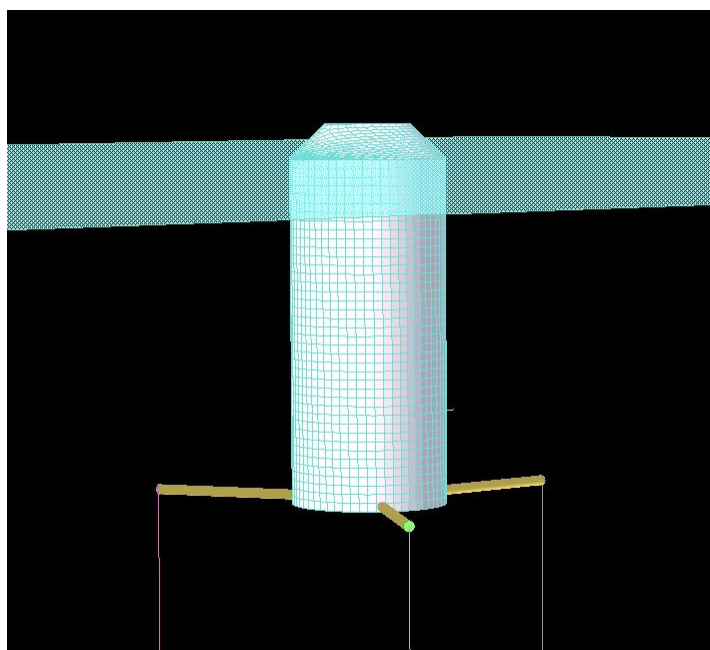


Figure A.1: Reference model in HydroD

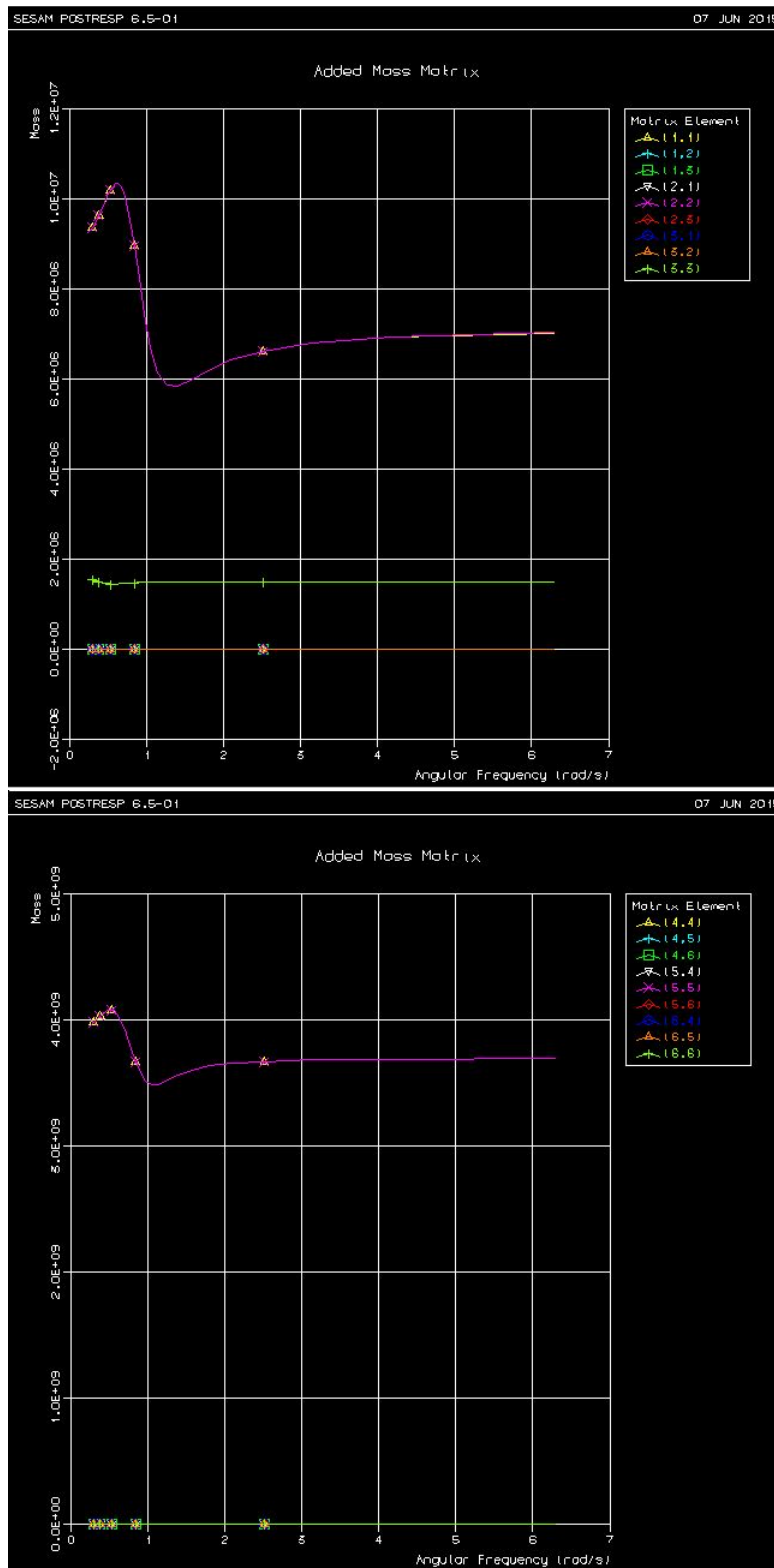


Figure A.2: Added mass; Force translation and moment rotation mode

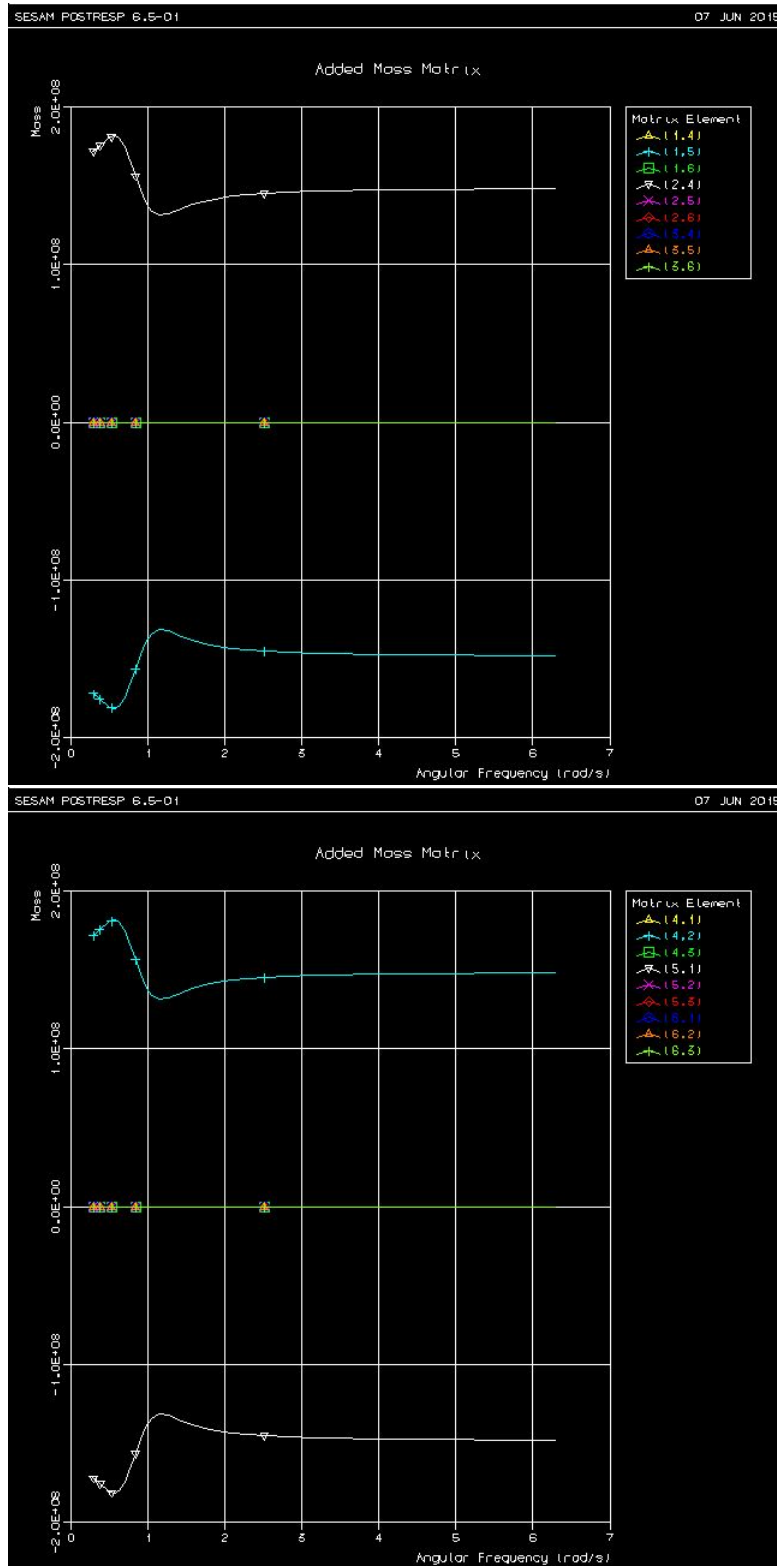


Figure A.3: Added mass; Force rotation and moment translation mode

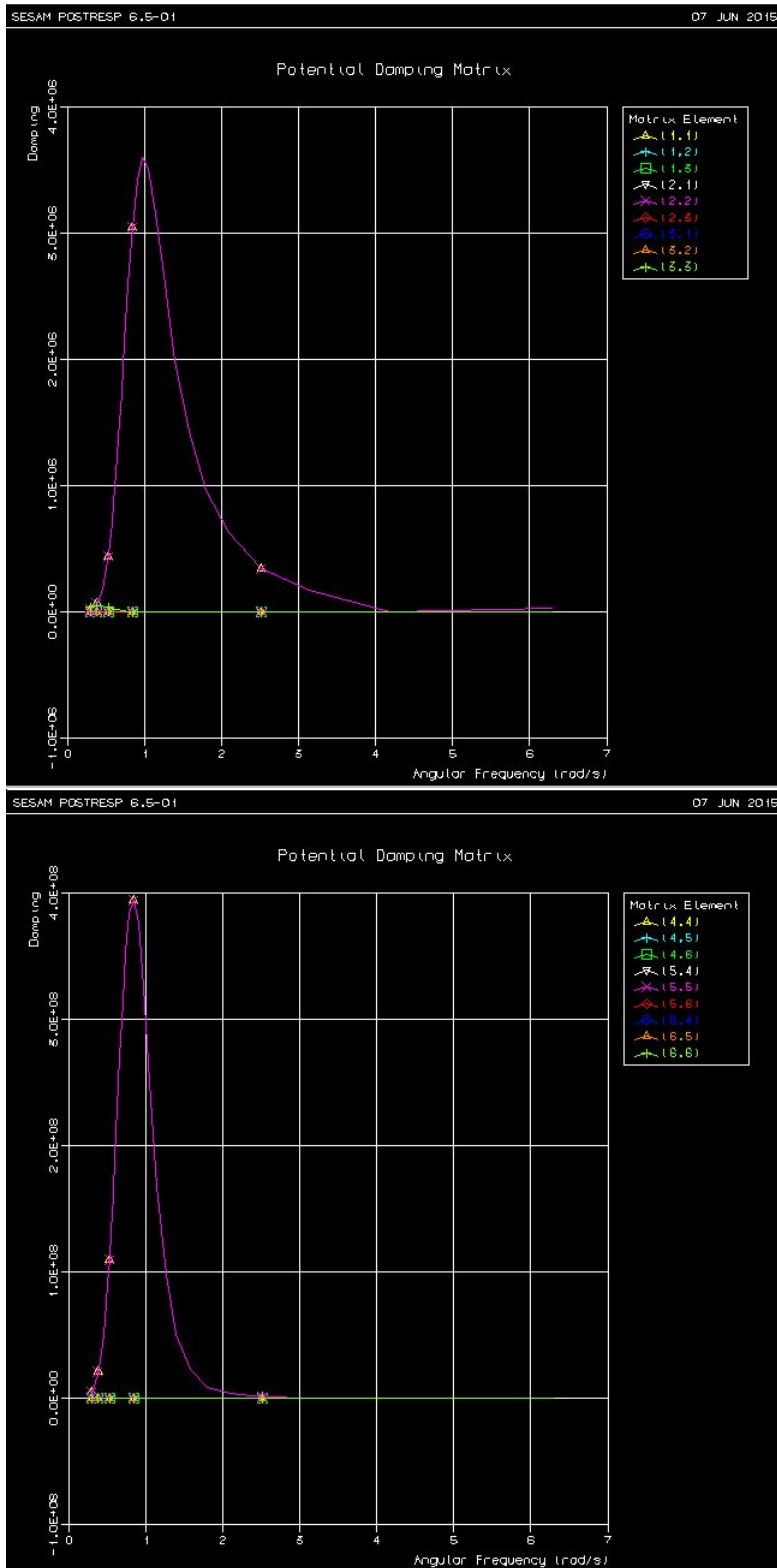


Figure A.4: Potential damping; Force translation and moment rotation mode

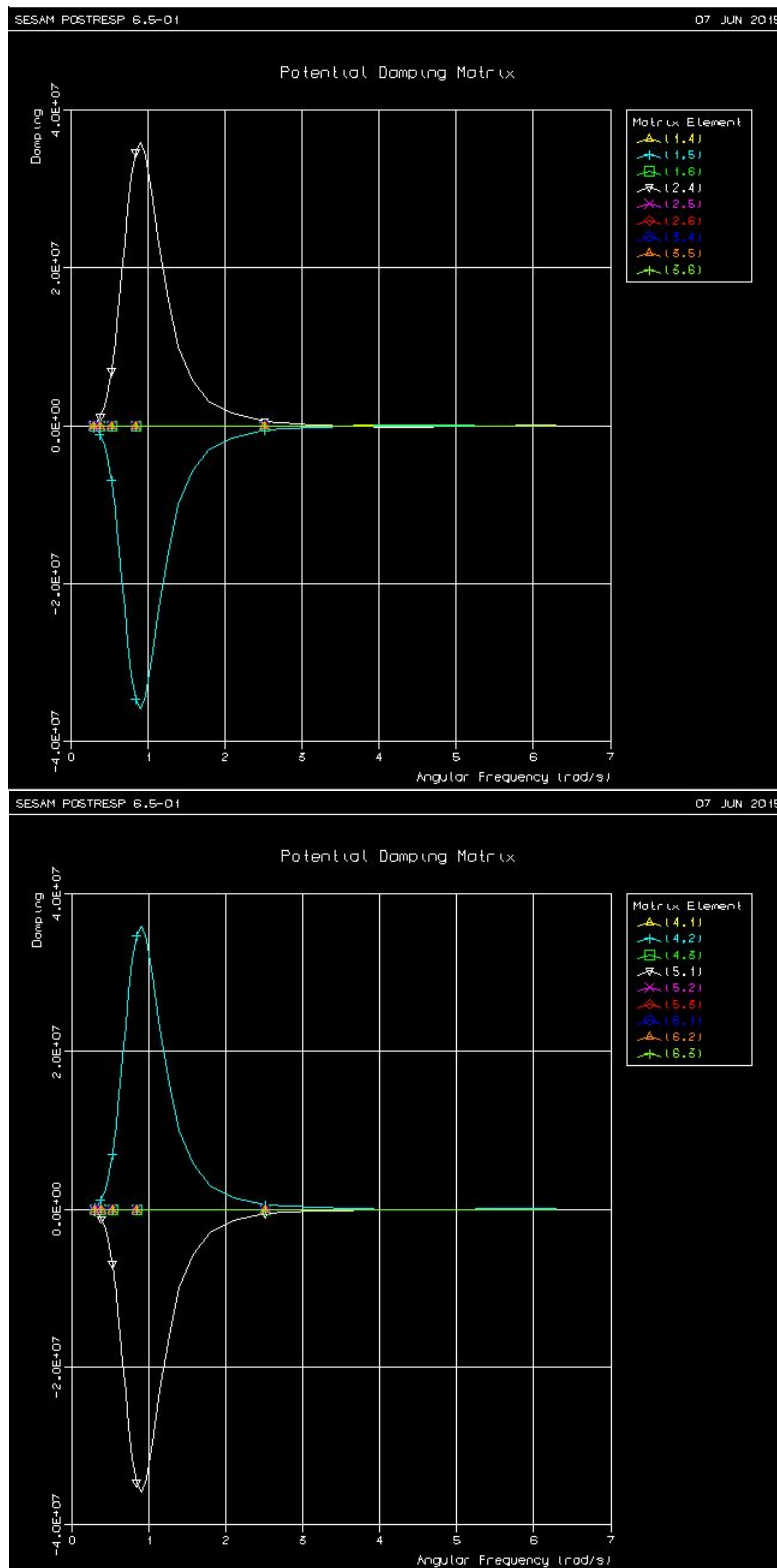


Figure A.5: Potential damping; Force rotation and moment translation mode

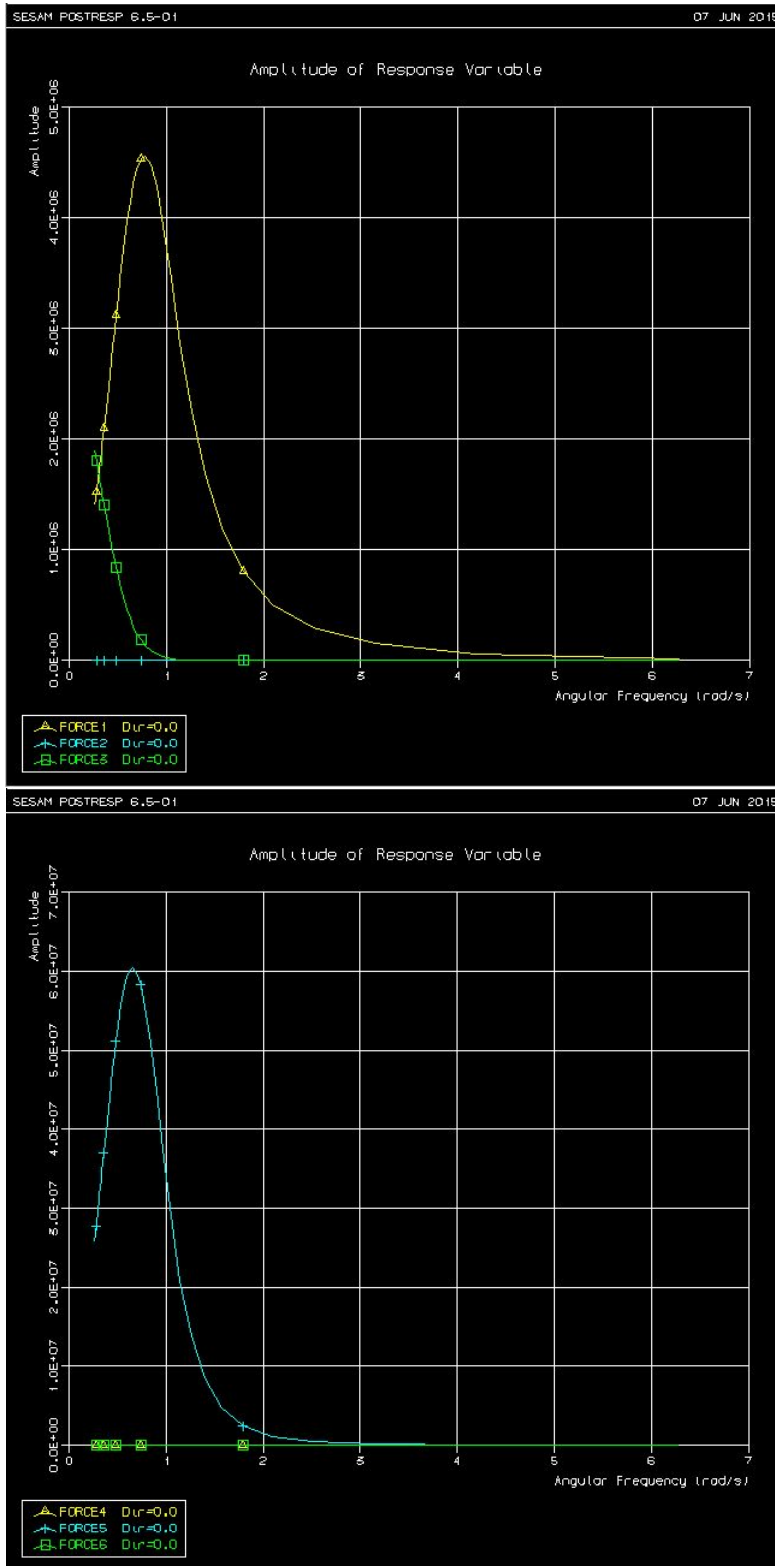


Figure A.6: Excitation forces and moments from HydroD (Postresp)

Appendix B

Decay Test

The plots from the time domain response of the decay test are presented in the following section of the appendix. The post processing module of SIMA has been used to produce these plots. The test parameters used are presented in table 7.1.

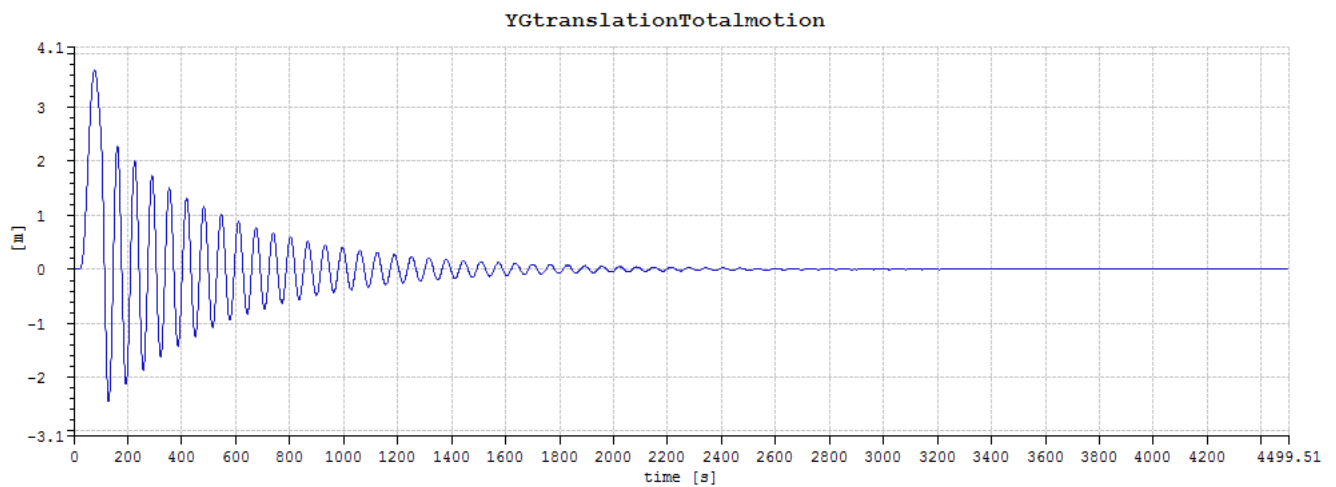


Figure B.1: Decay test: Surge

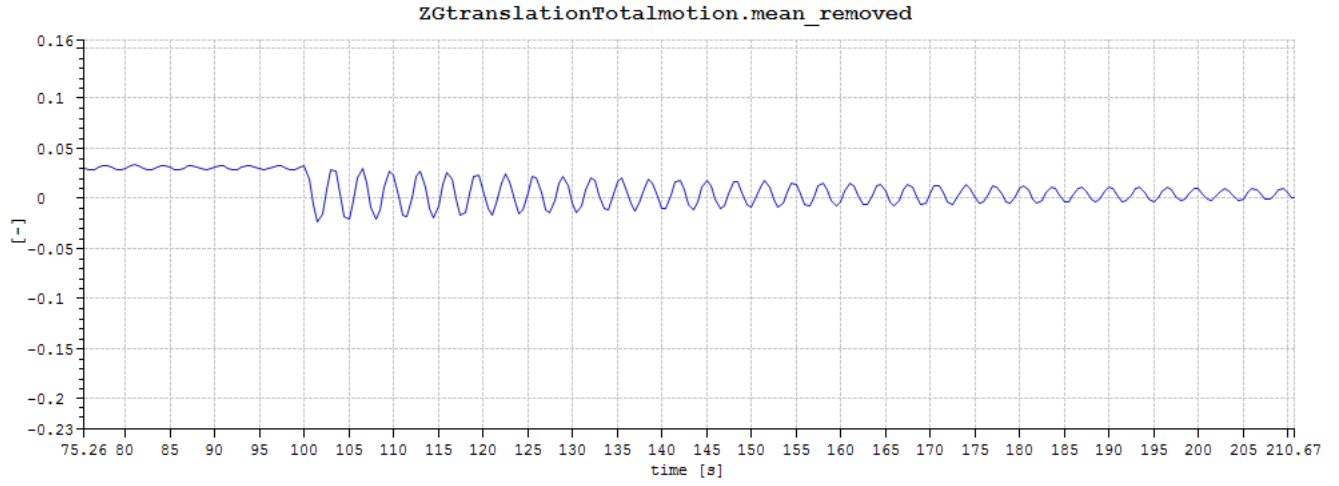


Figure B.2: Decay test: Heave

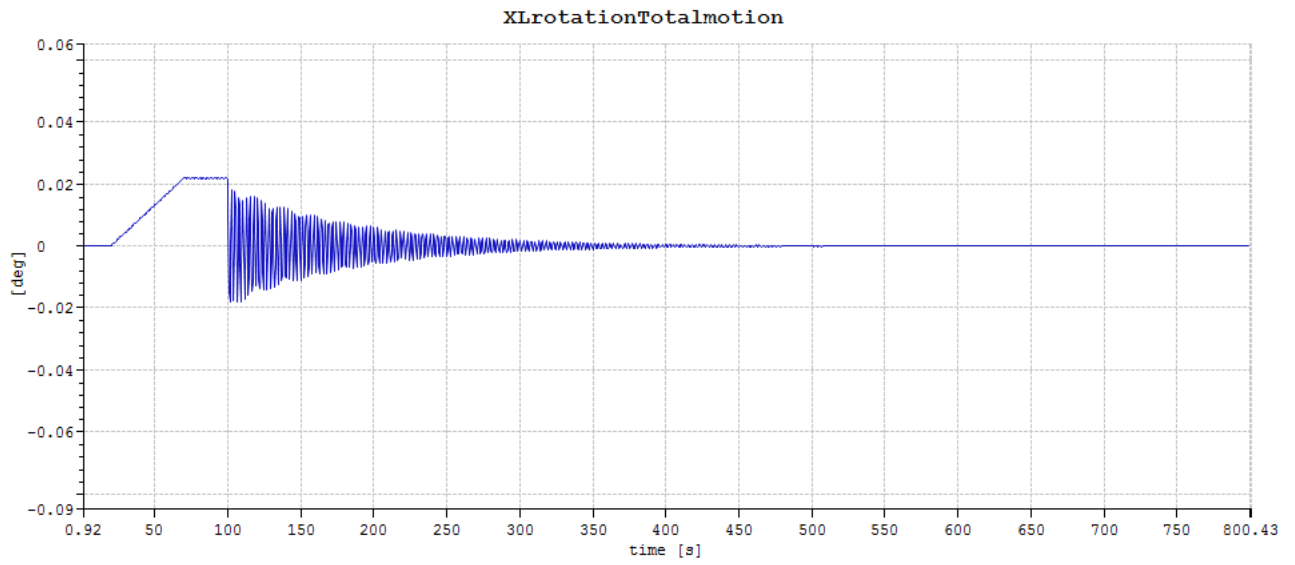


Figure B.3: Decay test: Roll

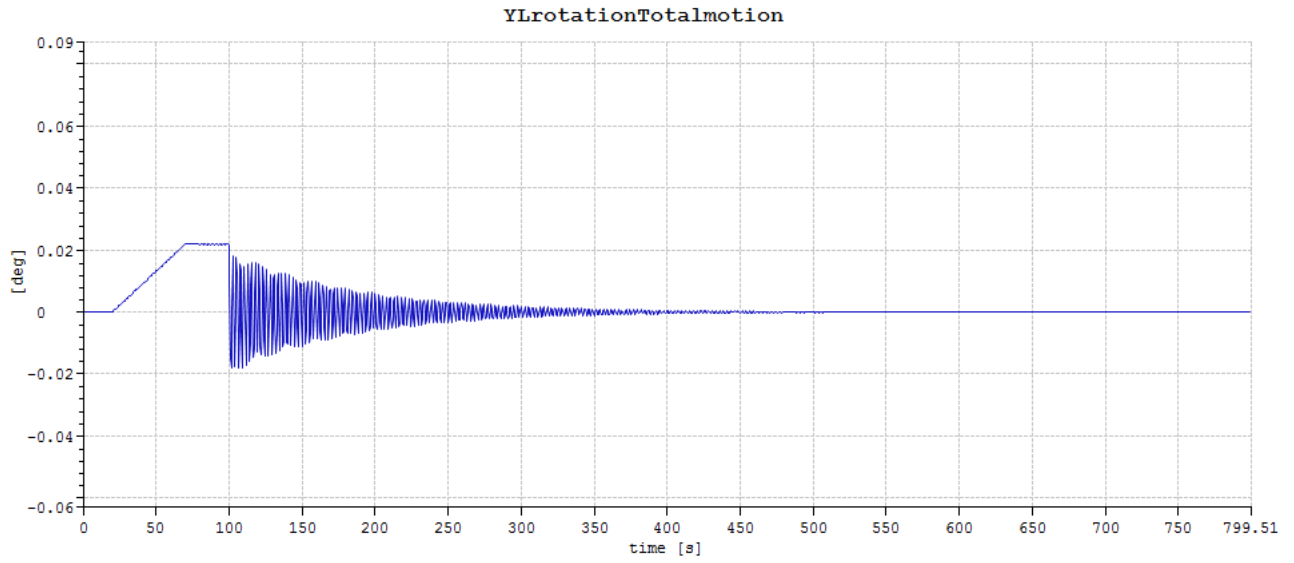


Figure B.4: Decay test: Pitch

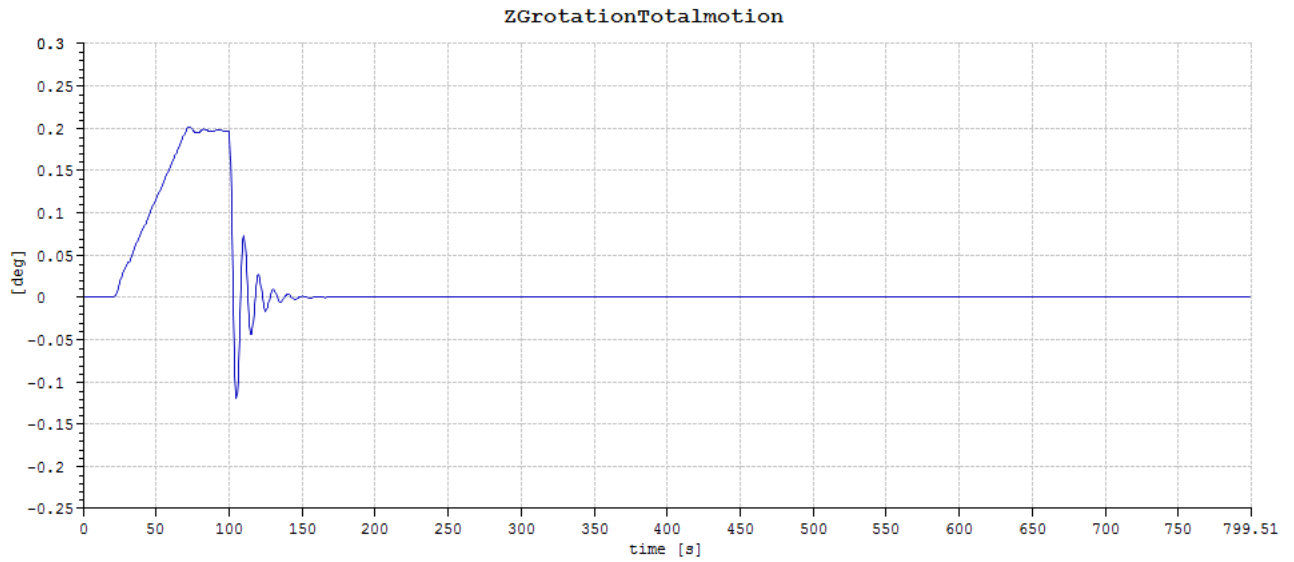


Figure B.5: Decay test: Yaw

Appendix C

Damping Calculations

Contents

- =====Decay test post-processing =====
- ===== Reading input =====
- ===== Calculating Damping Ratio =====

```
clc
```

```
clear all
```

```
==== Decay test post-processing =====
```

```
Written By Sindre Moldenhagen
```

```
===== Reading input =====
```

```
formatSpec='%f %f';
```

```
sizeA=[2 inf];
```

```
%-----Input from concept model -----
```

```
surgeid = fopen('decay_surge.dat','r');
```

```
%swayid = fopen('decay_sway.dat','r');
%heaveid = fopen('decay_heave.dat','r');
%rollid = fopen('decay_roll.dat','r');
%pitchid = fopen('decay_pitch.dat','r');
%yawid = fopen('decay_yaw.dat','r');

m1 = fscanf(surgeid,formatSpec,sizeA);
%m2 = fscanf(swayid,formatSpec,sizeA);
%m3 = fscanf(heaveid,formatSpec,sizeA);
%m4 = fscanf(rollid,formatSpec,sizeA);
%m5 = fscanf(pitchid,formatSpec,sizeA);
%m6 = fscanf(yawid,formatSpec,sizeA);

A1=m1';
%A2=m2';
%A3=m3';
%A4=m4';
%A5=m5';
%A6=m6';

%_____Input from reference model _____

%surgeidref = fopen('decay_surgeref.dat','r');
%swayidref = fopen('decay_swayref.dat','r');
%heaveidref = fopen('decay_heaveref.dat','r');
%rollidref = fopen('decay_rollref.dat','r');
%pitchidref = fopen('decay_pitchref.dat','r');
%yawidref = fopen('decay_yawref.dat','r');
```

```
%m1ref = fscanf(surgeidref,formatSpec,sizeA);
%m2ref = fscanf(swayidref,formatSpec,sizeA);
%m3ref = fscanf(heaveidref,formatSpec,sizeA);
%m4ref = fscanf(rollidref,formatSpec,sizeA);
%m5ref = fscanf(pitchidref,formatSpec,sizeA);
%m6ref = fscanf(yawidref,formatSpec,sizeA);

%A1ref=m1ref';
%A2ref=m2ref';
%A3ref=m3ref';
%A4ref=m4ref';
%A5ref=m5ref';
%A6ref=m6ref';

%==== Removing start-up period =====

Y1=A1(20:900,2);
T1=0.5:0.5:0.5*length(Y1);

%Y2=A2(20:950,2);
%T2=0.5:0.5:0.5*length(Y2);

%Y3=A3(20:350,2);
%T3=0.5:0.5:0.5*length(Y3);

%Y4=A4(20:950,2);
%T3=0.5:0.5:0.5*length(Y4);

%Y5=A5(20:950,2);
%T5=0.5:0.5:0.5*length(Y5);
```

```
%Y6= A3(20:450,2);
%T6=0.5:0.5:0.5*length(Y6);

%_____

%Y1ref=A1ref(20:950,2);
%T1ref=0.5:0.5:0.5*length(Y1ref);

%Y2ref=A2ref(20:950,2);
%T2ref=0.5:0.5:0.5*length(Y2ref);

%Y3ref=A3ref(20:350,2);
%T3ref=0.5:0.5:0.5*length(Y3ref);

%Y4ref=A4ref(20:950,2);
%T4ref=0.5:0.5:0.5*length(Y4ref);

%Y5ref=A5ref(20:950,2);
%T5ref=0.5:0.5:0.5*length(Y5ref);

%Y6ref= A3ref(20:450,2);
%T6ref=0.5:0.5:0.5*length(Y6ref);

%==== Finding peaks and location of peaks =====

[pk1,locs1]=findpeaks(Y1);
[i1,p1]=size(pk1);

%[pk2,locs2]=findpeaks(Y2);
```



```
%[i2,p2]=size(pks2);

%[pks3,locs3]=findpeaks(Y3);
%[i3,p3]=size(pks3);

%[pks4,locs4]=findpeaks(Y4);
%[i4,p4]=size(pks4);

%[pks5,locs5]=findpeaks(Y5);
%[i5,p5]=size(pks5);

%[pks6,locs6]=findpeaks(Y6);
%[i6,p6]=size(pks6);
%_____

%[pks1ref,locs1ref]=findpeaks(Y1ref);
%[i1ref,p1ref]=size(pks1ref);

%[pks2ref,locs2ref]=findpeaks(Y2ref);
%[i2ref,p2ref]=size(pks2ref);

%[pks3ref,locs3ref]=findpeaks(Y3ref);
%[i3ref,p3ref]=size(pks3ref);

%[pks4ref,locs4ref]=findpeaks(Y4ref);
%[i4ref,p4ref]=size(pks4ref);

%[pks5ref,locs5ref]=findpeaks(Y5ref);
%[i5ref,p5ref]=size(pks5ref);
```

```

%[pks6ref,locs6ref]=findpeaks(Y6ref);
%[i6ref,p6ref]=size(pks6ref);

```

= Calculating Damping Ratio =====

From SIMA, The natural periods are defined by their respective response spectrums.

```

T_n1 = 78.6;
T_n2 = 64;
T_n3 = 3;
T_n4 = 2.56;
T_n5 = 2.56;
T_n6 = 9.58;

```

```

T_n1ref = 73.5;
T_n2ref = 63;
T_n3ref = 2.5;
T_n4ref = 1.82;
T_n5ref = 1.82;
T_n6ref = 9.14;

```

```

for j=1:i1-1
delta1(j)= log(pks1(j)/pks1(j+1));
lambda1(j)= delta1(j)/(sqrt(4*pi^2+delta1(j)^2));
xaxisi1(j)=(pks1(j)+pks1(j+1))/2;
end

```

```

%==== Calculation Linear and quadratic damping coefficients =====

```

```
id    = ((4*pi)/T_n1)*lambda1
b_e1  = fliplr(id);
dum1  = 16*pks1/(3*T_n1);
dum2  = dum1(1:length(b_e1));
dum3  = dum2';
x_be1=fliplr(dum3)
scatter(x_be1,b_e1)

id =
```

```
0.0122    0.0034    0.0035    0.0035    0.0034    0.0035
```

```
x_be1 =
```

```
0.0903    0.1032    0.1186    0.1360    0.1551    0.2504
```


Appendix D

Response Spectra

D.0.1 Case 1

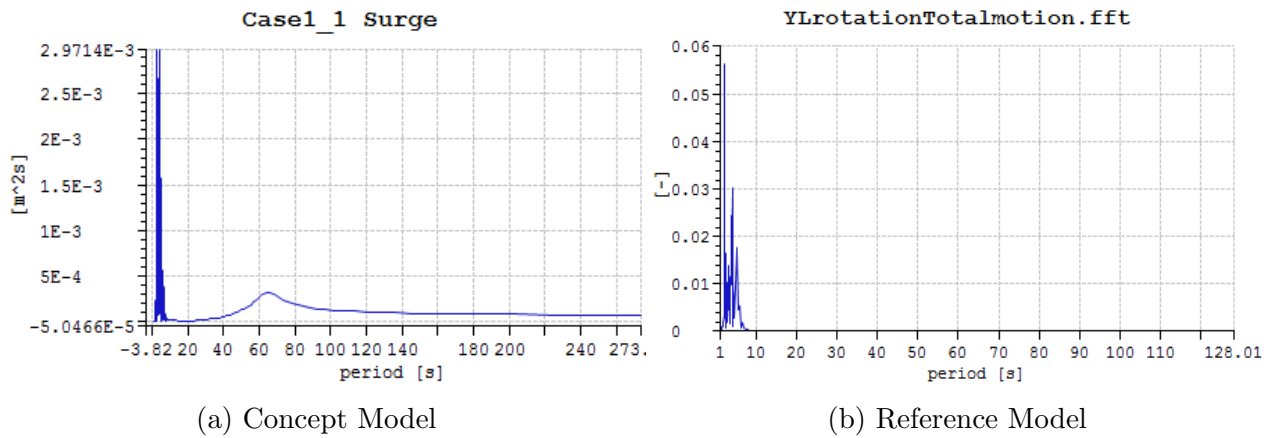


Figure D.1: Surge spectra for C1-1

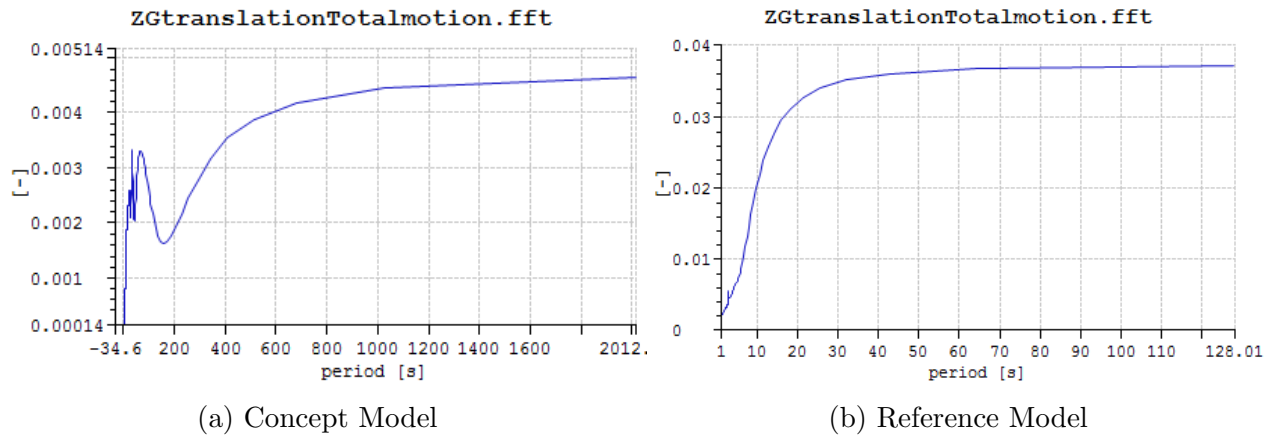


Figure D.2: heave spectra for C1-1

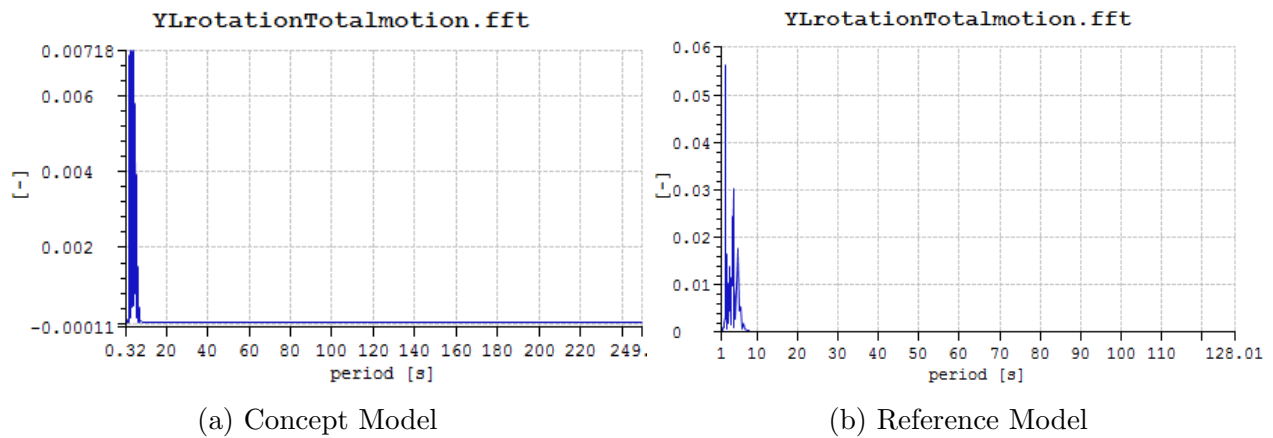


Figure D.3: Pitch spectra for C1-1

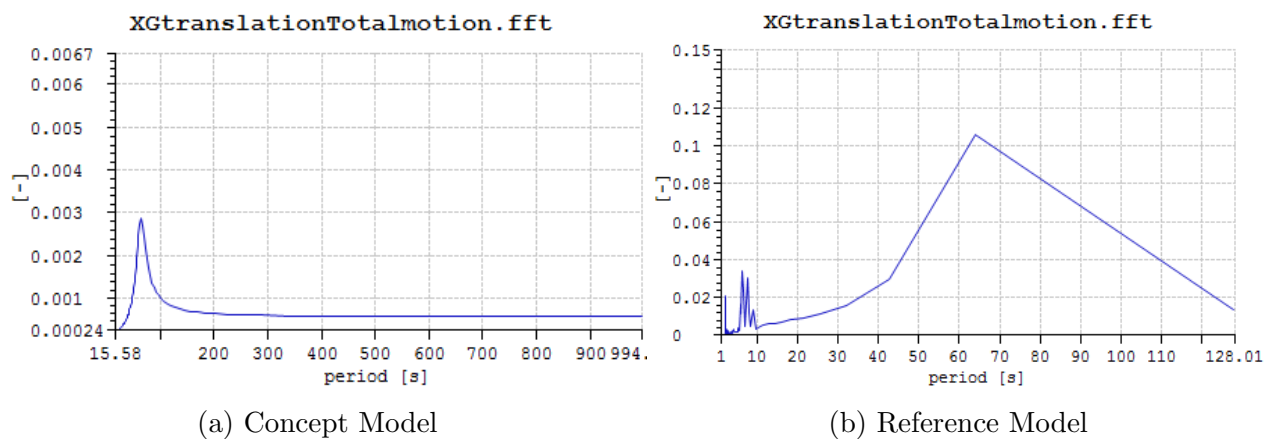


Figure D.4: Surge spectra for C1-2

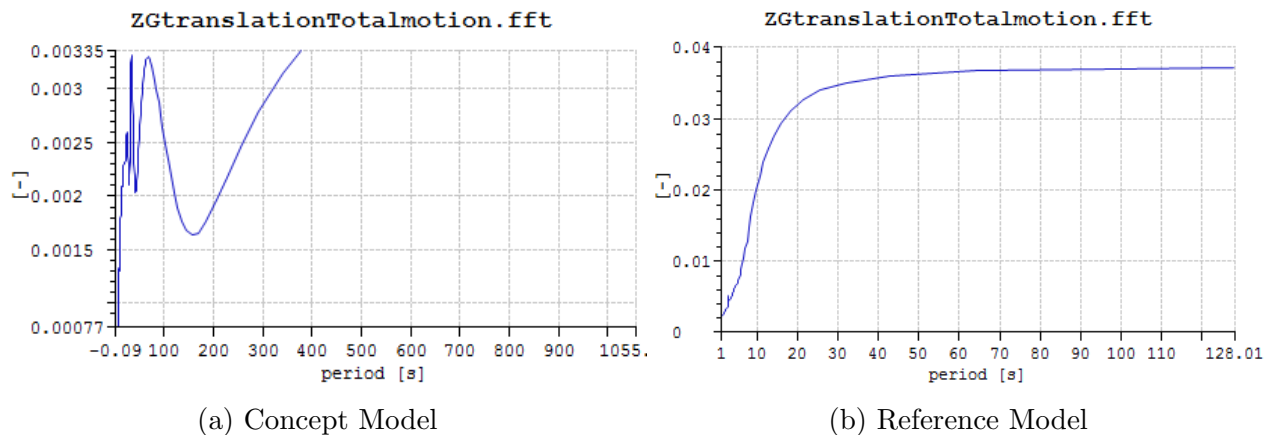


Figure D.5: heave spectra for C1-2

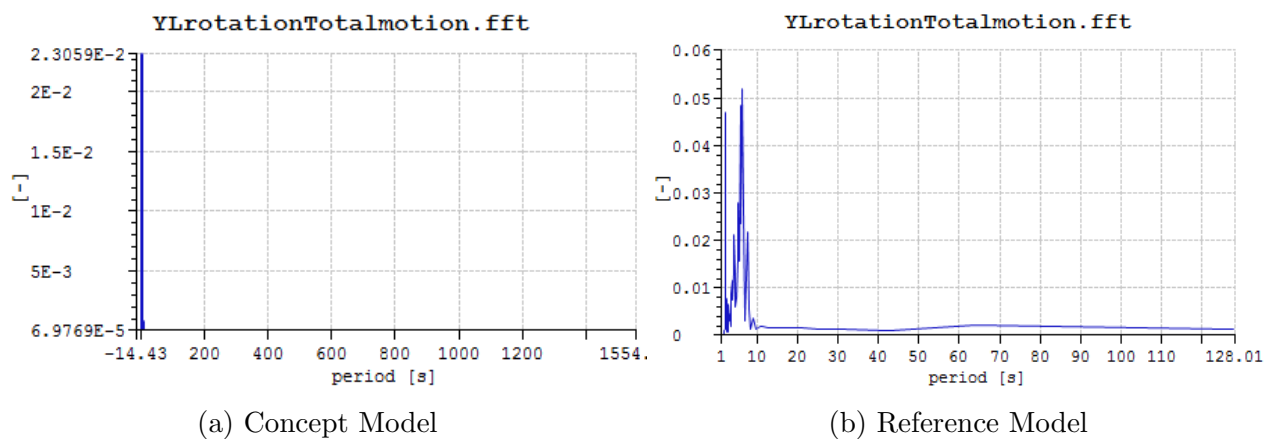


Figure D.6: Pitch spectra for C1-2

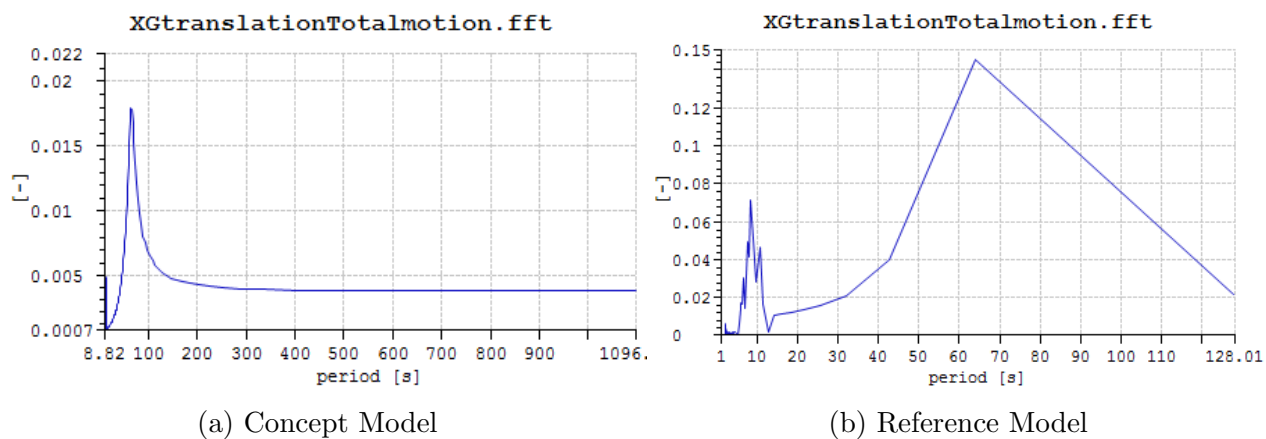


Figure D.7: Surge spectra for C1-3

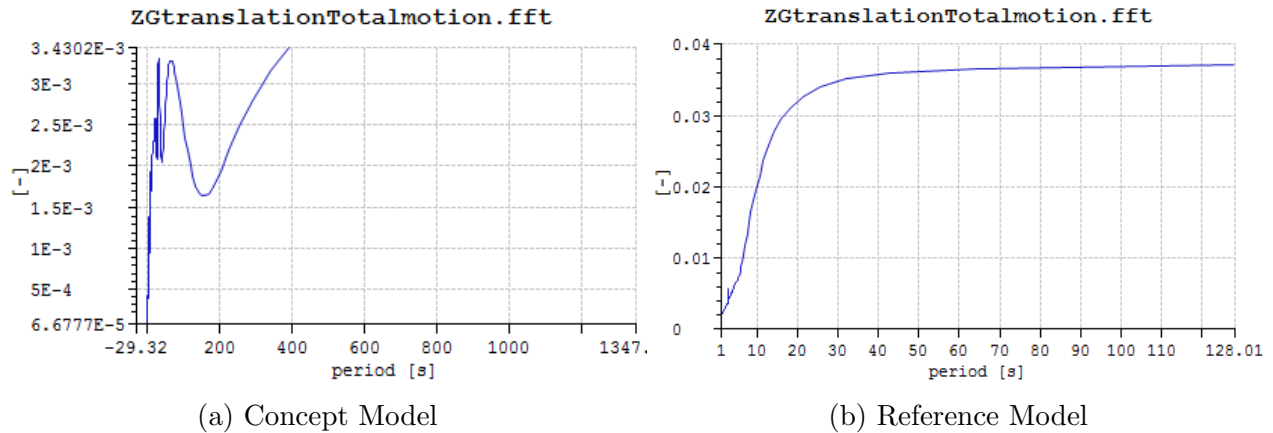


Figure D.8: heave spectra for C1-3

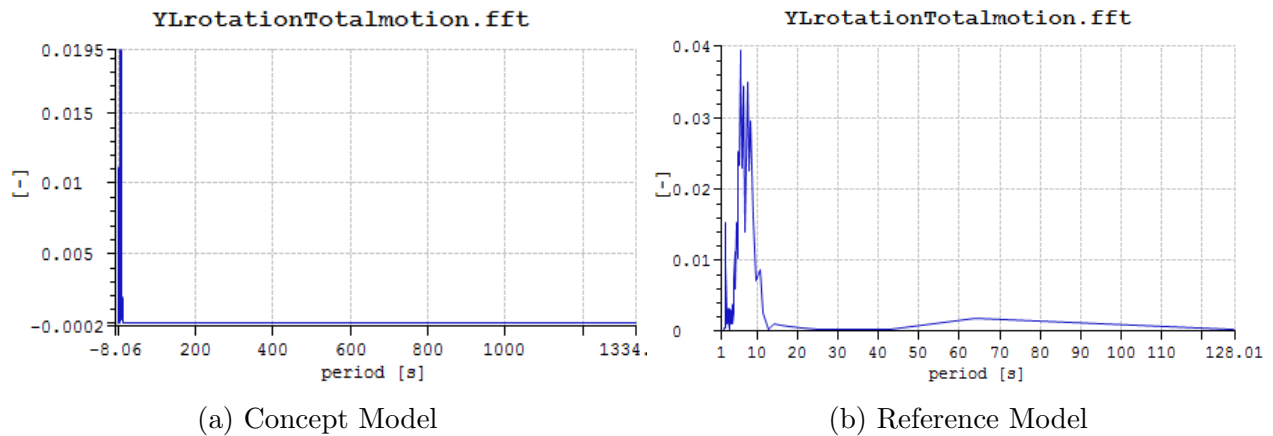


Figure D.9: Pitch spectra for C1-3

D.0.2 Case 2

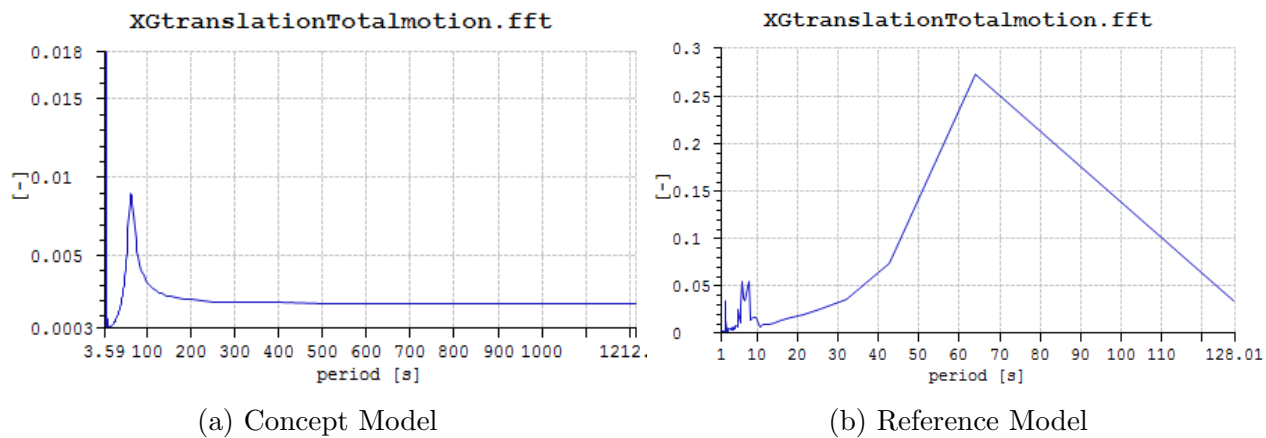


Figure D.10: Surge spectra for C2-1

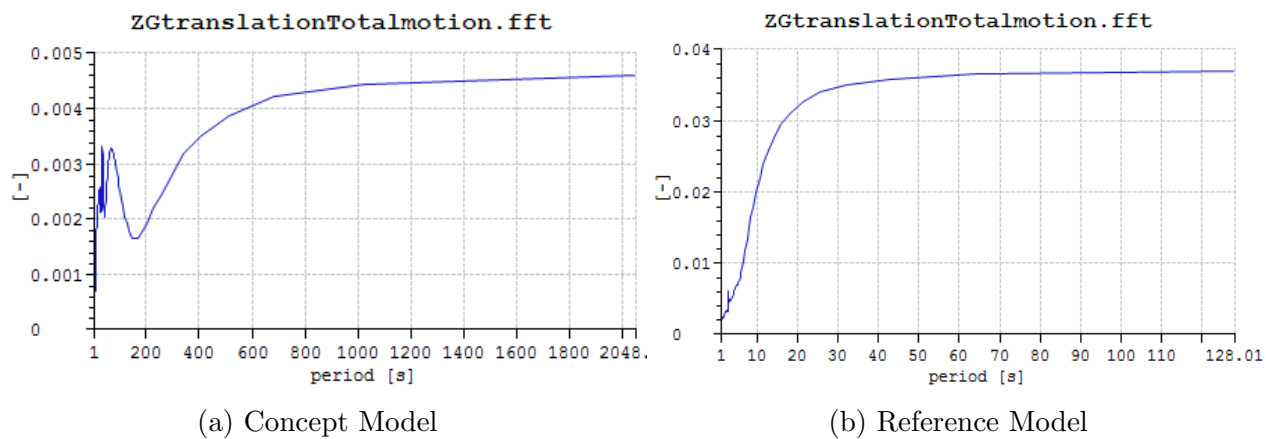


Figure D.11: heave spectra for C2-1

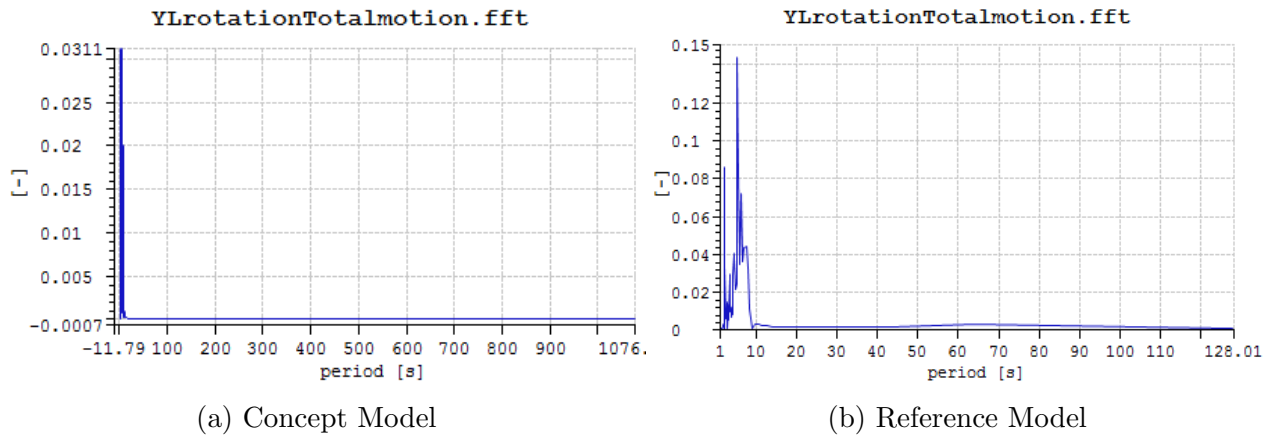


Figure D.12: Pitch spectra for C2-1

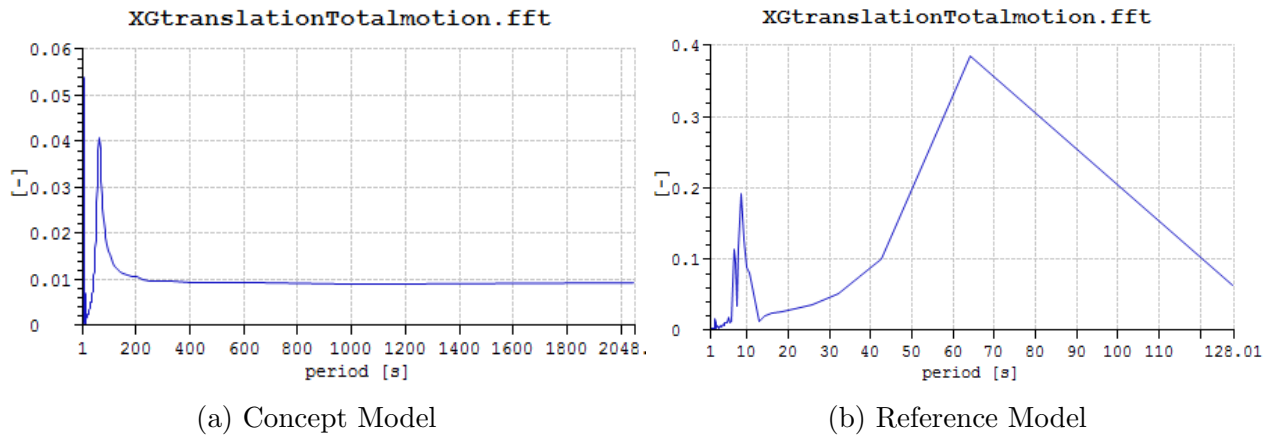


Figure D.13: Surge spectra for C2-2

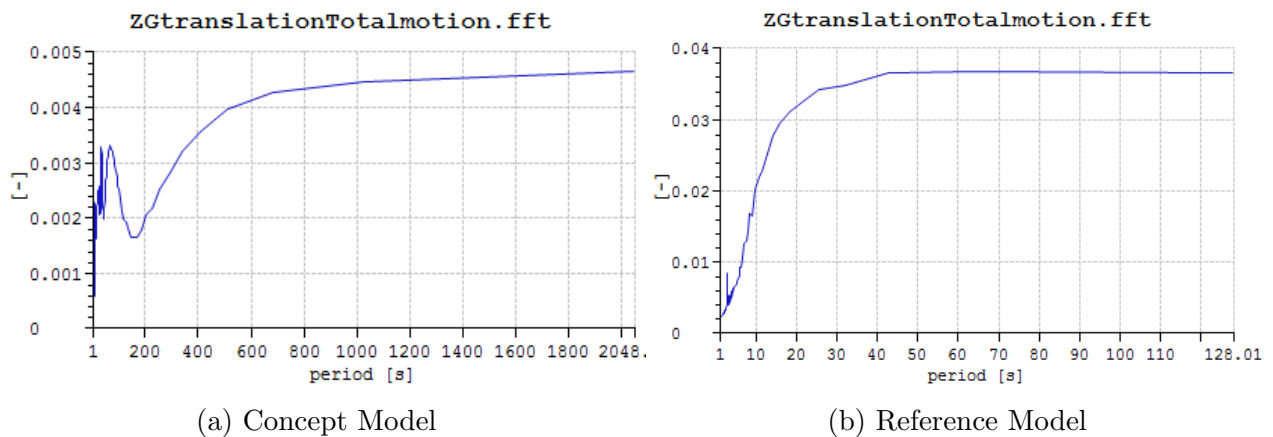


Figure D.14: heave spectra for C2-2

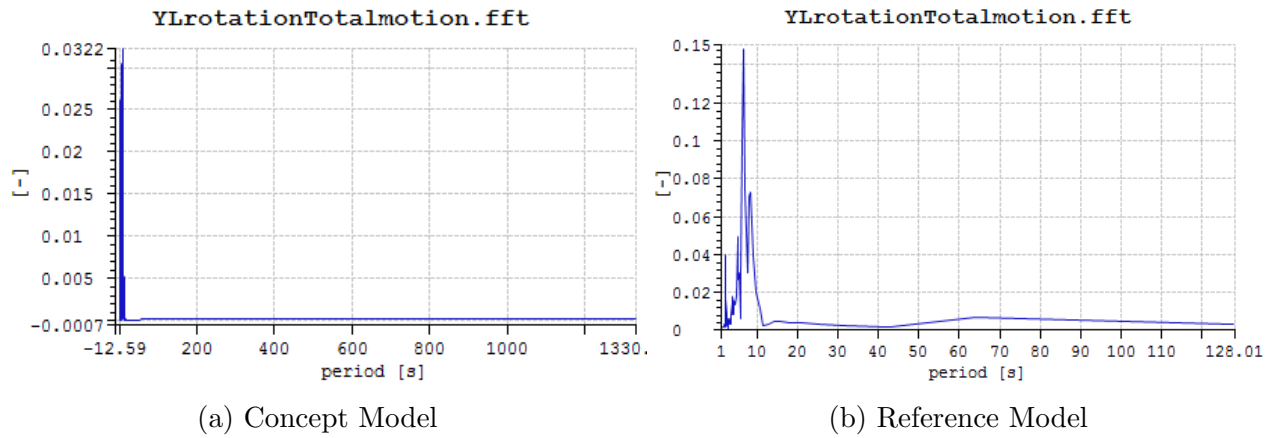


Figure D.15: Pitch spectra for C2-2

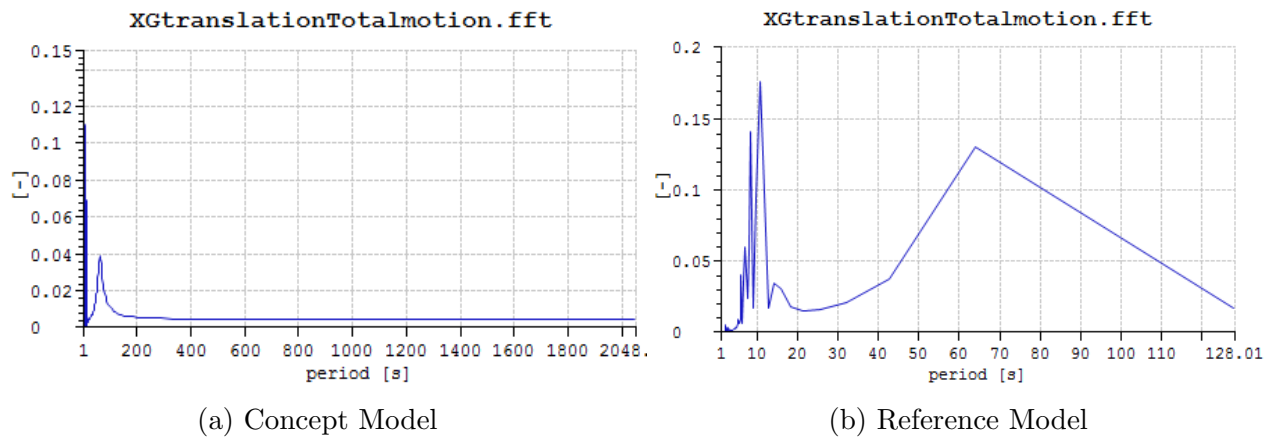


Figure D.16: Surge spectra for C2-3

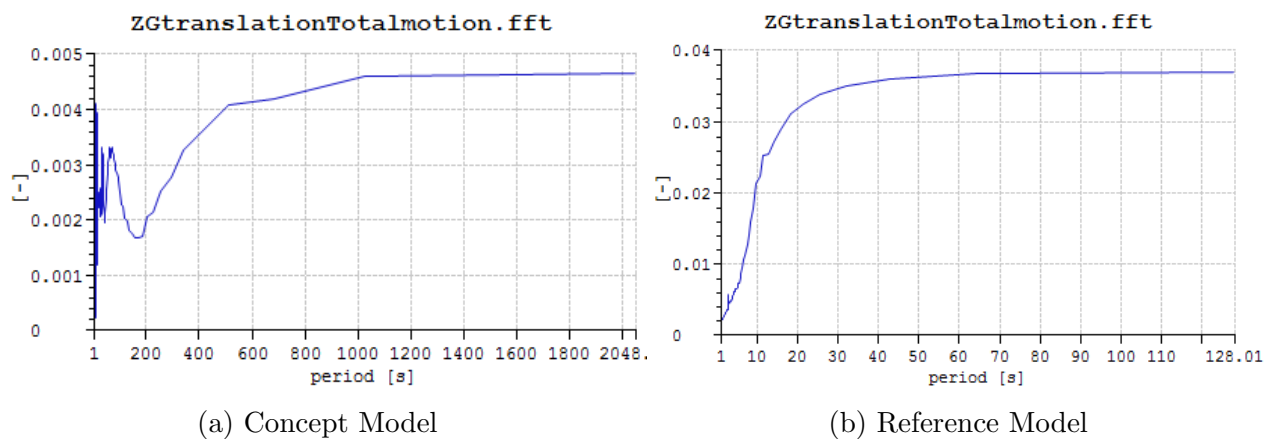


Figure D.17: heave spectra for C2-3

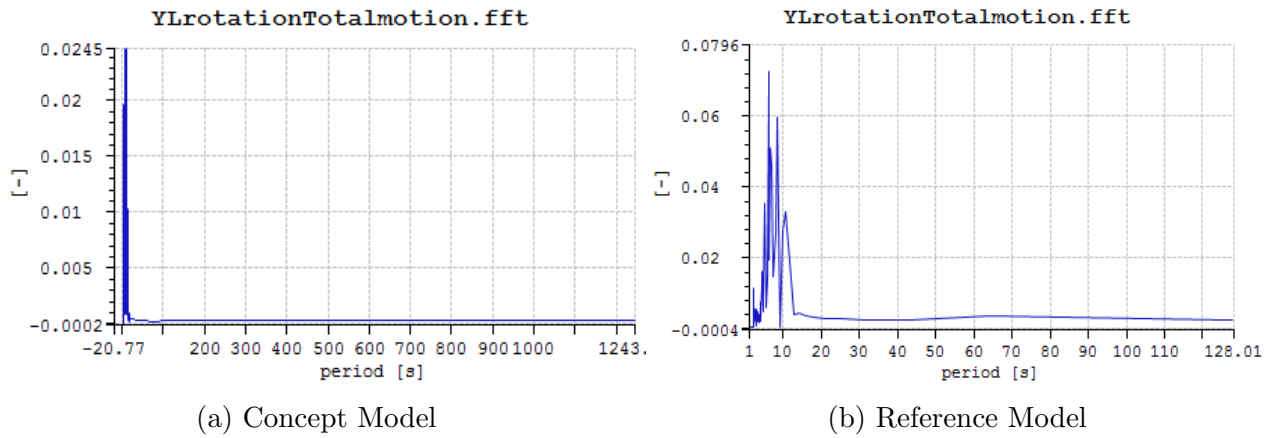


Figure D.18: Pitch spectra for C2-3

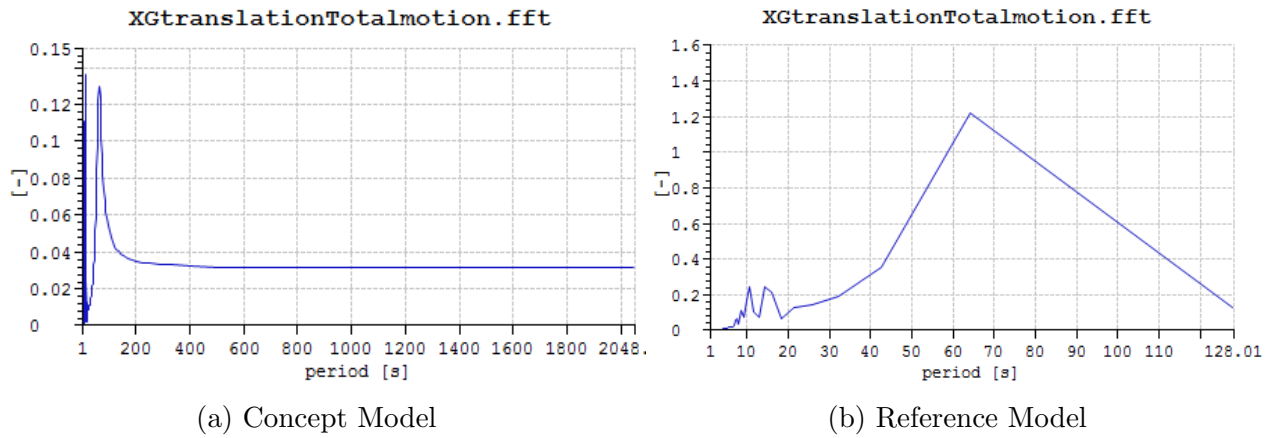


Figure D.19: Surge spectra for C2-4

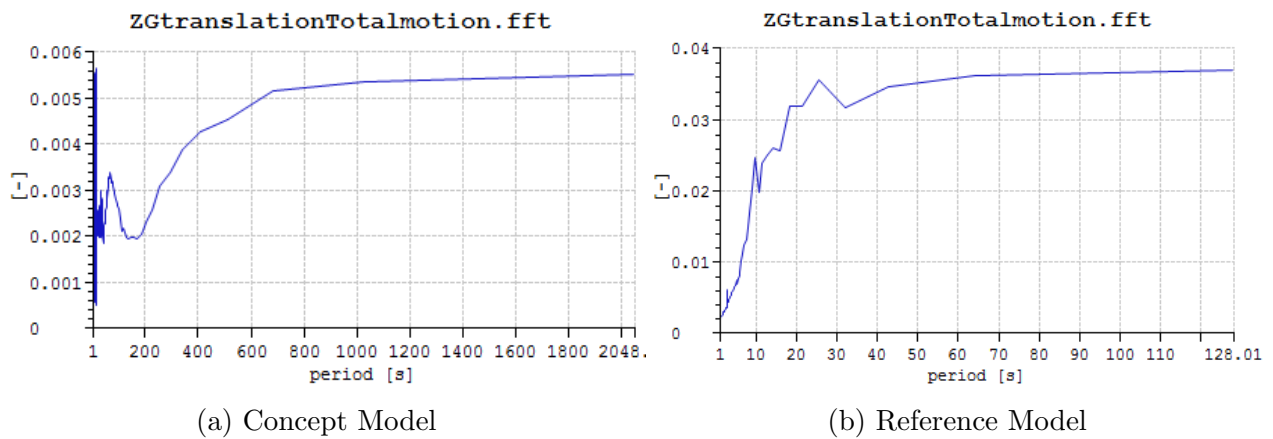


Figure D.20: heave spectra for C2-4

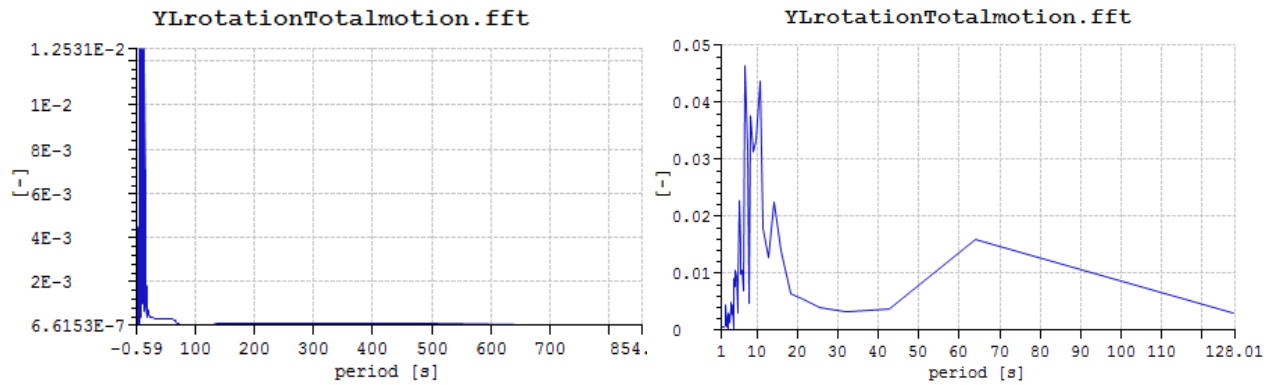


Figure D.21: Pitch spectra for C2-4

D.0.3 Case 3

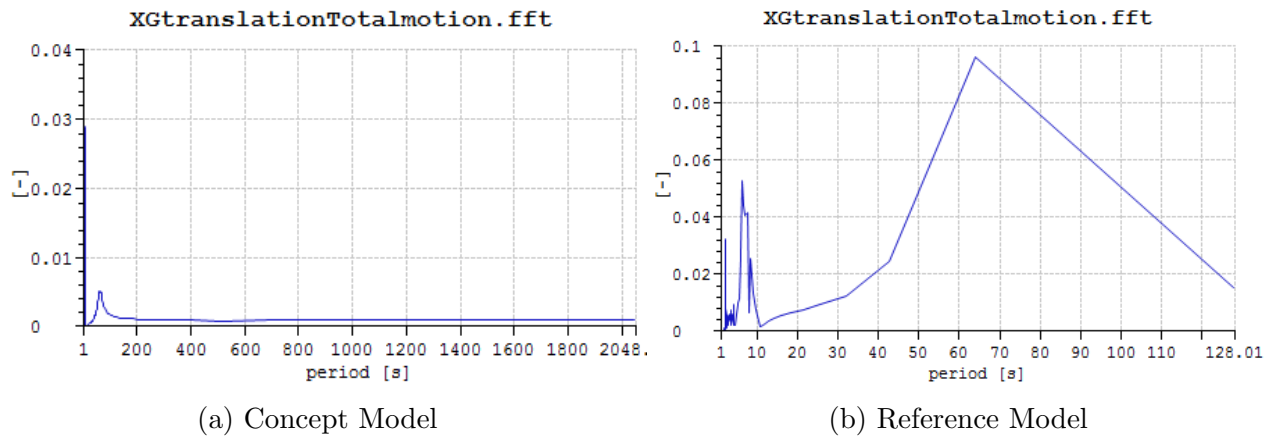


Figure D.22: Surge spectra for C3-1

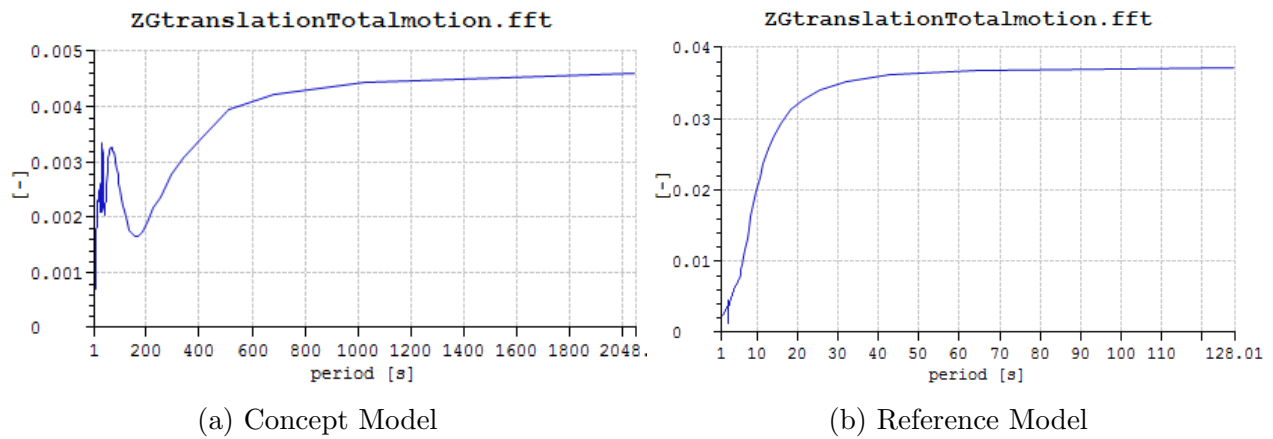
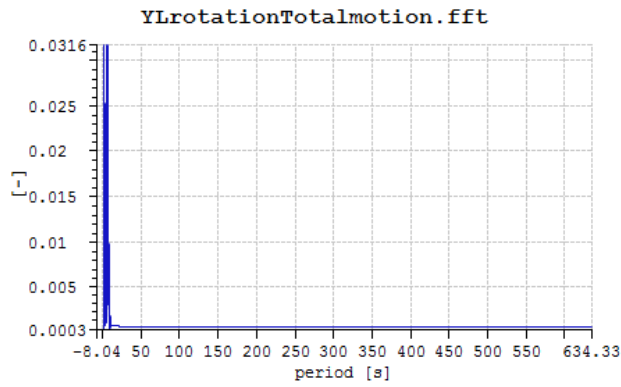
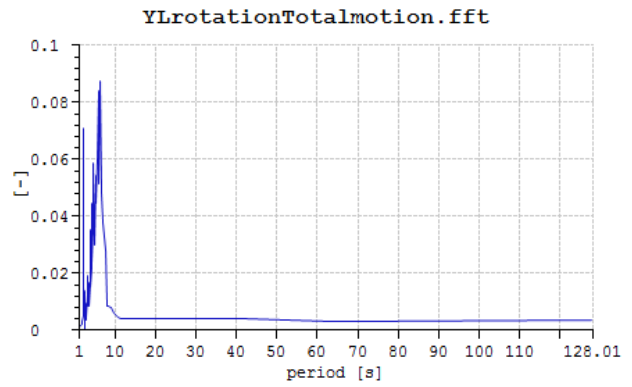


Figure D.23: heave spectra for C3-1

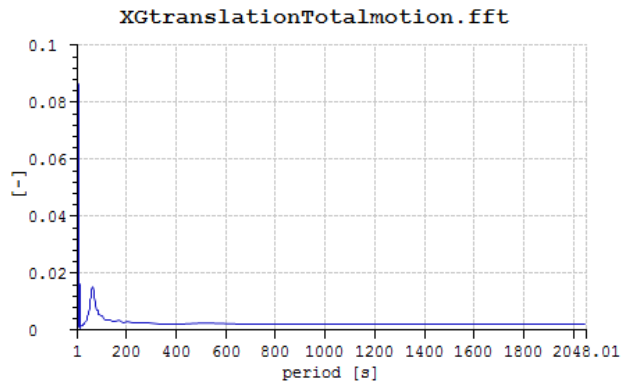


(a) Concept Model

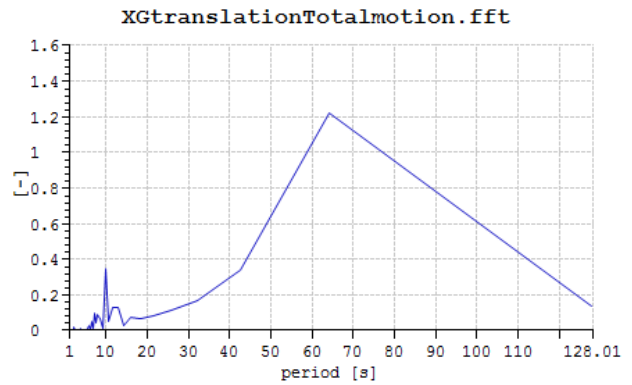


(b) Reference Model

Figure D.24: Pitch spectra for C3-1

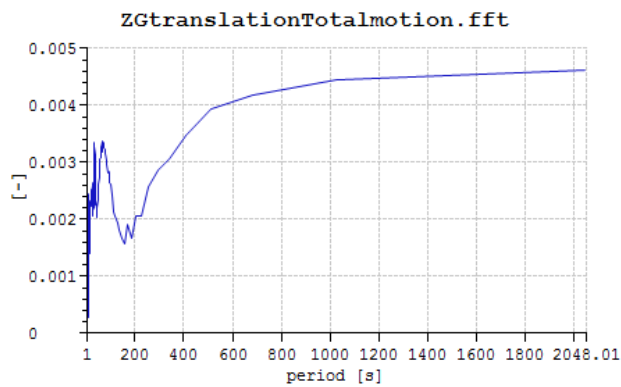


(a) Concept Model

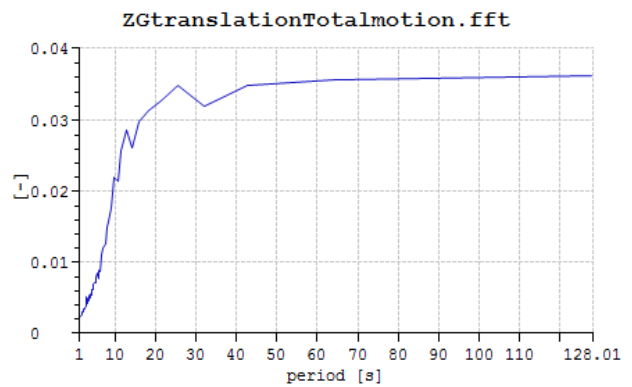


(b) Reference Model

Figure D.25: Surge spectra for C3-2



(a) Concept Model



(b) Reference Model

Figure D.26: heave spectra for C3-2

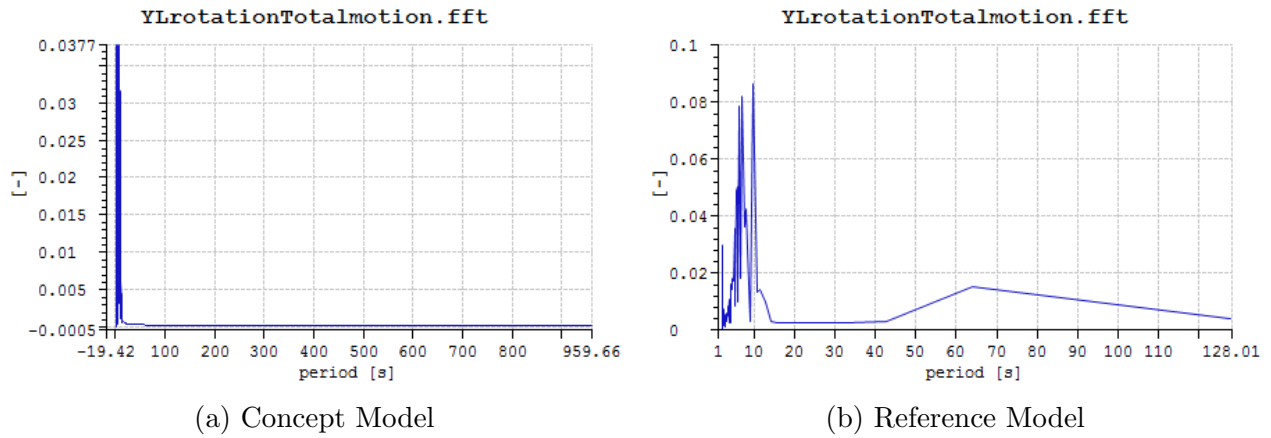


Figure D.27: Pitch spectra for C3-2

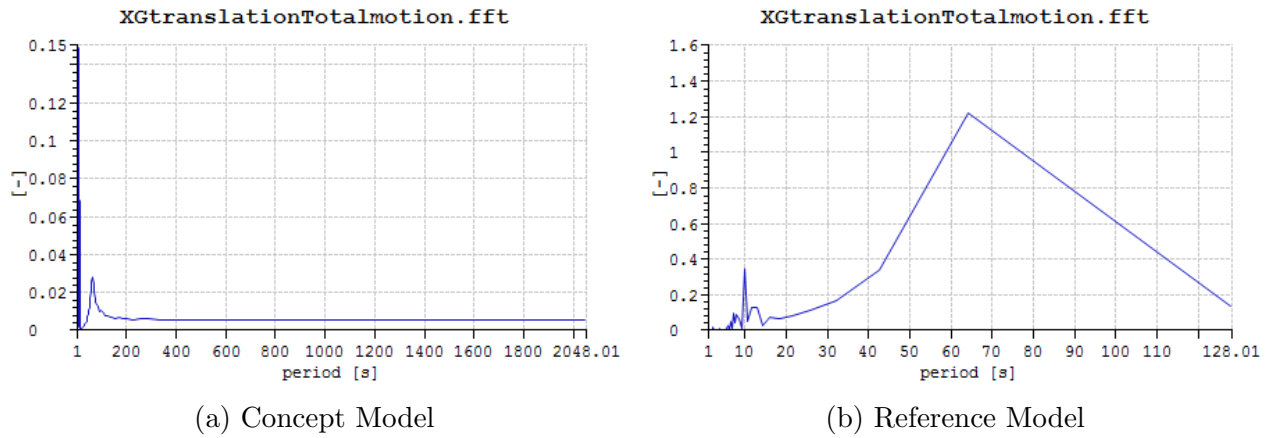


Figure D.28: Surge spectra for C3-3

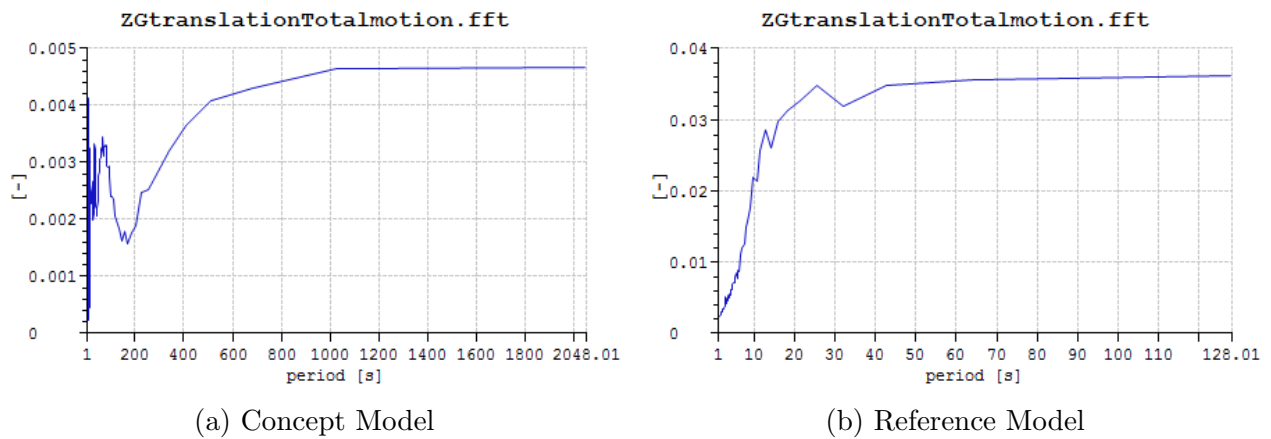
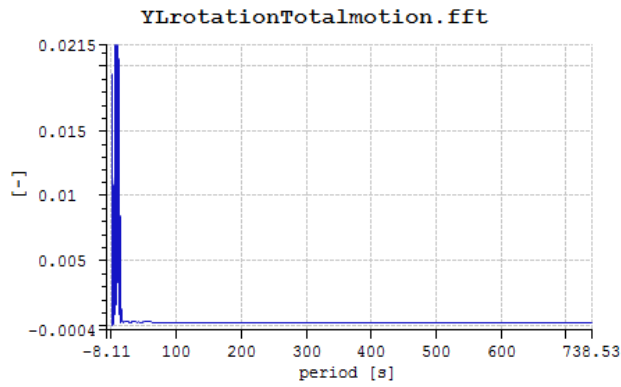
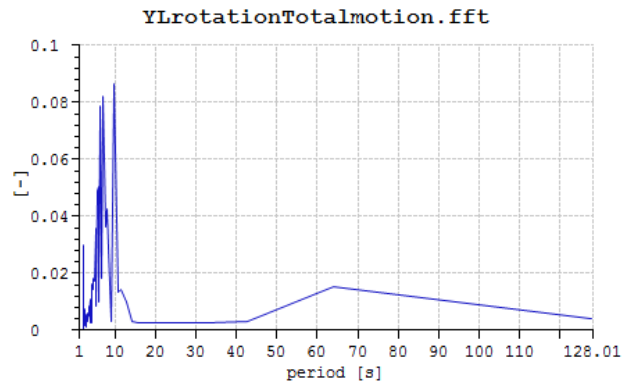


Figure D.29: heave spectra for C3-3

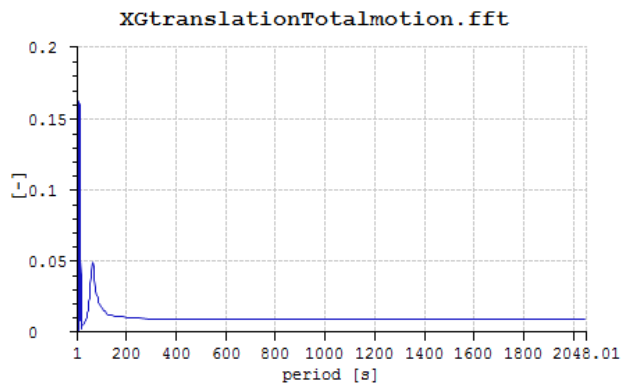


(a) Concept Model

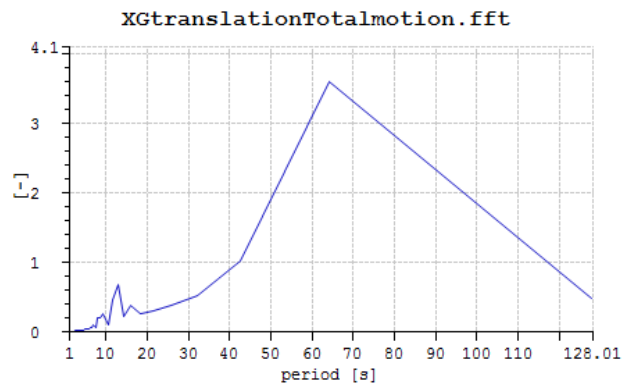


(b) Reference Model

Figure D.30: Pitch spectra for C3-3

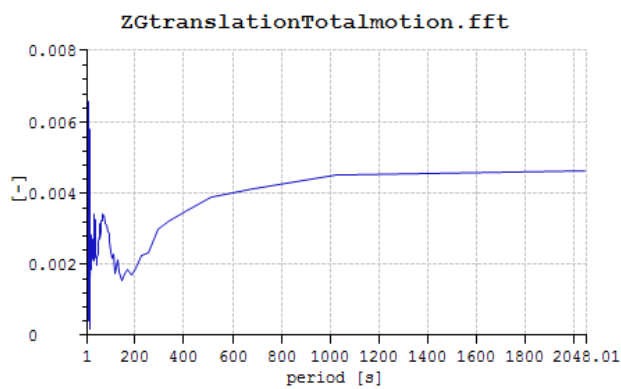


(a) Concept Model

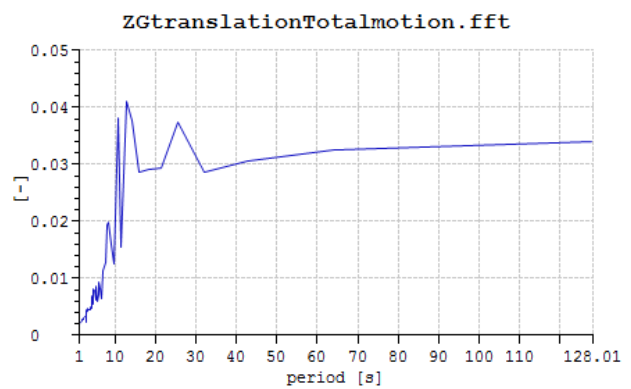


(b) Reference Model

Figure D.31: Surge spectra for C3-4

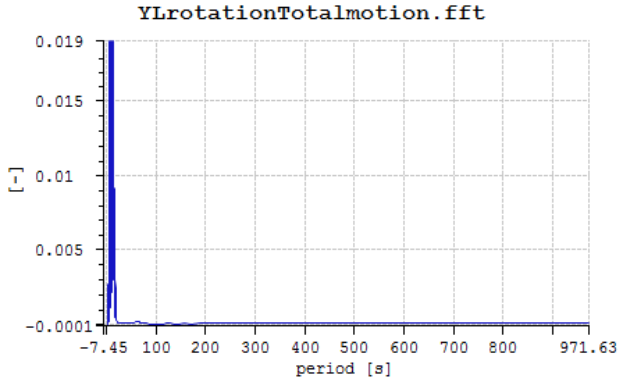


(a) Concept Model

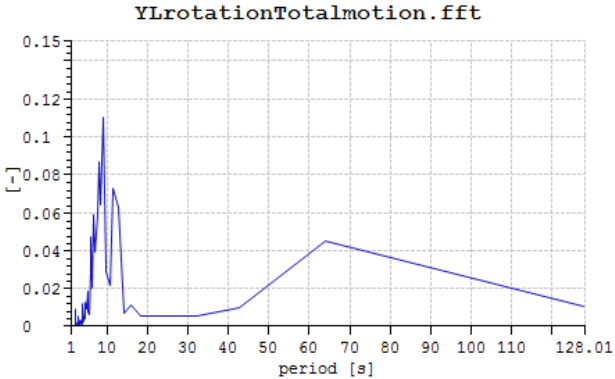


(b) Reference Model

Figure D.32: heave spectra for C3-4



(a) Concept Model



(b) Reference Model

Figure D.33: Pitch spectra for C3-4

D.0.4 Case 4

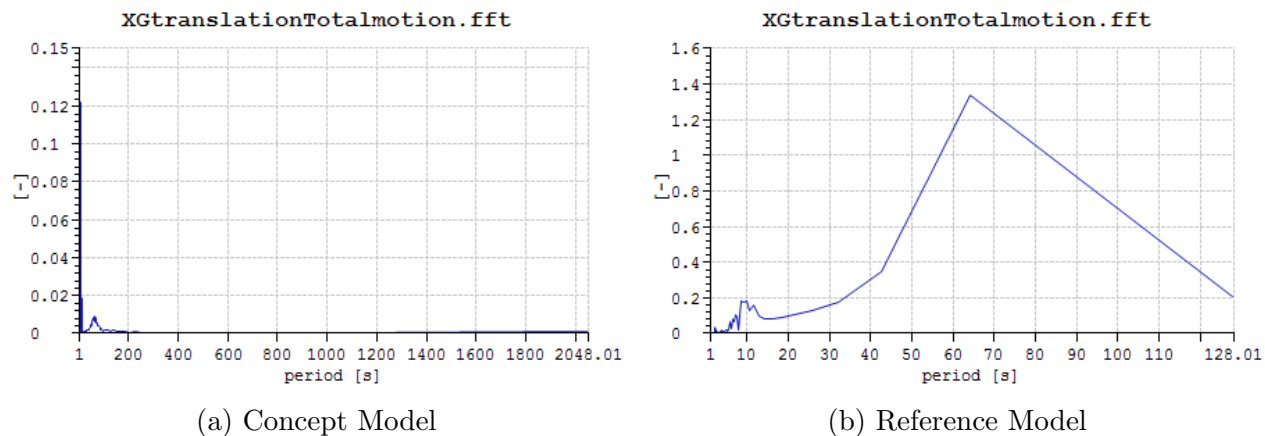


Figure D.34: Surge spectra for C4-1

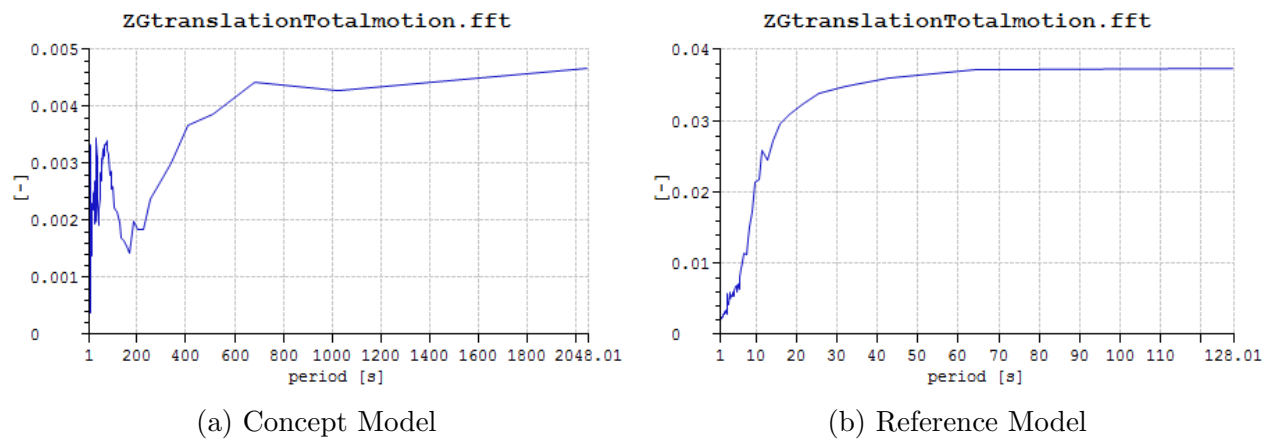


Figure D.35: heave spectra for C4-1

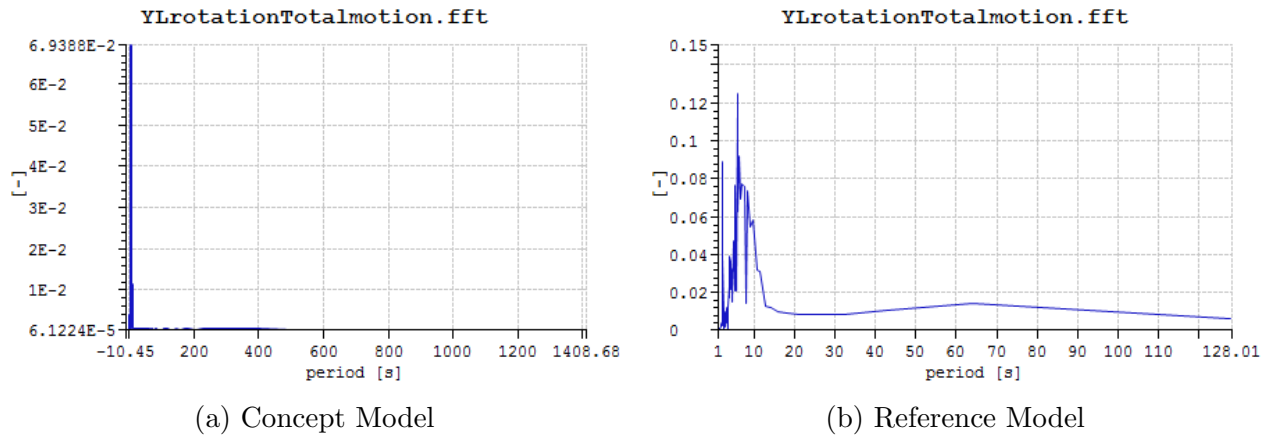


Figure D.36: Pitch spectra for C4-1

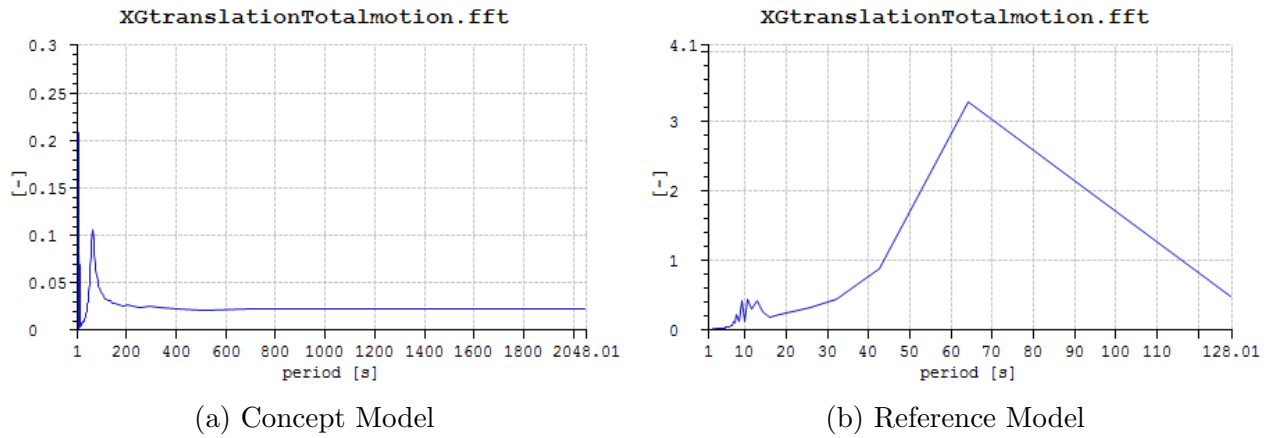


Figure D.37: Surge spectra for C4-2

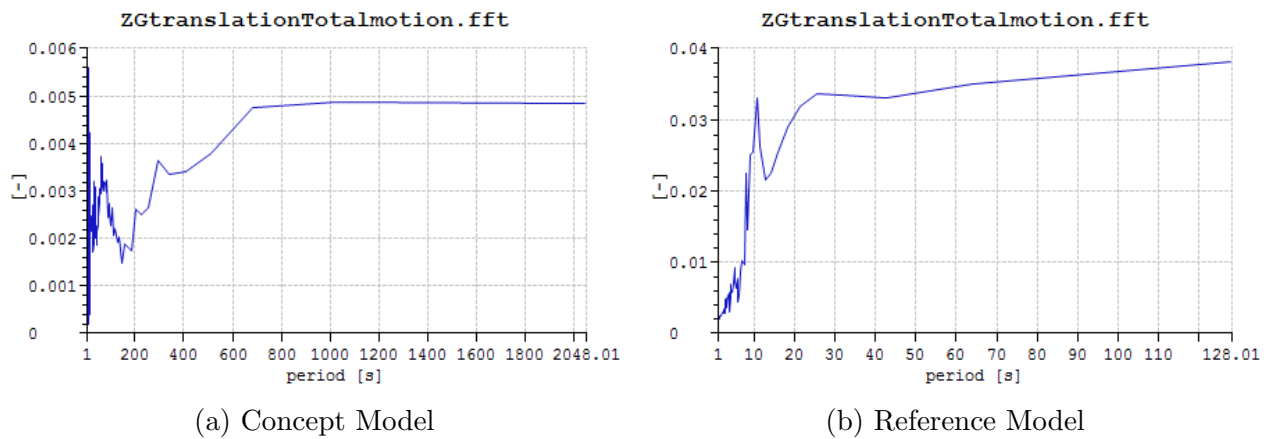
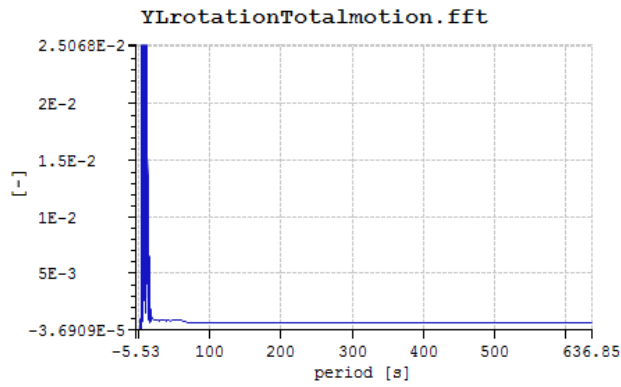
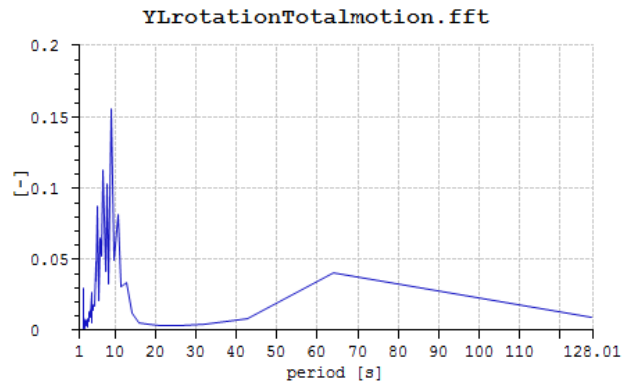


Figure D.38: heave spectra for C4-2

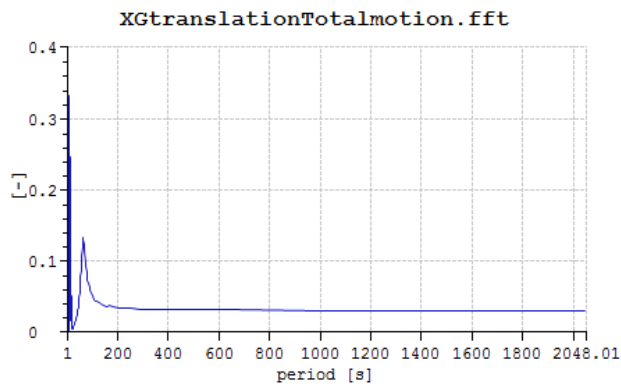


(a) Concept Model

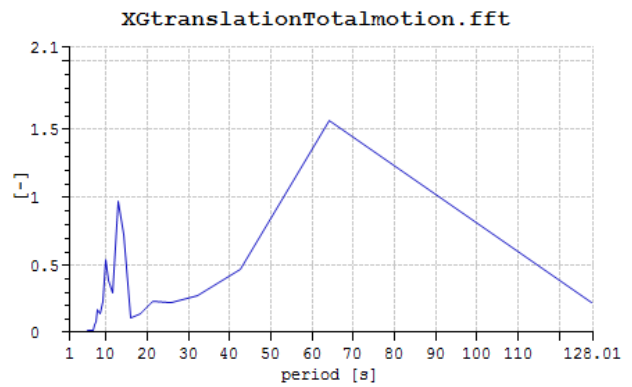


(b) Reference Model

Figure D.39: Pitch spectra for C4-2

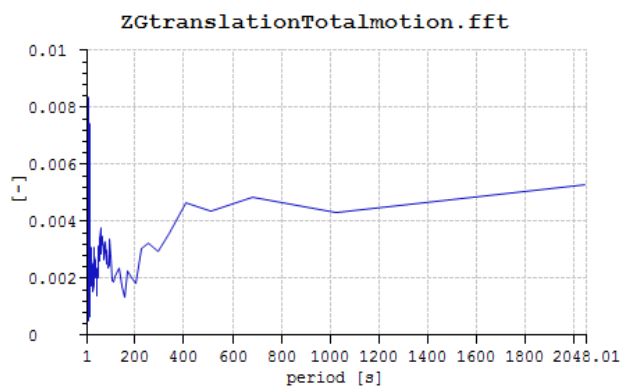


(a) Concept Model

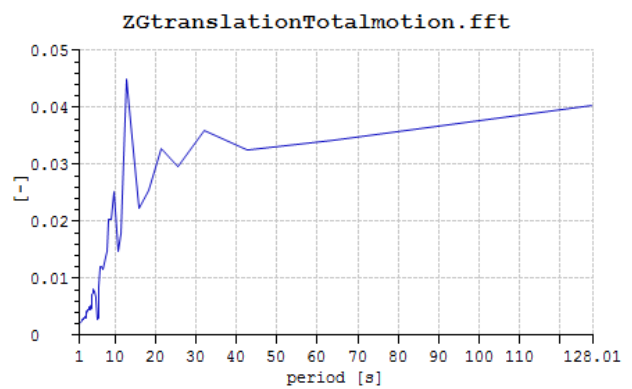


(b) Reference Model

Figure D.40: Surge spectra for C4-3

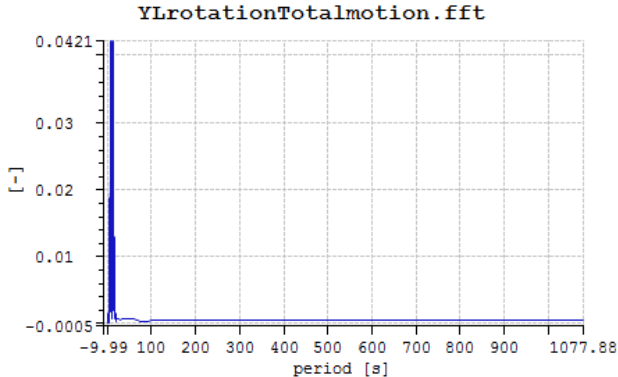


(a) Concept Model

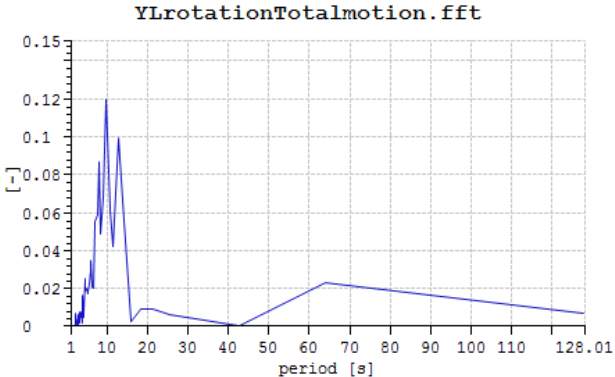


(b) Reference Model

Figure D.41: heave spectra for C4-3



(a) Concept Model



(b) Reference Model

Figure D.42: Pitch spectra for C4-3